Universität für Bodenkultur

University of Natural Resources and Life Sciences, Vienna

Department Wasser-Atmosphäre-Umwelt

Institut für Siedlungswasserbau, Industriewasserwirtschaft und Gewässerschutz

Leiter: Univ.Prof. DI Dr. Thomas Ertl

Toxicological effects of Cd-containing Quantum Dots on selected mammalian cell lines

Masterarbeit
Zur Erlangung des akademischen Grades
Diplomingenieur

eingereicht von

ELISABETTA DE VITO-FRANCESCO

Betreuer	Maria, Fürhacker
Mitbetreuer	Florian, Part

Matrikelnummer 01541711

05.2018

ACKNOWLEDGEMENTS

I would like to warmly thank Dr. Florian Part, my co-supervisor, for helping me in this new and interesting field and being available for any doubt. I would like to address another deep thanks to Ass. Prof. Seta Küpcü, who patiently showed me the basics of the practical part of my research. My additional acknowledgements go to my supervisor Prof. Maria Fürhacker, who always enlighteningly mentored me. Finally, I would direct special regards to Prof. Eva-Kathrin Ehmoser, who kindly welcomed me in her laboratory for allowing me to accomplish my work.

TABLE OF CONTENTS

Acknowledgements I

Table of figures VII

Table of tables XV

Table of abbreviations XVII

Abstract 1

1 Introduction 3

2 Aims Scopes 5

3 General background 7

3.1 Engineered Nanomaterials and Applications 7
3.2 Quantum dots 10

3.2.1 History of Quantum Dots 10

3.2.2 Definition and typologies 10

3.2.3 Physico-chemical Properties 12

3.3 Quantum dot Applications 19

3.4 Potential exposure routes, environmental Distribution and fate 23

3.5 Nanotoxicity 24

3.5.1 Nanomaterial-specific toxicity mechanisms (nanotoxicity) 24

3.5.2 Exposure and toxicokinetics 32

3.5.3 Bioassays to assess nanotoxicity 34

3.5.4 Flow cytometry 36

3.6 Cell lines and cell culture 38

3.6.1 CHO cell line 39

3.6.2 U937 macrophages 40

4 Materials And Methods 41

4.1 Quantum dot Characterization 41

4.1.1 Cd-based quantum dots used 41

4.2 Optical characterization 44

4.2.1 Determination of absorbance/emission spectra 44

4.2.2 Determination of hydrodynamic diameter 45

4.3 Assessment of cell viability 46

4.3.1 CHO cell line used in the study 46

4.3.2 U937 cell line used in the study 47

4.3.3 Flow cytometry 47

4.3.4 AlamarBlue® assay 51

4.4 QD Localization in cells 62

4.4.1 Confocal laser scanner microscope 62

5 Results And Discussions 65

5.1 QD characterization 65

5.2 Cell Viability...68

5.2.1 Flow Cytometry..68

5.2.2 Determined dose-response relationship by using AlamarBlue® assay.............................76

5.2.3 Localization of quantum dots 90

5.3 Discussion of obtained results...92

6 Summary... 97

7 Conclusions... 101

8 Outlook 103

9 References... 105

10 Annex 109

10.1 Sample preparation for flow cytometry 109

10.2 Sample prepatation for AlamarBlue® assay 111

10.3 Sample preparation for fluorescence microscopy..117

10.4 AlamarBlue® assay incubation times results 118

TABLE OF FIGURES

Figure 3.2.1. Spherical structure of a QD. The orange central sphere shows the inner metalloid core. The outer grey sphere represents the protective shell. Finally, the outer molecules represent the biocompatible coating layer. 12

Figure 3.2.2. Schematic representation of electron excitation and energy emission in a semiconductor. 14

Figure 3.2.3. Dependency relation between the increasing energy emitted and the decreasing size of the quantum dots. When the nanoparticles are small the band-gap is higher and therefore the colour emitted shits to the blue part (Sigma-Aldrich®, Quantum Dots). 15

Figure 3.3.1. Waterborne pathogens C. parvum (red) and G. Lamblia (green), detected with 605nm-QDs and 565nm-QDs respectively, 10µm scale (Zhu et al., 2004). 20

Figure 4.1.1. Schematic representation of QD types: bare-QD (CdTe core and NAC coating) (a), shelled QD (with additional ZnS shell) (b), shell-doped QD (Fe dopants added in the shell layer) (c), and core-doped QD (Fe dopants added in the core part) (c). 42

Figure 5.1.1. Absorbance and normalized fluorescence spectra (broken and solid lines) of bare-, shelled, shell-doped, core-doped QDs according to Part et al. (submitted). 65

Figure 5.1.2. Comparison of particle number vs HDD distributions over time (0 – 18 days) of bare-QD (A), shell-doped QD (B) and core-doped QD (C) (taken from Part et al., submitted). 67

Figure 5.2.1. From flow cytometry analysis dot-plots (side scatter signal on y-axis, forward scatter signal on the x-axis) show the gated population (blue) for a) untreated cells, b) treated cells (100 *µg/mL of NAC-CdTe QDs), c) treated cells that additionally contain Hoechst and 7-AAD stains. Single-parameter histograms from flow cytometry analysis using fluorescence channel FITC-A d) represents untreated cells, e) treated cells, and f) displays stained-treated cells. Dot-plots at the bottom of the Figure show the two populations created from the analysis of the histograms for g) untreated cells, h) treated cells, i) stained-treated cells.* *68*

Figure 5.2.2. From flow cytometry analysis after no incubation. The dot-plots (side scatter signal on y-axis, forward scatter signal on the x-axis) show the gated populations (blue and orange) for a) untreated cells, 1×10^6 cells/mL, b) PI-stained-untreated cells, 1×10^6 cells/mL. Single-parameter histograms show fluorescence intensity detected in the channel PE-A. Histograms c) is untreated cells, and d) is PI-stained-untreated cells. Dot-plots at the bottom of the Figure show the populations created during the analysis of the histograms c and d, for e) untreated cells, f) PI-stained-untreated cells. *71*

Figure 5.2.3. From flow cytometry analysis after 24h of incubation. The dot-plots (side scatter signal on y-axis, forward scatter signal on the x-axis) show the gated populations (blue and orange) for a) untreated cells, 1×10^6 cells/mL, b) PI-stained-untreated cells, 1×10^6 cells/mL. Single-parameter histograms show fluorescence intensity detected in the channel PE-A. Histograms c) is untreated cells, and d) is PI-stained-untreated cells. Dot-plots at the bottom of the Figure show the populations created during the analysis of the histograms c and d, for e) untreated cells, f) PI-stained-untreated cells. *72*

Figure 5.2.4. From flow cytometry analysis after no incubation. The dot-plots (side scatter signal on y-axis, forward scatter signal on the x-axis) show the gated populations (blue and orange) for a) treated cells, 1×10^6 cells/mL, 100µg/mL NAC-CdTe, b) PI-stained-treated cells. Single-parameter histograms show fluorescence intensity detected in the channel PE-A. Histograms c) is treated cells, and d) is PI-stained-treated cells. Dot-plots at the bottom of the Figure show the populations created during the analysis of the histograms c and d, for e) treated cells, f) PI-stained-treated cells. *73*

Figure 5.2.5. Flow cytometry analysis after 24h incubation. The dot-plots (side scatter signal on y-axis, forward scatter signal on the x-axis) show the gated populations (blue and orange) for a) treated cells, 1×10^6 cells/mL, 100µg/mL NAC-CdTe, b) PI-stained-treated cells. Single-parameter *histograms show fluorescence intensity detected in the channel PE-A. Histograms c) is treated cells, and d) is PI-stained-treated cells. Dot-plots at the bottom of the Figure show the populations created during the analysis of the histograms c and d, for e) treated cells, f) PI-stained-treated cells.* *74*

Figure 5.2.6. Change of fluorescence intensity of different U937 cells density as a function of incubation time. *76*

Figure 5.2.7. Change of fluorescence intensity of U937 cells treated with NaN_3 as a function of NaN_3 concentration and incubation time *77*

Figure 5.2.8. Dose-response relationship of U937 cells incubated with NAC-CdTe QDs after 18.5 and 24 hours (green and yellow bars, respectively). The fluorescence intensity was normalized related to the control (untreated) sample. *78*

Figure 5.2.9. Comparison of fluorescence intensity of the U937 cells, incubated with NAC-CdTe (yellow), NAC-CdTe/30%Fe:ZnS (orange) and NAC-30%Fe:CdTe/ZnS (blue) and 20% in volume AlamarBlue® stain. *80*

Figure 5.2.10. Fluorescence intensity of U937 incubated with NAC-30%Fe:CdTe/ZnS and 20% volume AlamarBlue® stain for 2, 4, 18 an 24h. For each concentration value, the incubation times are grouped, from the shortest to the longest. *81*

Figure 5.2.11. Comparison of fluorescence intensity of U937 incubated with AlamarBlue® stain and with NAC-CdTe, NAC-CdTe/ZnS, NAC-CdTe/30%Fe:ZnS, NAC-30%Fe:CdTe/ZnS and $CdCl_2$ (concentration values of $CdCl_2$ are shown in brackets). *82*

Figure 5.2.12. Comparison of fluorescence intensity of U937 incubated with NAC-CdTe, NAC-CdTe/ZnS, NAC-CdTe/30%Fe:ZnS, NAC-30%Fe:CdTe/ZnS, $CdCl_2$ and $FeCl_2$ (concentration values of $CdCl_2$ and then of $FeCl_2$ are shown in brackets). *84*

Figure 5.2.13. Comparison of fluorescence intensity of U937 incubated with $FeCl_2$ (concentrations in brackets) and $CdCl_2$. *85*

Figure 5.2.14. Sigmoidal function for curve fitting, exposure-concentration graph, with QDs concentrations from the second set of experiments, in logarithmic scale, % fluorescence signal for viability (inhibition of the cells), calculation of IC_{50} values for each different QDs type. 87

Figure 5.2.15. Comparison of fluorescence intensity values of media, media and AlamarBlue®, of background correction, of QD, and of before and after background correction samples. Data from shelled-QD incubated with U937 for 24h. 88

Figure 5.2.16. Comparison of background correction with only AlamarBlue® and media and background correction comprehending the QD fluorescence intensity. 89

Figure 5.2.17. Localization of NAC-CdTe/ZnS Quantum Dots, 1 µg/mL, after 24 hours of incubation, using confocal laser scanning microscopy. Bright field image of U937 macorphages(nucleus and membrane depited) (a). Fluorescent image of illuminated nuclei (stained with Hoechst) with DAPI filter channel (b). Fluorescent image of illuminated quantum dots (red arrows) (c). Overlay of the three micrographs (d).. 90

Figure 5.2.18. Localization of NAC-CdTe/ZnS QD 1 µg/mL inside the U937 samples after 24 hours of incubation, 3D visualization. NAC-CdTe/ZnS red dots, figure a). NAC-CdTe/30%Fe:ZnS red dots, figure b). Nuclei of the macrophages are enlightened in blue colour. Quantum dots are not localized inside the nuclei, but on the bottom and top layer of the sample and between the cells, probably inside their cytoplasm.. 91

Figure 10.1.1. Schematic description of treated sample preparation, for following flow cytometry analysis.. 109

Figure 10.1.2. Schematic description of untreated sample preparation, for the following flow cytometry analysis.. 109

Figure 10.1.3. Schematic representation of background sample preparation, for the following flow cytometry analysis.. 110

Figure 10.1.4. Schematic description of the staining steps, after the incubation for the following flow cytometry analysis. 110

Figure 10.2.1. Schematic description of the composition of samples to be analysed with the AlamarBlue® assay...111

Figure 10.2.2. Schematic procedure to prepare the NaN_3 *dilutions for preliminary analysis with AlamarBlue® assay.*..111

Figure 10.2.3. Schematic procedure to prepare the QD dispersions in Test 1, for further analysis with AlamarBlue® assay...112

Figure 10.2.4. Schematic procedure to prepare the QD dispersions in Test 2, for further analysis with AlamarBlue® assay...113

Figure 10.2.5. Schematic procedure to prepare the QD dispersions in Test 3.b, for further analysis with AlamarBlue® assay...113

Figure 10.2.6. Schematic representation of the calculation of the Cd counterpart from $CdCl_2$*, and procedure to obtain diluted solutions for further AlamarBlue® assay analysis.* 114

Figure 10.2.7. Schematic representation of the calculation of the Fe counterpart from $FeCl_2$ *and of the NAC organic ligand, and procedure to obtain diluted solutions for further AlamarBlue® assay analysis.* 114

Figure 10.2.8. Example of cell counting and cell suspension preparation...115

Figure 10.2.9. Well plate layout of example of samples of Test 1...115

Figure 10.2.10. Well plate layout of bare-QD and shell-doped QD-spiked samples.............................116

Figure 10.2.11. Well plate layout of core-doped QD and shelled-QD-spiked samples. 116

Figure 10.2.12. Well plate layout of ionic counterparts sample. $CdCl_2$ is displayed in green and $FeCl_2$ in orange. 117

Figure 10.3.1. Procedure for fixation, staining and glass preparation of the six samples, for fluorescence microscopy analysis. 117

Figure 10.4.1. Comparison of fluorescence intensity of U937 incubated with NAC-CdTe, Test 2. 118

Figure 10.4.2. Comparison of fluorescence intensity of U937 incubated with NAC-CdTe/30%Fe:ZnS, Test 2. 118

Figure 10.4.3. Comparison of fluorescence intensity of U937 incubated with NAC-CdTe, Test 3.a. 119

Figure 10.4.4. Comparison of fluorescence intensity of U937 incubated with NAC-CdTe/ZnS, Test 3.a. 119

Figure 10.4.5. Comparison of fluorescence intensity of U937 incubated with NAC-CdTe/30%Fe:ZnS, Test 3.a. 120

Figure 10.4.6. Comparison of fluorescence intensity of U937 incubated with NAC-30%Fe:CdTe/ZnS, Test 3.a. 120

Figure 10.4.7. Comparison of fluorescence intensity of U937 incubated with $CdCl_2$, Test 3.a. 121

Figure 10.4.8. Comparison of fluorescence intensity of U937 incubated with NAC-CdTe, Test 3.b. 121

Figure 10.4.9. Comparison of fluorescence intensity of U937 incubated with NAC-CdTe/ZnS, Test 3.b. 122

Figure 10.4.10. Comparison of fluorescence intensity of U937 incubated with NAC-CdTe/30%Fe:ZnS, Test 3.b. 122

Figure 10.4.11. Comparison of fluorescence intensity of U937 incubated with NAC-30%Fe:CdTe/ZnS, Test 3.b. 123

Figure 10.4.12. Comparison of fluorescence intensity of U937 incubated with $CdCl_2$, Test 3.b.............123

Figure 10.4.13. Comparison of fluorescence intensity of U937 incubated with $FeCl_2$, Test 3.b.............124

TABLE OF TABLES

Table 4.3.1. Schematic representation of dilutions and concentrations of QD dispersion for the conducted test with AlamarBlue® assay. 51

Table 4.3.2. Schematic representation of dilutions and concentrations of NaN3 solution for the preliminary test with AlamarBlue® assay. 52

Table 4.3.3. Schematic representation of dilutions and concentrations of CdCl2 solution. 52

Table 4.3.4. Schematic representation of dilutions and concentrations of FeCl2 solution. 53

Table 4.3.5. Schematic representation of dilutions and concentrations of NAC solution. 53

Table 4.3.6. Calculation steps for raw data correction of Absorbance intensity signal. 59

Table 4.3.7. Calculation steps for raw data correction, absolute and normalized fluorescence intensity. 60

Table 4.4.1. Schematic representation of dilutions and concentrations of QD dispersion for the conducted test with CLSM. 63

Table 5.2.1. IC50 values, with standard error R2 from sigmoidal curve fitting after 24h incubation of QDs/Cd and U937 cells. 87

TABLE OF ABBREVIATIONS

mg	milligram
µg	microgram
mL	millilitre
µL	microlitre
nm	nanometre
mmol	millimol
µM	micromolar
eV	Electron volt
ENM	Engineered Nanomaterial
NP	Nanoparticle
QD	Quantum Dot
mQD	magnetic Quantum Dots
CNT	Carbon Nanotubes
SWCNT	Single Walled Carbon Nanotube
MWCNT	Multi Walled Carbon Nanotube
R&D	Research and Development
Cd	Cadmium
Te	Telluride
Zn	Zinc
S	Sulphide

Fe	Iron
NAC	N-acetyl-L-cysteine
CLSM	Confocal laser scanner microscope
DIC	Differential interference contrast
TEM	Transmission electron microscope
ICP-AES	Inductively coupled plasma atomic emission spectroscopy
ICP-OES	Inductively coupled plasma optical emission spectroscopy
MRI	Magnetic Resonance Imaging
MTS	(3-(4,5-dimethylthiazol-2-yl)-5-(3-carboxymethoxyphenyl)-2-(4-sulfophenyl)-2H-tetrazolium)
TNFα	Tumour necrosis factor alpha
IL1-α	Interleukin alpha
ELISA	Enzyme-linked immunosorbent assay
MTT	3-(4,5-dimethylthiazol-2-yl)-2,5-diphenyltetrazolium bromide
PEI	Polyethylenimine
PEG	Polyethylene Glycol
MPA	Mercaptopropionic acid
GSH	Glutathione
TOPO	Tri-n-octylphosphine Oxide
DHLA	Dihydrolipoic Acid
FRET	Fluorescence resonance energy transfer
BRET	Bioluminescence resonance energy transfer
DRAM	Dynamic random-access memory
MEG	Multiple exciton generation
NADH	Nicotinamide adenine dinucleotide
ATP	Adenosin triphosphate

FITC	Fluorescein isothiocyanate
PE	Phycoerythrin
PI	Propium iodide
7-AAD	7-Aminoactinomycin D
PL QY	Photoluminescence quantum yield
PdI	Polydispersity index
FWHM	Full width half maximum
CHO	Chinese hamster ovary cells
BAC	Bacterial artificial chromosome
UV/VIS	Ultraviolet/visible
ROS	Reactive oxidative species
HDD	Hydrodynamic diameter
DLS	Dynamic light scattering
CLS	Collective light scatter
SSC-A	Side scattering channel
FSC-A	Forward scattering channel
IC_{50}	Inhibition concentration for 50% of living system

ABSTRACT

Quantum dots (QDs) are an engineered nanomaterial-type within the size range of 1 – 10 nm, exhibiting semiconducting and fluorescent properties, and higher reactivity than the bulk counterparts. Despite the wide applications (e.g. bioimaging, drug delivery, components in electronic devices), little is known about QDs toxicological effects and standardised toxicity methods. This research focused on the assessment of potential adverse effects of four types of NAC-coated Cd-based QDs (CdTe, CdTe/ZnS, CdTe/30%Fe:ZnS, 30%Fe:CdTe/ZnS) using in vitro bioassays, while attempting to develop a fast-screening and reproducible method to assess cytotoxicity by flow cytometry analysis. CHO cells (1×106 cells/mL) were incubated with NAC-CdTe (100 µg/mL) for 24h at 37°C. However, overlapping spectra of the viability determination stain (7AAD, Hoechst and PI) and of the QD's characteristic emission may have occurred. Therefore, cell viability assessment were proceeded via the AlamarBlue® assay, showing the dose-response behaviour. Macrophages U937 (5×105 cells/mL) were incubated with QDs (concentrations between 0.05 – 100 µg/mL), CdCl2 and FeCl2 solutions (0.3 – 30 µg/mL, 0.12 – 12 µg/mL, respectively), at 37°C for 0, 2, 4, 20, 24 hours. Due to lower half inhibition concentration value (IC50) for dissolved Cd ions (21.5 µg/mL) compared to these of QDs (66.6 µg/mL in average), and to viability reduction posed by Fe II counterparts (at 12 µg/mL), the release of these ions from the QD cores and the uptake into the cells was assumed as possible toxicity trigger factor. The images from the fluorescent microscopy analysis showed internalized QDs by the macrophages at a very low concentration (1 µg/mL) at which no significant viability decrease was observed. In conclusion, further tests are needed to better understand uptake mechanisms of QDs into cells, toxicity trigger factors and possible differences in QD types and their influence on cells.

GERMAN ABSTRACT

Quantum Dots (QDs) sind künstliche Nanomaterialen in der Größenordnung von 1-10 nm, die neben albleitenden und fluoreszierenden Eigenschaften auch generell eine höhere chemische Reaktivität als größere Partikel haben. Obwohl sie inzwischen in unterschiedlichsten Gebieten (Bildgebung, gezielte Wirkstoffabgabe, Elektronik) Verwendung finden, ist weder viel über ihre toxikologische Wirkung bekannt, noch gibt es standardisierte Methoden um diese zu bestimmen. Diese Arbeit beschäftigt sich mit der Erfassung von potentiell schädlichen Wirkungen von vier NAC-überzogenen cadmiumhaltigen QDs (CdTe, CdTe/ZnS, CdTe/30%Fe:ZnS, 30%Fe:CdTe/ZnS) mithilfe von in vitro Bioassays, sowie der Entwicklung einer schnellen Screening Methode für deren Zytotoxizität mittels Flow Cytometry. Dafür wurden CHO-Zellen (1×106 cells/mL) mit QDs NAC-CdTe (100 µg/mL) über 24h bei 37°C inkubiert. Da es unter Umständen zu überlagernden Spektren zwischen den Farben (7AAD, Hoechst and PI) und den charakteristischen QD Emissionen gekommen ist, wurde die weitere Analyse mit dem AlamarBlue® Assay durchgeführt. In weiterer Folge wurden die Makrophagen U937 (5×105 cells/mL) mit QDs (Konzentrationen 0,05 – 100 µg/mL) bzw. CdCl2 und FeCl2 Lösungen (0,3 – 30 µg/mL bzw. 0,12 – 12 µg/mL) bei 37°C für 0, 2, 4, 20, 24 Stunden inkubiert. Aufgrund der niedrigeren mittleren inhibitorischen Konzentration der gelösten Cd-Ionen (21,5 µg/mL) gegenüber den QDs (durchschnittlich 66,6 µg/mL) und der reduzierten Viabilität durch Fe-Ionen (12 µg/mL), wurde die Zellaufnahme der gelösten Ionen aus den QDs als potentielle Gründe für die Toxizität angenommen. Da die Bilder der Fluoreszenzmikroskopie von Makrophagen schon bei sehr niedriger Konzentration (1 µg/mL), absorbierte QDs zeigten, jedoch noch kein signifikanter Rückgang der Viabilität gemessen werden konnte, sind weitere Tests notwendig um Aufnahmemechanismen und Gründe für die Toxizität und potenziell unterschiedlichen Effekte verschiedener QDs Typen festzustellen.

1 INTRODUCTION

Engineered nanomaterials are uprising materials which find applications in several and different fields (from food packaging to cosmetics), and because of this their presence in the environment is increasing. However, these materials are still classified as emerging contaminants: contaminants which are not yet included in the routing monitoring program, and a possible future regulation may be stipulated depending on the ecotoxicity, public perception and occurrence in the environment.

In the past decades, toxicity tests have been conducted in order to assess the effects that those materials may induce to human being and to the environment. Many different methods have been applied and many different nanomaterial types as general model have been used to evaluate the potential ENMs toxicity. Some examples are silver and copper oxide (Ag and CuO) as representative nanoparticles used in the study of Piret et al. (2017), whose toxicity was assessed with cell viability assays (MTS, ATP content, caspase-3/7 activity) and immune assays (ELISA of proinflammatory cytokines IL1-β and TNF-α) (Piret et al., 2017). The study of Müller et al. (2014) studied the interaction among hydroxyapatite (HA) nanoparticles and cells using inductively-coupled plasma optical emission spectrometry (ICP-OES), MTT assay and bright-field transmission electron microscopy (BF-TEM) (Müller et al., 2014). Those were just two examples among the variety of toxicity assessment. Quantum dots, nanoparticles with size range within 1 – 10 nm, may be used as well as model to evaluate the toxicity of ENMs in general. Their characteristics of fluorescence emission and very small size allow to study potential internalization (and therefore effects) in cell culture, thanks to the possibility to track them and their penetration through cell membranes. Parallelly, those qualities may make them more difficult to be detected than compared to NP types. In this study effects of Cd-based QD incubated with cell lines were studied through flow cytometry, viability assay and microscope detection.

2 AIMS SCOPES

This study is aimed to assess the potential toxic effects of four types of quantum dots (QDs), NAC-CdTe, NAC-CdTe/ZnS, NAC-30%Fe:CdTe/ZnS and NAC-CdTe/30%Fe:ZnS, while attempting to develop a fast-screening and reproducible method. For this, two selected mammalian cell lines were used as representative potential end points: the Chinese Hamster Ovary cell line (CHO) and the suspended macrophages cell line U937. Fluorescence microscopy and flow cytometry was used to detect and localize QDs. The AlamarBlue® assay was conducted in order to detect the quantum dots and to assess cell viability. The objective of this study was to develop and optimize a protocol in order to assess cytotoxicity of QDs.

The study's scopes included the development of sample preparation protocol for:

- hydrophilic QD dispersions
- quantification of cell viability for both flow cytometry and AlamarBlue® assay
- localization of QDs within cells by using fluorescence microscopy

Based on the literature, it has been assumed that the studied quantum dots are likely to induce cytotoxicity effects to the cells used. The hypothesised reasons are related to the presence of heavy metal material in the core and to their ability to penetrate cell membranes.

3 GENERAL BACKGROUND

3.1 ENGINEERED NANOMATERIALS AND APPLICATIONS

Nanomaterials are defined as a natural, incidental or manufactured material containing particles in an unbound state or as an aggregate or agglomerate, and where more than 50% of the particles have dimension within the range of 1 – 100 nm (EC, 2011). According to International Organization for Standardizations (ISO, 2015), nanomaterials can be sub-classified into nano-objects and nanostructured materials. Nano-objects are defined as materials having one or more dimensions in the nanoscale. Nanostructured materials present nanoscale inner or surface structure. Furthermore, nano-objects are classified into three more different types according to number of nanoscale dimensions: nanoparticle, nanofiber and nanoplate. All the three dimensions of the first type lie in the nanoscale range. If just two dimensions are nano-confined the material is defined as nanofiber. Finally, nanoplate are nano-objects with just one nano-dimension. It is important to note that this study focuses on engineered nanomaterials (ENMs), which are designed for a specific purpose or product (ISO, 2015). Those are widely used in different products and for various applications – from medicine, Research and Development (R&D) to commercial applications.

According to Piperigkou et al. (2016) ENMs can be classified as following:

- Material type
    - Metallic, materials which contain metals and their compounds
    - Carbon, Carbon Nanotubes (CNT), Single Walled Carbon Nanotube (SWCNT), Multi Walled Carbon Nanotube (MWCNT), fullerenes, graphene
    - Organic, agglomeration of organic molecules, biomolecules or bio-macromolecules
    - Boron nitride
    - Mineral

  - Silicon

- Shape
  - Spherical
  - Aerogel
  - Nanotubes
  - Nanofiber
  - Nanorods
  - Nanoballs
  - Nanosheets
  - Nanowires
  - Nanofibrils

- Application
  - Industrial, electronical devices
  - Medical, bioimaging

In the following, some examples of nano-objects are listed (Piperigkou et al., 2016):

- Carbon Nanotubes (CNTs)

  They present an augmented surface area to size ratio. The consequences are the tendency to aggregate, the increase of interaction with biomolecules and a higher surface reactivity.

- Metal oxide nanoparticles

  They are more and more used for industrial and commercial application, for instance as pigments and sunscreen ingredients. Some examples are zinc oxide (ZnO) and titanium dioxide (TiO_2).

- Metal nanoparticles

  Metallic compounds like Au, Ag and Cu are used as ENMs because of their antibacterial properties.

- Non-metal oxide nanoparticles

SiO_2 is a non-metal oxide ENM which is used in cosmetics, as an additive to drugs, in food industry, for biomedical applications and in biosensors.

- Biopolymers

  These are ENMs which derive from different natural resources or materials, like cellulose. They can be obtained from crude oil. Or they can be produced by chemical synthesis, from bio-derived polymers.

According to Hansen et al. (2016), at the European market, nano-TiO_2, -SiO_2 and -Ag are most frequently used. However, it is still unclear the effective total amount, all the existing types and the hazard of nanomaterials (Foss Hansen et al., 2016). The authors established a new online inventory for nanomaterial products, called The Nanodatabase (www.nanodb.dk). This database contains the description of the product, specifying the type of nanomaterial included in it. It also gives the possibility to have some information concerning the potential exposure and hazard effects of the related ENM. To date, the number of listed nano-based products accounts for more than 3000. The majority of the products were listed under the categories of “health and fitness” (55% of the products), “home and garden” (21%) and “automotive” (12%). Specifically concerning nanomaterial, the most used ones in the products were:

1. Silver
   Across all the categories
2. Titanium oxide
   in “health and fitness” and “home and garden”
3. Gold
   in “appliance”, “health and fitness” and “home and garden”
4. Titanium
   in “automotive”, “health and fitness” and “home and garden”
5. Phosphate
   in “appliance”

Nevertheless, it was outlined that for many products it was not possible to identify the ENM type used in a product. This was caused by the lack of information from the producer itself. For example, 89% of products in category “automotive”, 79% in “electronics and computer” and 80% in “home and garden” were unknown (Foss Hansen et al., 2016). This lack of information complicates to derive exposure scenarios and consequently to assess potential risks. In the following, a special type of semiconductor ENMs is examined because this type was the object of research in this thesis.

3.2 QUANTUM DOTS

3.2.1 History of Quantum Dots

In the 1970s so-called quantum wells have been developed. They are considered as the precursors of quantum dots. Quantum wells present only one dimension in the nanoscale range, hence they belong to the nanofiber class. They are thick foil layers of nanometre dimension, in which the electron-hole charge carriers are trapped. Thanks to this characteristic they show a discrete excitation absorption spectrum, an observation first reported by Dingle et al. in 1974. During the same period, the term nanotechnology has been recovered by a Japanese Scientist N. Taniguchi. He understood the importance of nano-objects for the electronic industry, with this small and reactive material it was possible to build faster and more complex circuits (Bassi et al., 2013). The further development of nanomaterials was enabled by the enhancement of the electron beam lithography, instrumentation which allowed the production of 40-70nm size material (Bassi et al., 2013; Boxberg and Tulkki, 2018).

Later on, in the 1980s zero-dimension QDs were elaborated in more detail. In 1980 a Russian physicist, Ekimov, developed QDs in glass crystals. In 1984 an American chemist Louis E. Brus studied QDs in colloidal solutions, and he managed to derive the dependency relationship between energy emitted and size. However, it was necessary to wait for a decade to finally obtain a successful synthesis of colloidal CdX (X = Te, Se, S) as they are known nowadays (Zhu et al., 2013).

3.2.2 Definition and typologies

Quantum Dots are three-dimensionally confined nanocrystals, with size comprehended in the range of approximately 1 – 10 nm. According to the ISO definition (ISO, 2015), quantum dots are classified as nano-objects, and more precisely as nanoparticles, having all the three dimensions confined in the nanometre scale. Besides the small size, another significant characteristic for QDs is the ability of emitting fluorescent light when excited by a source of light in the UV and visible spectrum (Bassi et al., 2013; Semonin et al., 2012).

These semiconductor nanocrystals can be composed of different elements of the period table. According to the different groups, in which these elements belong to, QDs are classified as follow (Bonilla et al., 2016; Zhu et al., 2013):

- atoms of the groups II – VI
  e.g., cadmium sulphide (CdS), cadmium selenide (CdSe), cadmium telluride (CdTe);

- atoms of the group III – V
  e.g., indium phosphate (InP), indium arsenide (InAs), gallium arsenide (GaAs), gallium nitride (GaN);

- atoms of the group IV
  e.g., carbon (C), silicon (Si), germanium (Ge).

This last group of QDs are called emerging quantum dots, because of their just recent development and recent discovery of good optical properties. They are known to be more biocompatible then the heavy metal-based ones.

Silicon has been considered as a material with poor optical properties. However, during the 1990s its light emission and the absorption spectrum were studied in more detail. This material surprisingly revealed efficient optical characteristics. Their simultaneous advantage and disadvantage consists of good biocompatibility but high oxidative degradability. Because of this, they present then the need of surface modification.

The carbon-based QDs are a new class of nanoparticles and they have been discovered during purification of single-walled carbon nanotubes. Their wide success is due to their special optical property: they possess up-converted photoluminescence, which means that they are able to emit in the full spectrum of visible light. Moreover, under near infra-red light excitation they can also exhibit photoluminescence emission in the near infra-red spectrum (Zhu et al., 2013).

3.2.3 Physico-chemical Properties

Structural properties

The QD may be composed, as shown in Figure 3.2.1, of three layers of a spherical structure:

- a metalloid crystalline core
- a protective shell
- an outer more biocompatible coating.

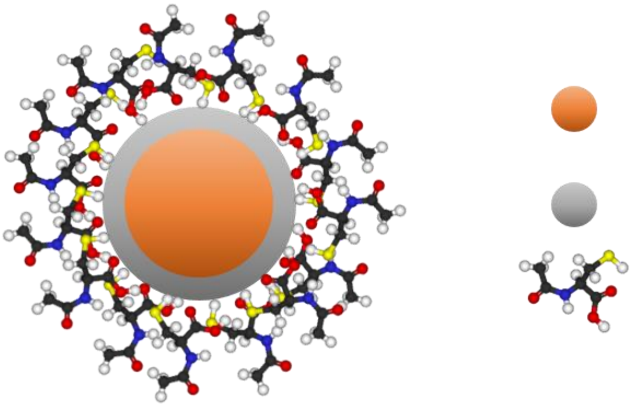

Figure 3.2.1. Spherical structure of a QD. The orange central sphere shows the inner metalloid core. The outer grey sphere represents the protective shell. Finally, the outer molecules represent the biocompatible coating layer.

The core is usually composed of metal complexes:

- Basic Metals with Semimetal

  Indium or gallium combined with arsenic (group III and V respectively). They create indium arsenide, InAs, or gallium arsenide, GaAs.

- Transition Metals with Non-metals

  Zinc or cadmium (group II) combined with selenium (group VI). They create zinc selenide, ZnSe, or cadmium selenide, CdSe.

- Transition Metals with Semimetals

  Cadmium or zinc combined with tellurium (group VI). They form zinc telluride, ZnTe, or cadmium telluride, CdTe (Hardman, 2006).

The core structure is then optionally overcoated with an outer protective shell. This is composed of transition metals and non-metals, such as ZnS. Or it can be composed of transition metals and semimetals, such as ZnTe. It is known that this additional layer enhances the optical properties of the nanoparticles and enhance the protection of the inner core against deterioration.

These core-shell QDs present hydrophobic characteristics. Therefore, an outer coating layer is usually added either to shell, or to the core directly if the shell is not present. This additional layer makes the particles hydrophilic hence water-dispersible, it increases colloidal stability in aqueous media and biocompatibility. For example, QDs can be coated with organic ligands having carboxyl functional groups, such as N-acetyl-L-cysteine (NAC). Other examples for frequently used, hydrophilic coatings are polyethylene glycol groups (PEG), mercaptopropionic acid (MPA), or glutathione (GSH) (Hardman, 2006; Lai et al., 2013; Ulusoy et al., 2015).

Semiconductor properties

QDs are defined as semiconductor materials. Their distinctive property is that their electrical conductivity behaves partly as insulator and partly as metal material. Semiconductors could be crystalline or amorphous solids, presenting higher resistance than metals but lower than insulators. The main properties shown by this kind of material are:

- Variable conductivity

  Semiconductors usually do not have optimum conductivity properties. However, thanks to the addition of some doping or gating, they could be transformed into conductor materials.

- Heterojunctions

  Exchange of electrons between different doped semiconductors.

- Excited electrons

  Electron-hole pairs are created when a difference in electric potential occurs, after energy excitation.

- Light emission

In some semiconductors (like in case of QDs), instead of releasing heat, when the electrons return to the normal state they emit light.

- Thermal energy conversion

Optical properties

The fluorescent properties of the QDs are enabled by their chemical composition, by their three-dimension nanoscale range and by the three-dimensional confinement of energy carriers (quantized energy) (Bimberg and Pohl, 2011; Hardman, 2006).

QDs are defined as semiconductor materials because of their chemical composition. The electrons in these semiconductor materials are empowered to change their energy state level after excitation. As it is shown in Figure 3.2.2 an electron can be in its ground state (or Valence Band), when it is stable at its original energy level, Figure 3.2.2 a). Or it can be in its excited state (or conduction band), when it jumps to higher levels after being excited, Figure 3.2.2 b). Finally, when it returns to the initial state the same energy is released as emitted light or fluorescence radiation, Figure 3.2.2 c). When the electron jumps from the valence band to the conduction band (see Figure 3.2.2 b)), it leaves am empty space (hole) in the initial band. From this, the physical behaviour of the electron after being excited has been named electron-hole pair.

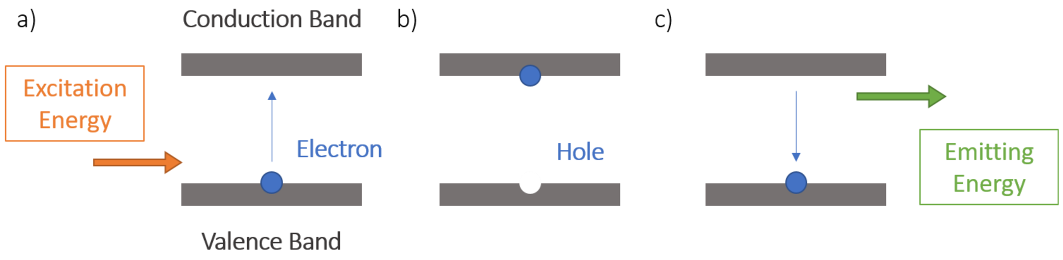

Figure 3.2.2. Schematic representation of electron excitation and energy emission in a semiconductor.

The Bohr radius is defined as the average distance between the valence and the conduction band. The effective distance between the ground state and the excited one is named band-gap in semiconductor materials (Bonilla et al., 2016). When the particles reach a size smaller than the Bohr radius and when they are three-dimensionally confined in the nano scale, it is guaranteed that their energy levels are quantized. Moreover, according to the Coulomb potential energy, the electron and the created hole mutually attract each other. Therefore, the small dimensions of the material induce simultaneous consequences: the creation of quantized energy levels and the more frequent interactions electron-hole. This characteristics allow the electrons to change their level of energy and therefore to emit fluorescent light (Semonin et al., 2012). Furthermore, the energy emitted is directly proportional to the value of this distance: the higher the band-gap, the higher the energy emitted (Bonilla et al., 2016). The difference with the bulk counterparts is based exactly on this behaviour. In the bulk materials, the band-gap has dimensions greater than the Bohr radius. Hence, the quantization of energy levels does not occur and the interactions between hole and electron are not as frequent as in nanomaterial. Therefore when the electrons in bulk materials are excited they do not emit quantized energy as fluorescent light when returning to the ground state (Semonin et al., 2012). Moreover, this behaviour outlines the difference among the semiconductors and the conductors. These last ones indeed do not present the electron-hole band-gap inner structure, hence no emission of energy due to electron movement occurs (Bonilla et al., 2016).

Depending on the value of the band-gap of the electron-hole pair, different amount of energy, in different wavelengths (or colours) is emitted, as it is explained in Figure 3.2.3. The larger the distance between the valence and the conduction band, the more energy is required to excite the electron. Therefore, higher energy is emitted during the electron's return to the ground state. This means that the colour of the light emitted varies depending on the particle's size. It is known that the band-gap distance increases with the decreasing of the particle's size. As a consequence, smaller QDs require more energy to be excited, and they emit higher emission values. The fluorescent light released shifts to blue colour. On the other hand, the bigger the particles, the smaller is the distance between electron and hole. Consequently, less energy is required to excite the nanoparticle and lower energy is emitted. In this case, smaller amount of energy means higher wavelength values and a red shift in the visible light spectrum (Bonilla et al., 2016).

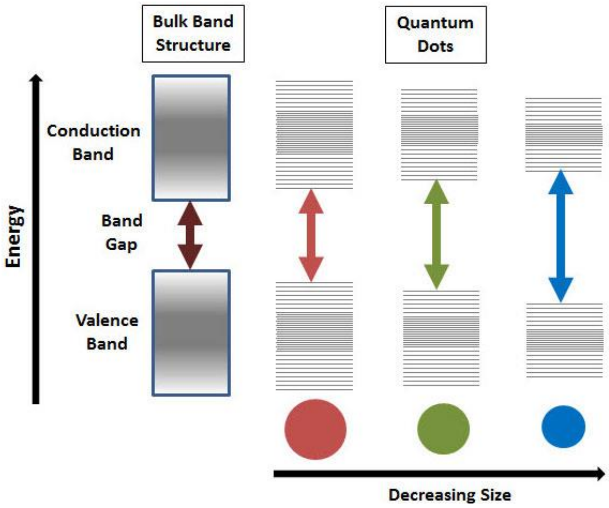

Figure 3.2.3. Dependency relation between the increasing energy emitted and the decreasing size of the quantum dots. When the nanoparticles are small the band-gap is higher and therefore the colour emitted shits to the blue part (Sigma-Aldrich®, Quantum Dots).

Remarkably, the different colours of emission can be influenced by different aspects of the particles: core size and composition, surface coating and shell composition. Among these characteristics the most influent are the core size and composition. Varying these characteristics is possible to customize the emission profile, stabilizing a specific wavelength peak in the whole range of electromagnetic spectrum (from UV to NIR). On the contrary, the shell composition and the surface composition could influence the photoluminescence but not the emission range in a significant way as the previous aspects (Midha et al., 2015). The size of the QDs usually varies between 1 and 10 nm, which can mainly be tuned by the reaction time and temperature during their synthesis. For instance, concerning the production of CdSe, when cadmium oleate reacts with trioctylphosphine, CdSe is created, and the longer this reaction is kept the bigger their crystals become. However, if the temperature is lowered, the growth stops. Therefore it is possible to control the QDs dimensions by stopping the reaction at certain specific moments by cooling it down (Bonilla et al., 2016).

Contrary to organic dyes, QDs present the characteristic of having a wide range of excitation spectrum and very narrow emission range. This means that it is possible to use one single excitation wavelength to excite many different types of QDs at the same time. This occurs because the energy emitted by the QDs depends on their chemical composition and on their size, as previously explained. Therefore, each different type of QD present a specific emission wavelength peak. This is a useful optical property for quantum dots application, mainly in the bioimaging field or for optoelectronic devices (e.g., LEDs). For example, it is possible to use different types of QDs having different sizes to track different specific cells and detect all of them at once with the same source of light (Bonilla et al., 2016).

Quantum dots present a high photostability and are not so prone to photobleaching (loss of intensity due to the damage of the chemical part of the dye because of photochemical damage) compared to organic dyes. They can be subjected to repeated cycles of excitation and then still emit with high brightness and fluorescence quantum yield values (Bonilla et al., 2016). Moreover, QDs present a high resistance to degradation for example to the metabolic one (Bonilla et al., 2016).

On the contrary, the organic dyes exhibit a narrow excitation and a wide emission spectrum. Depending on the type of organic dye, it is necessary to excite each of them with a specific wavelength value. Therefore, in order to make more than one organic dye emit at the same time, it would be necessary to have multiple different wavelength energy sources. Moreover, their wide emission spectrum makes it more difficult to distinguish a dye from autofluorescence background (e.g. like from proteins), because their wavelength emission may overlap (Bonilla et al., 2016). Finally, because of the organic characteristics of these kind of dyes, they present a lower photostability compared to QDs.

Surface properties

Their compositional characteristics make them more favourable compared to the organic dyes. Their surface properties make them tuneable, organic ligands can be bound to their surface and improve their properties. For instance, the presence of these organic ligands controls the hydrophilic or hydrophobic properties, therefore improving their colloidal stability. The addition of functional groups directly to the organic ligands is called functionalization or bioconjugation. This allows further surface modifications, such as labelling with antibodies of interest (Bilan et al., 2015).

The QD’s surface properties play also a significant role regarding their potential toxicity. The surface of the QDs is characterized by higher reactivity compared to the bulk counterpart. The smaller the diameter of the particle, the higher is the surface to volume ratio: the volume of each particle is reduced to nanoscale dimensions, but at the same time due to the creation of much more individual material the surface area increases. The direct consequence is an increase of the chemical reactivity of the particle because more available surface induces more opportunities for reactions with the surrounding biological environment. Indeed, if the surface tends to be active the nanoparticles may have more tendency to bind with external atomic and molecular structures, such as proteins. Another related effect is the potential toxicity that QDs may induce (Elsaesser and Howard, 2012). The hypothesis of nanotoxicity has been developed because if these nanoparticles are able to interact with very small living or vital entities, like cells or proteins, they may be able to penetrate inside them and they may be inclined to cause then negative effects (Fu et al., 2014).

Preparation of QDs

The methods for synthesis vary according to the different material used for the QDs. For example, the synthesis of silicon-based QDs consists of solution-phase-based methods, micro emulsion synthesis, and thermally induced disproportionation of solid hydrogen silsesquioxane. Instead, the synthesis of carbon-based particles can be carried out following two methods: top-down and bottom-up approaches. The top-down method consists of using a laser ablation and electrochemical oxidation: QDs are created from a larger carbon structure. The bottom-up method is related to solution chemistry methods: QDs are formed from molecular precursors (Zhu et al., 2013). Even different is the cadmium-based QDs preparation: it can be carried out according to two different approaches, physical or chemical. The physical approach consists of epitaxial growth and nanoscale patterning by combining high-resolution electron beam lithography and subsequent etching. However, this production method presents some disadvantages as defection formation, size non-uniformity, poor interface quality, damage to the bulk of the crystal itself (Zhu et al., 2013). The chemical method works by using pyrolysis of organometallic and chalcogen precursors, a rapid nucleation, and then a slower and steady growth. A typical protocol is: heating up tri-n-octylphosphine oxide (TOPO) under argon or nitrogen atmosphere, afterwards a hot solution of precursors material is injected to initiate rapid homogeneous nucleation. The final step consists of lowering quickly the temperature of the solution, and letting the crystal grow for some time (Zhu et al., 2013).

Water disperseability

QD are often synthesized using non-polar organic solvents, therefore they are hydrophobic. This is the reason why, QDs are often further surface modified in order to obtain hydrophilic properties. A first method used is ligand displacement with molecules with thiol groups. This means that the hydrophobic part of the organic solvent is exchanged for hydrophilic ligands, such as carbonyl-terminated organic acids. A ligand molecule can be composed of various units: polyethylene glycol (PEG), which enhances the hydrophilicity; any functional group such as -COOH, -NH_2, -OH, biotin, to permit further modification of the QD’s surface; dihydrolipoic acid (DHLA) which makes the QD’s surface an anchor for other materials. A second method to obtain water-disperseability is encapsulation. The particle is encapsulated in a layer of amphiphilic diblock or triblock copolymers, or of silica coating, or of phospholipid micelles. In this way more biocompatible QDs are created: the hydrophobic ends of amphiphilic molecules bind to the hydrophobic part of the particle (via hydrophobic interactions), hence the hydrophilic part extends towards the aqueous environment around (Bonilla et al., 2016; Zhu et al., 2013).

3.3 QUANTUM DOT APPLICATIONS

The use of QDs is becoming more and more frequent due to their outstanding optical properties. One of the sector where the QDs are applied is in biological imaging (e.g., *in vivo* imaging, for *in vivo* cancer imaging and treatment, for cell tracking and intracellular delivery, pathogen and enzyme detection, and for monitoring drug delivery). Another category of application of QDs is in food science: for targeted detecting and monitoring foodborne pathogens, protein tracking and food packaging. Finally, a different but wide field of application is the electronics: QDs are used for LED components, lasers, flash memories and photovoltaics devices (Bimberg and Pohl, 2011; Bonilla et al., 2016; Piccinno et al., 2012; Piperigkou et al., 2016; Semonin et al., 2012).

Biological imaging applications

Fluorescence resonance energy transfer (FRET) is a method of resonance where conformational changes and interaction between different molecules are measured, usually for proteins. The principle of this device is the transfer of energy among two fluorophore dyes, from the excited one, called donor, to the second one called acceptor. Usually, the dyes involved in FRET are organic and one is linked to the carbon terminal of the protein and another one linked to the nitrogen one. The emission wavelength value of the donor and the excitation wavelength value of the acceptor must overlap. On the contrary the excitation of both donor and acceptor must not overlap, guaranteeing in this way that the only light emitted is by the acceptor (Bonilla et al., 2016). According to these rules, QDs can replace the organic classical dyes because of the unique characteristics of the ENMs. Indeed, they can be excited by the same wavelength source and emit at different values, therefore there would be an overlapping of the excitation spectra but not for the emission. A study tested the behaviour of a QDs, having an emission maximum at a wavelength of 585 nm, used as donor dye and the organic fluorophore “Cy5” as acceptor, compared with the ordinary organic dyes couple “Cy3” and “Cy5”. The results of protein monitoring were the same even with the nanoparticle substitution: QDs-organic dye test presented a lower overlapping of emission and excitation, but compensated by the higher quantum yield of the QDs, hence more detectable (Bonilla et al., 2016).

QDs have also been used for *in vivo* imaging thanks to their high photostability in the first place and thanks to their strong signal, to the high brightness and uniform spectral profile (Bonilla et al., 2016; Midha et al., 2015). For example, the particles could be used in a bioluminescence resonance energy transfer (BRET) device, similar to the above discussed FRET, but with the substitution of the energy donor dye with a bioluminescent molecule activated by an enzyme (Bonilla et al., 2016). The QDs may be used in this case indeed as acceptor, and their fluorescence activated by an enzyme (Bonilla et al., 2016).

One of the most important and promising *in vivo* imaging application is targeted cancer detection and potential cure. Detecting a tumour is possible based on the technique of sentinel node lymph mapping. A blue dye is inserted in the lymphatic system surrounding the potential tumour area, in this way the sentinel lymph node (usually the first lymph node to which the cells of the cancer direct and spread) can be detected. The introduction of QDs instead of an organic dye may improve consistently this technique: due to the brighter fluorescence of the nanoparticles the localization of the sentinel node would be easier (Bonilla et al., 2016). The non-invasive cell tracking procedure is more in favour compared to the invasive one because of no cellular damage or alteration effects. The QDs may enhance the progress of this kind of technique, and so far two approaches of cell labelling with the QDs have been developed. A first one is based on penetration in the cell via endocytosis, and the second one is based on the binding of QDs to the cell's surface via the biotinylating of the cell's surface (Bonilla et al., 2016).

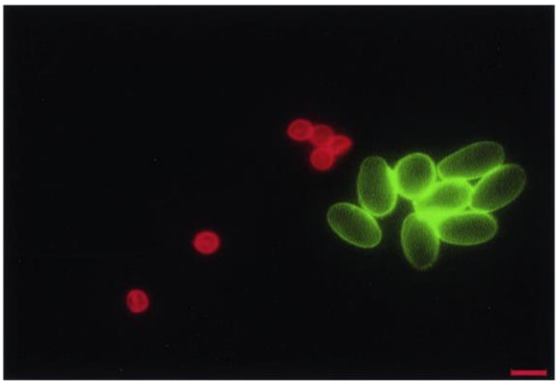

Figure 3.3.1. Waterborne pathogens C. parvum (red) and G. Lamblia (green), detected with 605nm-QDs and 565nm-QDs respectively, 10µm scale (Zhu et al., 2004).

QDs have been as well used in detection of pathogens, as for example waterborne pathogens, of microorganisms, of fungal populations and of viruses (Bonilla et al., 2016). An example, which outlines the before-mentioned optical characteristic of the QDs, is an example of success in detecting two different waterborne microorganisms, *Cryptosporidium parvum* and *Giarda lamblia*, at the same time (Figure 3.3.1). The use of QDs as fluorescent labels allowed to detect distinctively the two different microorganisms because after enlightening them with a unique source of light the emission released was of two different colours for the two different pathogens. They exhibited as well their enhanced photostability (Bonilla et al., 2016; Zhu et al., 2004).

Drug delivery applications

Furthermore, QDs may be used as therapeutic drug (or gene) delivery systems in cancer therapy or in cell tracking. This is due to the many advantages that nanoparticles may bring: prolonged drug circulation lifetime, specific and selective drug delivery and improved colloidal stability, and most important the possibility of more than one drug release per delivery per each QD (Piperigkou et al., 2016). However, QDs are not yet used for medical purposes but only in R&D because of their potential and not yet well studied toxicity effects (Bonilla et al., 2016).

Food industry applications

The main application in food industry for QDs is the tracking and the detection of food pathogens. For instance, simultaneous detection of *Escherichia coli* and *Salmonella typhimurium* was possible after having conjugated 525nm- and 705nm-QDs (emission peak value) to anti-*E. coli* and to anti-*Salmonella* antibodies. These finally successfully attached to the bacteria's surfaces, and after excitation it was possible to detect each of them individually and simultaneously (Bonilla et al., 2016; Wang et al., 2011). These fluorescent QDs are as well utilized as protein tracker in food. For instance, they may improve the understanding of the movement of gluten under thermal motions. It has been made possible because of the conjugation of CdSe/ZnS carboxyl-terminated QDs to gluten. The QDs showed good photostability, little bleaching (after repeated laser excitements) and long term bright stable imaging (Bonilla et al., 2016; Sozer and Kokini, 2014).

An innovative application of QDs in alimentary field is in food packing. This may be improved by the novel use of polymer nanotechnology. For instance, the manipulation of the polymer barriers with active components may give the packaging the skill of protecting the food against possible pathogens, against humidity, against oxidation. Besides, nanotechnology could be developed in order to be able to monitor the conditions of the food inside the packaging. Such nanosensors may indicate the level of degradation of the products, or microbial contamination occurrence (Piperigkou et al., 2016).

Electronical devices applications

QDs have been mostly applied in electronic field. For example, QDs are used as fluorescent semiconductors to manufacture near infrared lasers, at which the emission wavelength can be designed by controlling quantum dot's size and composition (Bimberg and Pohl, 2011). These nanoparticles might be attractive in the field of data storage. So far two semiconductor memories devices have been developed, which are called the "Dynamic random-access memory" (DRAM) and the "dots-based flash memory". The DRAM exhibits fast access time and good endurance, but poor retention time. A quantum dots-based flash memory has long retention time but poor writing time (Bimberg and Pohl, 2011). However, the widest electronical application of QDs is their use in LED screens and displays. QDs provide high brightness and colour saturation (SigmaAldrich, 2017).

Photovoltaics applications

The principle of a solar cell system consists of harvesting a fixed amount of energy derived from solar photons, presenting values between 0.4 and 4.0 eV. However, the solar cells possess just a defined band-gap values for energy absorption. Hence, the photons with lower energy than the solar cell's band-gap can not be absorbed, and photons with higher energy than the solar cell's band-gap are just partly absorbed. The problem is the dissipation of the shortage or excess of energy which could be instead stored (Semonin et al., 2012).

The use of QD-based semiconductors could avoid the energy dissipation and increase the efficiency of the primary photoconversion through enhancing the sensitivity of the already present semiconductors, or through forming QDs electronically coupled arrays to enhance the efficiency electron-hole conductivity (Semonin et al., 2012). The process of Multiple exciton generation (MEG) consists of the possibility for a solar cell to store twice the amount of energy than the defined band-gap, and to produce two or more electron-hole pairs. This procedure allows to avoid thermal dissipation energy and to guarantee a simple solar cell structure having just one absorber layer (Semonin et al., 2012). The nanostructure material allows many ways of energy control for the MEG procedure, compared to the bulk counterpart. This is because in this last one both the crystal momentum and the energy must be conserved, on the other hand in nanomaterials just the energy is needed to be conserved. Moreover the three-dimension quantum confinement improves the process itself: MEG is based on Coulomb interaction as the electron-hole pairs attraction in the QDs (Semonin et al., 2012).

3.4 POTENTIAL EXPOSURE ROUTES, ENVIRONMENTAL DISTRIBUTION AND FATE

As previously described ENMs show a wide range of applications (e.g., bioimaging, electronical devices, R&D, cosmetics, construction materials, etc…) (Part et al., 2016a). These larger amounts of ENMs induced the necessity of defining the effective amount present and released in the environment, and as a consequence the necessity of clarifying the potential harm to the environment (Part et al., 2016a).

One of the main challenge indeed is the attempt to define the exact amount of the ENMs in the market and in the environment. In order to solve this first problem, a first step is the delineation of potential exposure scenarios where QDs are likely to be exposed or released to the environment. So far, these potential exposure routes have not been completely understood yet and indeed they have been hypothesized only on the basis of similar materials (Hardman, 2006). In this study it has been assumed that QDs may be released along the life cycle of QD-containing products, in particular during: synthetisation/manufacturing, utilization and disposal/recycling. During the synthesis of the Nanoparticles, the most likely exposures routes are through dermal and respiratory pathways, while handling with QD-containing materials, such powders or aqueous dispersions. After inhalation of QD, these may reach the pulmonary tissues, and the smaller particles may reach and interrelate with alveolar parts. On the contrary, the bigger particles may deposit in the more superficial part of the apparatus, like bronchi. A relevant problem is the potential endocytosis incorporation of the particles inside the cells (Hardman, 2006). During the manufacturing process, the handling of raw materials, for instance $CdCl_2$ powder, or as well the prepared crystalline form of QDs may produce potential risk through dermal exposure or inhalation. On the other hand, during this initial phase, less likely accidental absorption mechanisms may occur by means the digestion pathways. Concerning QD-based electronical devices, for instance LED screens, the exposure or the release of QDs is very unlikely, as the materials are always incorporated into sealed structures and matrices, such as epoxy resins. However, chemical or mechanical stress during waste treatment processes (e.g. recycling or landfilling) may lead to unintentional QD release into the environment. During the recycling, discarded QD-containing products may end up in the wastewaters and solid waste streams. The disposal and the risk of leakage are the main concern regarding the potential exposure and sources of contamination. Furthermore, the fate, the potential risk of bioaccumulation and of toxicity of released ENMs are not fully understood (Hardman, 2006).

The term endpoint is connected to the kinds of effects which are measured in a toxicity tests, the most important ones to be considered are mortality, immobilization, reproduction changings, growth of individuals or populations or specific molecular/biochemical responses. Regarding, the potential end-points for human beings might be the liver, the kidneys and the lungs. This assumption is based on the already known information about heavy metal substance Cadmium. This tends to bioaccumulate and to distribute in all the body tissues, with main targets liver and kidney (Hardman, 2006).

3.5 NANOTOXICITY

3.5.1 Nanomaterial-specific toxicity mechanisms (nanotoxicity)

Toxicity is defined as the possibility of a chemical substance to cause adverse effects to human beings, animals and the environment. This is a concept strictly linked to the dose-response relationship. Thus, the most important parameters to define the toxicity of a compound are concentration and time of exposure. Considering then the specific topic of nanoparticles, the term toxicity turns into a more specific term, namely nanotoxicity. This is the potential harm to human beings, animals or the environment caused by nanoparticles.

According to the meta-analysis from Oh et al. (2016), which is based on 307 different studies, most of the QDs are composed of Cd, Se or Te, CdSe 63% and CdTe 29% (Oh et al., 2016). It is known how the Cd and Se substances cause acute and chronic toxicity towards vertebrates, hence being of relevant concern for human health and for the environment. Cadmium is potentially carcinogenic and bioaccumulative, its half-life in humans is around 15-20 years. It accumulates in the bodily tissues, with main target of liver and kidneys, and it is able to cross the blood-brain barrier and placenta. Selenium presents severe environmental and ecosystems impacts. Because of quantum dots may be composed indeed of these two materials it is highly necessary to take into consideration the potential risks which these particles might present towards the human health and towards the environment (Hardman, 2006).

So far, several nanotoxicity tests have been conducted and studied by using cell lines or in specific cases whole living organisms as biological simulating end-point systems. However, ENMs are a non-uniform group of substances having different shapes, elemental composition and morphologies and therefore it complicates to derive general conclusions regarding nanotoxicity. They differentiate from the others because of the element composition, the addition or not of a core-protective layer, or the addition of a hydrophilic coating layer. As a consequence, in various studies the obtained results concerning potential toxicity of ENMs showed different values of dose-response concentration, of units of measurement, of physicochemical properties among each other (Hardman, 2006). Besides the wide range of nanoparticles typologies, the complexity to fully understand the nano-specific toxic effect lays on the lack of information of the cell uptake mechanisms and of the interaction between nanoparticles and the living systems (Elsaesser and Howard, 2012).

According to Elsaesser and Howard (2012), the main concern about the toxicity of ENMs is the chronic low dose exposure over a life time rather than the high dose acute exposure, which could be easily detected and fixed. Moreover, in the case of nanoparticles, the dose metric should be related to the number of particles, determined by a certain size and shape, rather than the mass of the chemical substances. This different metric would be chosen because the reactivity of the surface area is better known, hence it may be possible to predict the potential harmful effects towards humans and the environment (Elsaesser and Howard, 2012).

In case of QDs, their specific toxic effects are also not fully understood. A meta-analysis by Oh et al. (2016) on the cytotoxicity of Cd-based QDs outlined that the QD-induced toxicity responses are mainly associated to the QD's specific physico-chemical properties, such as QD diameter, and to their specific surface properties, determined by the used type of surface ligands. Other relevant influencing factors are exposure time, exposure concentration values, assay type, cell type and cell origin (Oh et al., 2016). Moreover, Hardman (2006) summarized that both the physicochemical properties of ENMs and environmental attributes have been enlightened as important factors to take into account when assessing nanotoxicity. In particular, physico-chemical properties, such as size, concentration, composition, stability, surface charge, and surface coatings (bioactivity) are key factors regarding nanotoxicity (Hardman, 2006). In the following, some key factors regarding nanotoxicity are listed, focusing on QDs.

Size

The size of ENMs play an important role in nanotoxicity (Fu et al., 2014). It is assumed that the smaller the particle, the higher the potential damage to the cells. This is due to the ability of such small sized particles to easily penetrate the cell membranes or to reach the organelles, and therefore potentially cause cellular dysfunctions (Fu et al., 2014). Cytotoxicity of CdTe/CdS and CdTe/CdS/ZnS has been assessed in the study of Ulusoy et al. (2014). The QD were exposed to A549 adenocarcinoma lung cancer cells for 2 and 24 hours in concentration range between 0.002 – 600 µg/mL. The viability of the cell was then measured with the CellTiter-Blue assay method. The dose-response curves after 24 hours of incubation showed that smaller size QDs (3.68±0.74 nm) resulted in lower IC_{50} values, than larger QDs (4.31±0.76 nm) (83µg/ml and 100µg/ml, respectively). This means that smaller particles may cause higher negative effects compared to the bigger ones (Ulusoy et al., 2014).

Shape

Regarding the shape of ENMs, the study from Fu et al. (2014) suggested that different shape types cause different cytotoxicity effects. For example, a snowflake shape induces the strongest toxicity among the different shapes available. Fu et al. (2014) showed that hexagonal shaped showed higher toxicity, followed by rods, spheres, cylinders, and cubes. In another study, the effects of two differently shaped QDs (spherical and cylindrical) on the CHO cell line have been compared (Zhang et al., 2008). They observed that for smaller and more spherically shaped QDs, the uptake by the cells was easier, than for larger and cylindrically shaped QDs (Zhang et al., 2008).

Composition and disperseability

Besides size and surface capping materials, the composition of the same QDs might influence their adverse effects. Hauck et al. (2010) compared the difference between PbS and CdS QDs. These ENMs presented indeed different composition substances, sizes and shapes and surface chemistry composition. PbS were sphere-shaped with amino groups (onto the surface coating), and the CdS QD were rod-shaped and had carboxyl-terminated capping agents. The results showed that the composition revealed a higher influence in toxicity compared to the size, shape and surface characteristics (Fu et al., 2014; Hauck et al., 2010). Chiang et al. (2012) examined the influence of disperseability of nano-ZnO (Chiang et al., 2012). For this, nano-ZnO was dispersed in serum-free Dulbecco's modified Eagle's medium (DMEM) and in DMEM with addition of 10% of foetal bovine serum (FBS). They induced similar cytotoxicity effects, with the only difference that the serum-free samples showed reactive oxidative species (ROS) toxicity (Chiang et al., 2012; Fu et al., 2014). In conclusion, the disperseability of ENMs in a certain media could as well influence the cytotoxicity of the cells (the more disperseable the particle, the higher the potential induced toxicity). This is in accordance to a study from Mahto et al. (2010) on core-shell QDs, (CdSe/ZnSe), which were dispersed in aqueous media and, induced both ROS formation, oxidation and the release of cadmium ions (Fu et al., 2014; Mahto et al., 2010).

Transformation of QD components

One of the main QD-concern is related to the possibility of the cadmium ions releasing from the nanoparticle's core or shell materials (e.g. from CdTe/CdS QDs). The oxidation of selenium or sulphur compounds may be caused by the exposition of the QDs to air before the solubilisation, or the catalyzation by UV light, or by an oxidant solution like hydrogen peroxide. In summary, transformation processes in the environment are very likely and can significantly influence their hazardous properties. For example, after the deterioration/degradation of the shell, the core is more exposed to the environment. This process might accelerate further oxidation processes, consequently leading to a release of free cadmium ions, which cause acute toxicity. In sulphur-rich environments, like cell media, cadmium ions are likely to bind to sulfhydryl groups of mitochondria proteins in the cells. As a consequence, the thiol group is inactivated, inducing oxidative stress and mitochondrial dysfunction, with potential cell death (Derfus et al., 2004; Midha et al., 2015). Derfus at al. (2004) studied the effects of CdSe QD using hepatocytes cells (liver cells) and compared different test conditions (QDs were exposed to air or to UV-light). Results from the MTT assay showed how the viability of the cells was significantly reduced from 98% to 21% in the case of 30 minutes of air exposure of the QDs. In the case of UV light exposure, cell viability was reduced of 6, 42, 83 and 97% after incubation of 1, 2, 4 and 8 hours, respectively. Derfus at al. (2004) assumed that the reason relied on the oxidation processes of the chalcogenide atoms (S, Se, Te), which formed some oxides, and therefore Cd ions were released from the core. Further tests from the inductively coupled plasma optical emission spectroscopy (ICP-OES) confirmed the higher presence of dissolved Cd^{2+} ions in the previously UV-light oxidized and in the previously air-oxidized samples (126ppm and 82ppm), rather than standard conditions samples (6ppm) (Derfus et al., 2004). These results concerning the Cd ions toxicity are in accordance to the study of Kirchner et al. (2005). They incubated CdSe and CdSe/ZnS with MPA, silica or polymer coatings QD with MDA-MB-435S breast cancer cells. They calculated the concentration of cadmium ions related to the amount present in the QDs. Thanks to the method of counting the number of cells adherent on to the cell culture, they showed that with the increasing of the cadmium concentration in the incubated sample, the cells were initially prone to apoptosis, and afterwards to necrosis, which could be explained by the release of Cd^{2+} rather than of Zn^{2+} and Se^{2-} ions. Cadmium ions were present in concentrations of 10 µM maximum, the concentration of zinc and selenium ions was greater than 40 µM. Nevertheless, the cadmium concentration caused more negative effects than the Zn and Se ions. The study of Xu et al. (2010) showed similar results regarding the release of toxic heavy metals from QD materials. Different concentrations of Cd-based QDs (CdTe, CdTe/CdS, CdTe/ZnS and $CdTe/SiO_2$) have been incubated with unicellular algae, *Phaeodactylum tricorntum*. They measured firstly cadmium release rate, obtaining in decreasing order CdTe (8.78nm/ml×mg×h) > CdTe/CdS (2.63) > $CdTe/SiO_2$ (0.89) > CdTe/ZnS (0.72). Secondly, they measured the cytotoxicity induced and they showed corresponding values in term of decreasing cytotoxicity order: CdTe > CdTe/CdS > $CdTe/SiO_2$ > CdTe/ZnS. The correlation between decreasing cadmium ions release rate and decreasing cytotoxicity indicates the confirmation of the hypothesis that QD toxicity is mainly triggered by the release of toxic Cd ions (Xu et al., 2010). The cytotoxicity of CdTe/CdS and CdTe/CdS/ZnS was assessed in a concentration range between 0.002 – 600 µg/ml using A549 adenocarcinoma lung cancer cells. These were incubated for 2 or 24 hours using the CellTiter-Blue assay. The dose-response curves showed that QDs, which were coated by a thicker and additional ZnS shell, presented higher IC_{50} values (116.6 for small and 150.8µg/mL for larger NPs) compared to the ZnS shell-devoided NPs (83 for small and 99.9µg/ml for larger NPs). They assumed again that the reason may be related to the Cd ions release mechanism. This release occurs more likely in NPs without outer protective shell, rather than the shell-equipped ones (Ulusoy et al., 2014).

Surface/Coating/Shell Surface properties, determined by capping agents (coatings)

The previous examples showed how QDs may cause toxicity effects. A possible solution to reduce cytotoxicity effects could be the introduction of an additional/protective layer or coating of the core materials. This one would act like a physical barrier, limiting or avoiding the possibility of leaching the inner core materials (Midha et al., 2015).

The surface characteristics induce different toxicity effects. Hoskins et al. (2012) were examining two different types of core-shell NPs: nano-Fe_3O_4-PEI and Fe_3O_4-PEI-PEG. The first presented higher surface charges than the latter NP type. The non-PEG-coated QDs showed higher cytotoxicity and ROS formation in three different cell lines, (human SH-SY5Y, MCF-7 and U937) (Fu et al., 2014; Hoskins et al., 2012). Another example of cytotoxicity reduction after addition of PEG-silica-shell coatings was reported by Ulusoy et al. (2015). The authors assess the toxicity of differently coated CdTe/CdS/ZnS QDs, in a concentration range between 2 – 1000 µg/ml using A549 lung cells. They compared the different effects of QDs equipped with capping agents having either carboxyl group ligands (-COOH) or methoxy polyethylene glycol (mPEG). The -COOH QDs showed higher cytotoxicity effects than the mPEG one. The IC_{50} values measured were 152.1 and 282.9 µg/ml for the carboxyl group coating and for the mPEG coating respectively. (Ulusoy et al., 2015). In the tests conducted by Kirchner et al. (2005), CdSe and Cd/ZnS coated with PEG-silica, or with mercaptopropionic acid (MPA) were incubated with MDA-MB-435S breast cancer cells. The viability tests displayed that the uptake of the PEG-silica coated particles was lower compared to the MPA coated or polymer coated ones, which may also reduce the probability of direct Cd ions release (Kirchner et al., 2005). N-Acetyl-L-cysteine (NAC) organic ligands, or glutathione (GSH), or mercaptopropionic acid (MPA) ligands were used as coating layers for CdTe QDs in the study from Lai et al. (2013). They studied the toxicity effects of these different coated QDs using *Escherichia coli* bacteria as a model. The kinetics and thermodynamic information about microorganism's metabolism were evaluated. Their results reveal that when the QD concentration values increased, on the contrary the heat rate decreases. Moreover, the results showed inhibitory effect to the metabolic activity of the bacteria in the order from the highest to the lowest inhibitory intensity: MPA-CdTe > GSH-CdTe > NAC-CdTe QD. This confirmed again the dependency of the cytotoxicity on the surface chemistry of the nanoparticles (Lai et al., 2013).

Besides the use of surface coatings, the use of additional layers (e.g., ZnS shells) can also reduce the toxicity of ENMs. It may almost completely solve the problem of core-oxidation due to air exposure before solubilisation. Furthermore, it may partly reduce as well the core-oxidation due to UV-light exposure (Derfus et al., 2004; Midha et al., 2015). Derfus et al. (2004) carried out a comparison among ZnS shelled-QDs and QDs with no additional shells, while exposing them to air and UV light. The results obtained displayed that after air-exposure (for 12 hours), the release rate of Cd ions and the cytotoxicity effects were lower than in case of UV light exposure. This was probably due to the slower oxidation process leading to deteriorate the core materials. Nevertheless, also after UV-exposure for 8 hours, the oxidation process took place, reducing the viability of the cells (Derfus et al., 2004). Studies of Ulusoy et al. (2014) and of Xu et al. (2010) showed in addition that the ZnS shell addition induced less cytotoxicity after incubation with the chosen biological system. Ulusoy et al. (2014) assessed the viability of the cells with the CellTiter Blue assay, showing lower toxicity results for the ZnS shelled QD (IC_{50} value of 116.6µg/ml after 24 hours), compared to the non-shelled ones (IC_{50} value of 83µg/ml after 24 hours). They hypothesised that the ZnS shell may protect the nanoparticle from external agents (Ulusoy et al., 2014). Xu et al. (2010) found out as well how the CdTe QD equipped with ZnS shell presented the lowest cadmium release rate and the lowest reduction of viability (Xu et al., 2010). This confirmed the hypothesis of ZnS shell being a good first protection against the potential cytotoxicity of the QD.

Other attributes – Cell characteristics

Not only material-related physico-chemical properties determine ENM-specific toxicity effects, but also the environmental conditions (matrix-related properties). An example are the characteristics of the cells itself, such as their membrane or the ability of interaction with the ENMs.

Membranes are the barrier which separate the external environment from the inner cell. Intracellular membranes separate instead internal organelles of the cell from the cytoplasm. Both types of membranes are composed by phospholipids bilayers. They are permeable and they allow the selective transport of certain particles, like ions. If the size of the particle is lower than 100 nm ENMs may be uptaken and internalized by the cells through endocytosis (Elsaesser and Howard, 2012; Zhang et al., 2008). For example, Lai et al. (2013) studied membrane damage, in experiments at which CdTe QDs, coated with different capping agents (NAC, GSH and MPA), were incubated with *E. coli* bacteria. They tested the fluidity of the membrane of the bacteria, the viscosity of the lipid bilayer, by using membrane probes. They obtained reduction of fluidity properties when QDs were present in the samples. The permeability of the membrane has been afterwards analysed, showing as well an increased membrane damage when the QD concentration was increased (Lai et al., 2013).

Other aspects to be considered for cytotoxicity analysis are the characteristics of the cell line itself: some analysis showed cell uptake of the ENM, some others just adhesion on the surface. This arouse the assumption that besides material-related properties, the characteristics of the biological system are very likely to influence toxicity. For instance, Lai et al. (2013) showed by using transmission electron microscopy (TEM) that CdTe QDs were adhered on the surface of *Escherichia coli* bacteria. Furthermore, the results from Kirchner et al. (2005) showed by using differential interference contrast microscopy (DICM) that CdSe/ZnS QDs were also internalized into MDA-MB-435S breast cancer cells, and accumulated around the nucleus membrane. From the fluorescence microscope images of the study of Xu et al. (2010), the CdTe QDs were detected only in the cytoplasm of the unicellular algae *Phaeodactylum tricorntum*. Ulusoy et al. (2015) assessed the cytotoxicity of PEGylated QD using 3D tumour-like spheroid cultures of the lung cancer cell line A549. They presented higher viability results compared to the 2D related cells. This has been possibly explained because of the formation of the extracellular matrix (ECM) during spheroidal agglomeration of the cells themselves. This matrix potentially hampered and limited the QD transport towards the inner region (Kirchner et al., 2005; Lai et al., 2013; Ulusoy et al., 2015; Xu et al., 2010).

Proteins may be another influencing aspect in nanotoxicity, particularly the viability and vulnerability of the cells. They play an important role as enzymes in the cell apparatus, signalling molecules like hormones, or structural ones. ENMs have the same size and magnitude as the proteins. According to some researches nanoparticles may be able to interact with proteins or to alter their signalling processes, possibly causing neuro-degenerative diseases (Elsaesser and Howard, 2012). Moreover, the protein-ENM interaction plays an important role in the uptake process. Nanoparticles may interact with proteins contained in the serum of the cell culture, leading to the formation of a “protein corona”. The proteins are adsorbed around the ENM’s surface and consequently increase the ability to adhere onto the cell membrane. Therefore, ENMs may have higher chances to be uptaken by cells (Ulusoy et al., 2015).

ROS formation

The nanoparticles compared to their bulk counterpart present smaller size, higher surface to volume ratio and therefore higher surface reactivity. This may lead to oxidative stress generation after the creation of high amount of reactive oxygen species (ROS). The most relevant species are superoxide anion radicals, hydroxyl radicals, singlet oxygen and hydrogen peroxide (Fu et al., 2014). These are by-products of the cellular oxidative metabolism. In the mitochondria, the adenosine triphosphate (ATP) is generated and molecular oxygen is reduced to water via proton and electron transfer reaction. However, during the reaction process, not all of the oxygen is reduced, part of it is instead transformed into superoxide anion radicals, and then other oxygen-containing radicals, known as ROS (Fu et al., 2014). In small scale, the production of ROS is beneficial for the cellular signalling systems and induction of mitogenic responses. Thus, when there is an overproduction of these species, they can induce oxidative stress and cause therefore the failure in the redox activity maintenance by the cell system. The related effects may be (Fu et al., 2014):

- oxidation of the proteins hence the production of protein radicals because of malfunctioning of the cell
- lipid peroxidation

- DNA damages, to nucleic acids, or modulation of gene-expression
- potential modification of inflammatory signals transduction finally leading to genotoxic effects and possible cell death
- genotoxic effects which might cause age-related degenerative diseases (sclerosis, arthritis, cardiovascular diseases, inflammation, Alzheimer's Parkinson's diseases, diabetes and cancer)

One of the potential produced radicals is superoxide (O_2^-) which is a poor oxidant presenting low interactions with biological molecules. However, it becomes dangerous when it is transformed into another more reactive radical, such as hydroxyl species (OH^-). The only known protections against these radicals are antioxidants, reducing agents. While participating in redox reactions, they donate electrons or hydrogen atoms. In this way they avoid stress oxidation formation, and they ensure a normal function of the cell, without any premature destruction or malfunctions (Fu et al., 2014).

The generation of the ROS in high amounts it might be dependent on the cell type and at the same time it might be induced by ENMs. In particular, oxidative species may be created depending on the physico-chemical properties of the ENMs (e.g., size, shape, oxidation state, surface chemistry (coating), solubility or aggregation state) (Fu et al., 2014).

3.5.2 Exposure and toxicokinetics

It is assumed that nanoparticles might undertake the ADME process to enter and to distribute inside the human body or cells. This process is composed of four stages, which are part of the toxicokinetics:

1. Absorption
2. Distribution
3. Metabolism
4. Excretion

The main concern about the interactions between ENMs and the human body is the possibility to cross biological barriers. These barriers serve as shield against indeed external potential harmful substances. Therefore, if ENMs are able to pass them they may reach the blood stream and spread in the entire body – e.g., via the air-blood (in the lungs), brain-blood (the brain), or via the materno-foetal barrier. In addition, bioaccumulation of ENMs can also lead to negative effects (Elsaesser and Howard, 2012). However, the studies from Elsaesser and Howard (2012) have been carried out just as *in vitro* experiments. Nevertheless, *in vivo* studies would help to obtain deeper and more detailed results (Elsaesser and Howard, 2012).

The three main routes how ENMs may enter the body: through the skin, through the ingestion pathway (intestine) and through the airways paths (lungs).

The respiratory ways act as a potential entry pathway for the ENMs. The main problem is to understand and detect, which type of ENMs can penetrate and pass the air-blood-barrier. Once they overstep this, ENMs may have access to all the rest of the body, being able to reach other important organs, like the liver, spleen and even the heart. It has been hypothesized that the mechanism of penetrating through the respiratory ways is via endocytosis of the alveolar epithelial cells. The olfactory bulb system pathway presents a higher risk because of the ability of ENMs to reach the central nervous system in an easier way (Elsaesser and Howard, 2012).

The skin is composed of two main parts: the epidermis and the dermis. The first one is the outer layer that protects the inner body from the physical chemical agents and from the external environment in general. The dermis is a deeper layer which provides structural support of the skin. It has been shown that some particular substances, like drugs, can penetrate the skin barrier after dermal exposure. Some of these substances are: liposomes, poorly soluble materials (e.g., nano-TiO_2), and submicron emulsion particles containing lipophile ENMs (Piperigkou et al., 2016). The skin absorption of ENMs is dependent on size and surface chemistry. For instance, nano-TiO_2 is more likely to penetrate inside the epidermis apparat, probably mainly through hair follicles, wounds or lesions. Moreover, all the liposomes are able to easily enter through the skin: those with smaller size than 270 nm are more likely to be found in the dermis (Elsaesser and Howard, 2012; Piperigkou et al., 2016). However, the knowledge concerning ENM absorption and the related potential transfer from the skin to the inner systems is scarce and limited, and therefore further research is needed.

The third possible route for ENMs to enter the body is the gastro-intestinal (GI) path. This is related to the more frequent presence of ENMs, which are used for food packaging and food additives. It has been studied that ENM absorption via the GI path is mainly driven by particle's size, surface area, charge, presence or absence of ligands and also GI physiological characteristics. It has been assumed that the ENMs do not remain as free and colloidally stable particles in the GI tract, because they tend to aggregate or react with some component in the tract (Piperigkou et al., 2016). It has been hypothesized that ENMs may be able to translocate through the intestinal epithelium walls via transcytosis through initial endocytosis mechanisms, enable by the microfold cells (allowing the transport of microbes or particles across the epithelial cell layer) or through passive diffusion (Piperigkou et al., 2016).

The distribution phase is the phase in which the ENMs are supposed to spread inside the body and then into the different organs. Depending on the ENM type, these could target just specific or equally all the organs. The surface characteristics of the particle induce interactions with proteins. This causes effects on the tertiary structure of the proteins or effects concerning their dysfunction. These particles proteins interactions may lead to the possibility of membrane expansion and cellular penetration and apoptosis. The size characteristic of the ENMS may influence their distribution. It has been observed that bigger ENMs remain in the GI tract, whilst smaller ones translocate into other organs. They have been mainly found in the kidneys, liver, spleen, brain and lungs (Piperigkou et al., 2016).

The metabolism phase consists of the biotransformation of ENMs inside the body. This highly depends on the chemical composition of the particle and in particular on its surface composition. For example, the charge and the hydrodynamic diameter may influence the interactions with the proteins and therefore the possibility of passing through the biological barrier (Piperigkou et al., 2016).

The excretion part is when the particles could be finally expelled from the body. The related data are limited, however it is highly possible to assume that insoluble EMNs may remain and accumulate in tissues. Moreover, up to date there is no data regarding the presence of ENMs in the maternal milk (Piperigkou et al., 2016).

3.5.3 Bioassays to assess nanotoxicity

It has been previously explained how ENMs specifically induce toxicity. The induced effects have been measured by using bioassays and different cell models. In general, these methods aim to estimate the potency of a specific substance by measuring the biological response in a standard test (Panuganti, 2015). Bioassays can be conducted both *in vitro* and *in vivo*. Bioassays *in vivo* are based on the testing of reaction of specific substances in whole living organisms. Nevertheless, these are no more valid options because of the new European regulations on animal experimentation (Wernersson et al., 2015). The first methods are based on the measurement of the effects of the specific substance at subcellular level, after interaction with cells. Beside of ethical aspects, the advantages of *in vitro* methods rely on:

- the possibility to perform the experiment with short exposure time
- to obtain more specific and sensitive information, being evaluated at low organizational level
- lower costs.

For *in vitro* bioassay methods, usually considered to assess the nanotoxicity effects, are the so-called:

- MTS reduction assay
- ATP content assay
- TNF-α and IL1-α ELISA detection
- Caspase 3/7
- AlamarBlue® assay

The MTS reduction assay ((3-(4,5-dimethylthiazol-2-yl)-5-(3-carboxymethoxyphenyl)-2-(4-sulfophenyl)-2H-tetrazolium)), is based on the measurement of the reduction by viable cells of the salt tetrazolium into a coloured formazan product through the production of NAD(P)H by dehydrogenase. In this way, it is possible to mirror the cellular redox metabolism: reduced products correspond to readout products such as luminometry and colorimetry. Therefore, the higher the amount of the reduction products, the higher the viability of the cells analysed (Piret et al., 2017).

In the framework of the ATP content assay, the ATP amount in the cells, through the luciferase or ATP-consuming reactions, is measured. Whenever the content of the ATP present in the cell suspension to be tested is high enough, good viability conditions could be assumed. If the level of ATP decreases, less metabolic active cells are present in the sample (Piret et al., 2017).

TNF-α stands for tumour necrosis factor and IL1-α for interleukin. In this case the pro-inflammatory effect signals indicate when the viability of cell line starts to decrease (Piret et al., 2017).

Caspase is a group of protease enzymes, which induce cell death. In the course of the caspase 3/7 assay, the two enzymes which cause cell apoptosis, splitt a specific sequence of the DNA present in their substrates (Piret et al., 2017).

The last method listed, AlamarBlue® assay, consists of the measurement of the proliferation of a certain cell line. The sample is stained with AlamarBlue®, which is a non-toxic, water soluble blue dye, whose main component (resazurin, blue indicator) is reduced during metabolic activity of the cells (resorufin, red fluorescent indicator). Therefore, when the reduced component of AlamarBlue® is detected (high fluorescence signal), a good proliferation of the cells is occurring, which means high viability. On the contrary, low fluorescence signal reflects low metabolic activity and therefore low viability values of the cells.

3.5.4 Flow cytometry

Flow cytometry is a largely used method which allows the counting of cells and the analysis of their physical, external, internal properties (abcam, 2018; Bioscience, 2000). The principle consists of the use of a beam of light to detect the scatter signal (Forward Scatter Signal or Side Scatter Signal) and fluorescence signal, obtaining information concerning the physical properties of the cells (e.g. cell types, cell viability). A Flow Cytometer is composed of three main parts:

- Fluidics
- Optics
- Electronics

The first component is aimed to transport the sample inside the device and make the analysis possible through the meeting between the single line fluid and the laser beam.

The fluidic system works via hydrodynamic focusing: it is composed of an inner core, the fluid sample, and an outer sheat fluid. They are injected with different pressure values, low for the inner fluid and high for the outer one. In this way the inner fluid is forced to narrow down and to create a single line of cell, ready to be enlightened (AbDSerotec, 2017).

The most common source of light is laser, it produces a single wavelength of light (available in different values) at one or more discrete frequencies (AbDSerotec, 2017; Serotec). The source of light is positioned in a way that each ordered single cell can meet the laser beam and give back SSC, FSC or fluorescent signal. The optical components are aimed to detect those signals with a system of mirrors and sensors, and aimed to send those detected signals to the electronic parts to be stored as data. The Forward Scatter signal is light which is scattered after the meeting laser-cell in the forward direction within angle of 20°. It is collected then in a photomultiplier tube

(PMT), and its signal is related to the size of the particle: the higher the detected light the bigger the cell. On the other hand, the Side Scatter signal consists of the scattered light from the sides within an angle of 20 – 90°. This light is refracted by mirrors and filters systems and collected in a PMT. This signal's interpretation displays the inner structure of the cell and its granularity (abcam, 2018; AbDSerotec, 2017). The combination of these two signals allow the delineation of the types of cells. For example, both high values of FSC and SSC are characteristic of neutrophils or as well granulocytes. Or high FSC values but low SSC indicate monocytes, or medium values of FSC and very low values of SSC show presence of lymphocytes, or debris (abcam, 2018; Bioscience, 2000). The sample is usually stained with a fluorescent dye, enhancing specific characteristics of the cells. These dyes can be fluorophore-labelled surface receptors or intracellular molecules (DNA, cytokines) (AbDSerotec, 2017). The optics system is composed as well by separate channels and detectors. They are usually made of silicon photodiodes or more commonly of photomultiplier tubes. A system of filters selects the light which arrives from the scattering, before the detecting phase. Those filters are enabled to block or let pass through specific wavelength values. The four main filters are:

- Long Pass Filter
  It allows the transmission of wavelength values >520nm.
- Short Pass Filter
  Light transmission of <575nm.
- Band Pass Filter
  Wavelength values transmitted in a range of 620-640nm.
- Dichroic Short Pass Mirror
  It reflects light with wavelength >540nm and transmits light signals with wavelength <540nm (AbDSerotec, 2017).

Each different fluorescent dye is detected in a different channel. For example, the FITC fluorophore (Fluorescein Isothiocyanate) emits signals at wavelength within the range of 400 – 550 nm with its peak at 490 nm (blue), and it can be excited within the range of 475 – 700 nm, peaking at 525 nm (green). If the excited wavelength signal from the event is near enough to the peak value, the number of photons absorbed by the channel is high, which means more intense fluorescence signal emission. This is the reason why this stain is usually detected through the fluorescence channel with the 488 nm laser. The channel which guarantees the excitation and the emission of the fluorophores at their maximum values is generally labelled as channel -A.

The pulse intensity of an event (electric current from the PMT) is measured and converted by the Analog to Digital Converter (ADC) and calculated as sum of the signal intensity detected in time. The pulse intensity rises as the particle enters in the laser beam section area, reaching the highest value when it is centred and decreasing after it moves away from the laser section area (abcam, 2018; AbDSerotec, 2017). Finally, these stored and converted data can be visualized in a density graph: the side scatter signal on the y-axis and the forward scatter signal on the x-axis, in which each dot corresponds to the analysis of each different particle. Or data can be visualized in a histogram graph: the number of events on the y-axis and the intensity of the fluorescence of the defined channel on the x-axis. In order to obtain the desired result, specific settings need to be adjusted during the data acquisition. Those comprehend:

- the voltage of the channels and the correspondent possibility of choosing logarithmic scale, in order to amplify weak signals and narrow strong ones.
- The threshold level, the selection of a triggering value designates the minimum value at which a pulse is detected.
- The laser type, to obtain the maximum emission signal a specific laser wavelength needs to be selected, according to the used fluorophore.
- The fluorescence compensation. When using tandem dyes (two stains in one sample) overlapping emission signals can occur. In order to avoid this, flow cytometer device automatically apply mathematic compensation (abcam, 2018; AbDSerotec, 2017).

3.6 CELL LINES AND CELL CULTURE

Cell lines and cell cultures are widely used for research studies, due to their advantage of reproducibility and consistency of the experiments. The difference between normal cells and cultured ones is the number of divisions which occurs. The first one can divide a limited amount of times, on the contrary the second ones can reproduce for a longer period of time with a higher number of divisions. This procedure is known as immortalization and is accomplished thanks to natural or artificial transformations, through chemicals or viruses treatments (Verhoeckx et al., 2015).

There are two main methods for culture growth: adhesion and suspension. In the adhesion method the cells attach themselves to the surface of the vessel in which they are carried. This is composed of either plastic either surface coated with 1% solution of gelatine, collagen or fibronectin. Cells in suspension grow floating in a suspension environment (Verhoeckx et al., 2015). In both growing methods, the cells have to be in contact with just isotonic solutions or culture media. Isotonic solutions could consist of saline (0.9% NaCl), or phosphate buffer saline (PBS), which are developed in different types depending on the different cell culture typology. Culture media might consist of balanced salt solutions with the variable addition of amino acids or, vitamins, trace minerals, pH indicators and antibiotics, which play a crucial part in the cell growth (Verhoeckx et al., 2015). When a carbon dioxide (CO_2) and bicarbonate (HCO_3) media is used, it is mandatory to provide exogenous CO_2 in 5-7% in air. This is related to the fact that CO_2 influences the pH of the culture, which should be kept around 7.2-7.4, for most of the mammalian cells types (Verhoeckx et al., 2015). A required additional component to culture media is the serum, this provides fatty acids, transport proteins, and hormones. Despite the small differences among the batches and types, the most general types are FBS, foetal bovine serum, and FCS, foetal calf serum. They generally derive from slaughter houses and they consist of the part of cattle’s blood after blood-cells, platelets and fibrinogen removal. These serums are composed of electrolytes, antibodies, hormones, exogenous substances and protein (exception of the blood clotting ones) (Chanput et al., 2015; Verhoeckx et al., 2015).

3.6.1 CHO cell line

Chinese Hamster Ovary (CHO) is a cell line which is indeed derived by ovaries of Chinese Hamster, characterized by wide genetic and phenotypic diversity (Wurm, 2013). In the 1957 at Eleanor Roosevelt Institute of Cancer Research, Dr. T. Puck was able to obtain a cell line from 0.1 g of ovary tissue of Chinese hamster, provided by Boston Children’s Cancer Research Foundation (Wurm, 2013). They have always been used as laboratory mammals because of their small dimensions, their validity for tissue culture and radiation studies (low chromosome number). It has been used in many biology, medical and pharmaceutical researches since then (THEMESHAKER, 2017). In the very beginning CHO cell line applications were for molecular and classic cell genetics until 1970s, for being practical to culture, for having large chromosome and the simplicity to identify mutations (Wurm, 2013). Nowadays, they are mainly used as source for therapeutic protein pharmaceuticals. From the first cell line created, others were afterwards generated during time. For instance, CHO-K1 cell line is a derivative presenting less DNA than the original one. From this modified cell line, another one has been created, CHO-DXB11, with a lack of dihydrofolate reductase activity (DHFR activity), and later on CHO-DG44 (THEMESHAKER, 2017; Wurm, 2013). Due to this remodelling of the genomic structure, the CHO cell line has been defined as a “quasispecies” line (Wurm, 2013). This term identifies families of related (genomic) sequences, which are exposed to mutation conditions, and whose offspring are expected to present at least one mutation (Wurm, 2013). This cell line is relevant in the scientific research because of:

- fast and easy growth
- good stability, robustness and flexibility
- generation of recombinant proteins, with very similar functionality and structure compared to the original proteins
- no transmission of infectious agents in products manufacturing
- high volumetric production
- not presenting epidermal growth factor receptor (EGFR), good source for the EGFR mutation studies (THEMESHAKER, 2017; Wurm, 2013).

3.6.2 U937 macrophages

Macrophages are cells presenting antigen characteristics. They are developed by monocytes, which are circulatory precursor cells, from myeloid origin. Macrophages exhibit three main functions in the immune system: phagocytosis, antigen presentation and cytokine production (Chanput et al., 2015).

Specifically, U937 are (pro-)monocytic cell lines which can be developed into various types of macrophages. U937 has tissue origins (at their mature stage). Indeed, they have been derived from the isolation of histiocytic lymphoma of a 37 years-old man, pro-monocytic, human myeloid leukaemia cell line. This presents indeed advantages of:

- Monocytes
- Easy use
- Preparation of a uniform number of cell
- Culturing with a high number of passages (up to 25) without any damage
- Long period storage without any effects on their features or on their viability (Chanput et al., 2015).

4 MATERIALS AND METHODS

4.1 QUANTUM DOT CHARACTERIZATION

4.1.1 Cd-based quantum dots used

In the present study, the analysed QD is composed of an inorganic hydrophobic core-or core-shell structure, coated with organic ligands having carboxyl groups (-COOH). The coating used in this study was *N*-Acetyl-*L*-Cysteine (NAC), which enables to equip the QDs with hydrophilic properties. The inorganic core is composed of CdTe, the QD's shell of ZnS.

In this study four different types of NAC-capped QDs have been assessed regarding their potential toxicity. The used QDs are described and characterized in more detail in Part et al. (*submitted*). The typologies are listed in the following and schematically described in Figure 4.1.1:

- NAC-CdTe
- NAC-CdTe/ZnS
- NAC-CdTe/30%Fe:ZnS
- NAC-30%Fe:CdTe/ZnS

In the present study, the above listed QD were named respectively as:

- Bare QD
- Shelled QD
- Shell-doped QD
- Core-doped QD

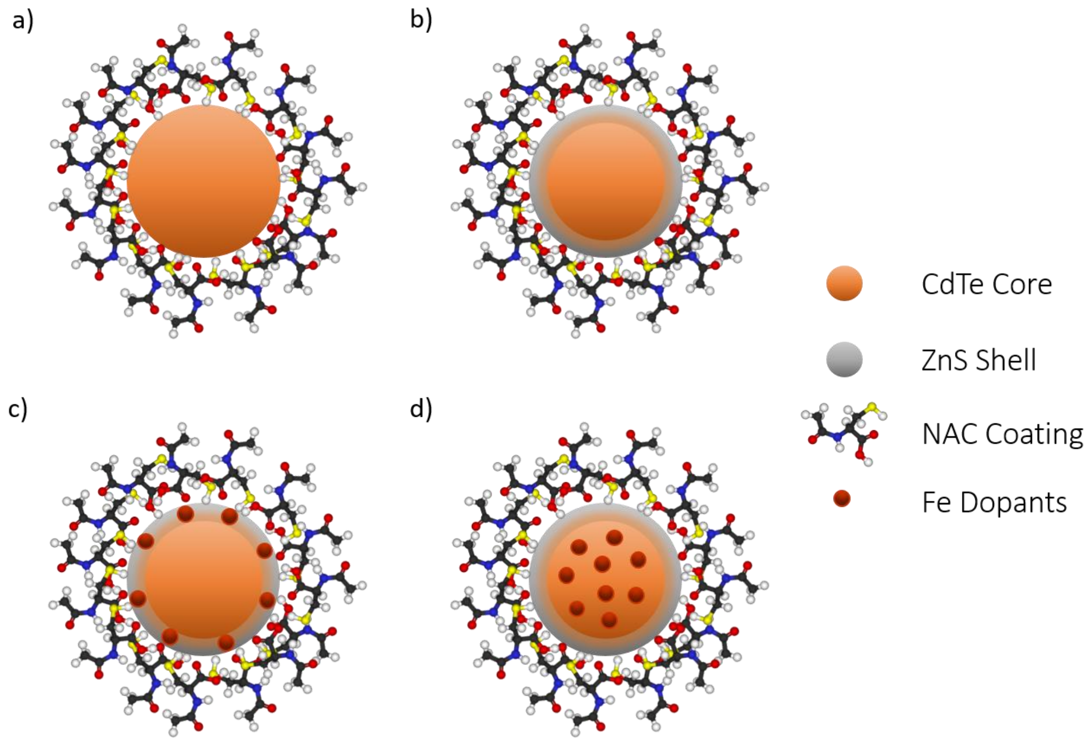

Figure 4.1.1. Schematic representation of QD types: bare-QD (CdTe core and NAC coating) (a), shelled QD (with additional ZnS shell) (b), shell-doped QD (Fe dopants added in the shell layer) (c), and core-doped QD (Fe dopants added in the core part) (c).

Note that the last two types of QDs show para- and superparamagnetic properties, respectively (Part et al., 2018), and can be used for multimodal imaging (e.g. for both fluorescence and magnetic resonance analyses).

Quantum dots preparation

All the QDs had previously been synthetized and characterized, as described in Part et al. (*submitted*). The QDs were provided in powder form from the Nanobiotechnology Department (BOKU) and could directly be used for cytotoxicity assessment. However, a brief description of the preparation methods can be found in the following.

Growth of CdTe cores

Tellurium powder (0.63 mmol) was mixed with sodium borohydride $NaBH_4$ (1.32 mmol) in 10 mL ultrapure water under N_2 atmosphere in order to obtain a NaHTe precursor solution. Under constant stirring the pH was adjusted to 8.3 via adding 1.0 mol NaOH. Meanwhile, $CdCl_2$ (0.5 mmol) and N-Acetyl-L-Cysteine (NAC) (1.25 mmol) were dissolved in 200 mL N_2 purged ultrapure water. These two solutions were then merged keeping the molar ratio for Cd : Te : NAC at 2 : 1 : 5. The growth of CdTe crystals was then initiated (oil bath at 140°C, for 45 minutes, rapidly cooled down in ice bath). Finally, a purification step was made with 2-propanol, lyophilization and ultrapure water (Part et al., *submitted*).

Deposition of ZnS shells

In a second step, ZnS was deposited onto the CdTe cores in order to obtain the shelled QDs. 20 mg of NAC-CdTe crystals had to be re-dispersed in 20 mL of ultrapure water and 0.5 mmol of zinc (II) chloride ($ZnCl_2$), 0.1 mmol of sodium sulphide • 9 H_2O (Na_2S• 9 H_2O) and 2.5 mmol of NAC were added. The mixture was heated for 45 minutes at 65°C in order to obtain NAC-CdTe/ZnS QDs. After purification steps, as mentioned above, Zn deposited on the QD's cores and NAC-CdTe/ZnS were formed (Part et al., *submitted*).

Iron doping of the core

In order to obtain NAC-30%Fe:CdTe/ZnS, 20 mg of NAC-CdTe crystals had to be re-dispersed in 20 mL of ultrapure water and 0.5 mmol $ZnCl_2$, 0.1 mmol of Na_2S and 2.5 mmol of NAC were added too. To the latter solution, iron (II) chloride•4H_2O ($FeCl_2$•4H_2O) (0.03 mmol) had to be added as well. This led to the formation of NAC-30%Fe:CdTe. In a further step, ZnS shells were deposited onto the QD's cores, as described above. In this study, NAC-30%Fe:CdTe/ZnS QDs are referred to core-doped QDs (Part et al., *submitted*).

Iron doping of the shell

In order to synthesize NAC-CdTe/30%Fe:ZnS, which are referred to as shell-doped QDs in this study, 20 mg of NAC-CdTe crystals had to be re-dispersed in 20 mL of ultrapure water and 0.5 mmol $ZnCl_2$, 0.03 mmol of Na_2S•9H_2O and 2.5 mmol of NAC were added too. The ratio for Cd : Fe needed to be fixed at 1 : 0.3, therefore 0.03 mmol of $FeCl_2$•4H_2O were added. After the heating bath and the purification step, as above described NAC-CdTe/30%Fe:ZnS QDs were obtained, as described in Part et al. (*submitted*).

Optical properties

In general, the photoluminescence quantum yield (PL QY) of QDs highly depends on reaction conditions, characteristic emission wavelengths maxima (Part et al., 2016b). In addition to the reaction condition, it is important to note that the pH in the dispersion media influences the PL QY of a QD.

In order to assess the cytotoxicity of the QDs two cell lines have been used (Chinese Hamster Ovary, CHO, and macrophages U937). In order then to assess the viability of these cells two methods have been utilized: flow cytometry and AlamarBlue® assay. Finally, in order to attempt to localize the QDs in the cells or in the cell surroundings, the confocal laser scanner microscope has been employed.

4.2 OPTICAL CHARACTERIZATION

In order to obtain information concerning the absorbance, fluorescence emission wavelength values and the dimensions of the quantum dots used in the present study three methods have been employed: UV/VIS spectrophotometry, fluorescence spectrophotometry, Dynamic Light Scatter.

4.2.1 Determination of absorbance/emission spectra

Materials used

The materials used for the absorbance spectrum evaluation are listed in the following:

- UV-VIS spectrophotometer (Hitachi UV 2900, Japan).
- Dispersion of bare-QD, core- and shell-doped QDs and shelled QDs, in concentrations of 10 mg/mL, diluted at 1:100, obtaining 0.1 mg/mL concentration.
- Ultrapure water (18.2 MΩ·cm at 25°C, MilliQ®, USA).
- Glass cuvette, 10 mm.

The materials used for the emission spectrum evaluation are listed in the following:

- Fluorescence spectrometer (LS 55, 230 V, PerkinElmer, UK)
- Dispersion of bare-QD, core- and shell-doped QDs and shelled QDs, in concentrations of 10 mg/mL, diluted at 1:100, obtaining 0.1 mg/mL concentration.

- Ultrapure water (18.2 MΩ·cm at 25°C, MilliQ®, USA).
- Glass cuvette, 10 mm.

Methods

In order to determine the absorbance and emission spectra of the studied QDs two methods have been utilized: UV/VIS Spectrophotometry and fluorescence spectrophotometry, respectively.

For the absorbance spectrum evaluation, the samples were prepared diluting at 1:100 the QD dispersions at concentration of 10 mg/mL. After sonicating of the new diluted samples for 30 seconds, these were pipetted into the glass cuvette and ready to be measured. The optical density value was settled to <0.1, in this way the self-quenching and homo-aggregation effects could have been avoided. The scan speed for recording was set at 400 nm/min and the wavelength range was fixed between 300 and 700 nm. In order to prevent background signal disturbance, absorbance values analysis with ultra-pure MilliQ water were initially performed as well. The value obtained are shown in the Results and Discussion chapter, QD characterization section.

The same diluted dispersions, which were prepared for the UV/VIS analysis, were used in order to determine the fluorescence emission spectrum with the fluorescence spectrophotometer. The dilutions were sonicated for 30 seconds and afterwards pipetted into the glass cuvette, ready to be analysed. The scan speed to record was set at 400 nm/min in this case as well. The excitation value was fixed at 470 nm and the excitation and emission slit-width at 4 nm. The spectrum at which the emission was recorded was within 400 – 700 nm. The results are displayed in the Results and Discussion chapter, QD characterization section.

4.2.2 Determination of hydrodynamic diameter

Materials used

The materials used for the absorbance spectrum evaluation are listed in the following:

- Dynamic Light Scattering (DLS, Zetasizer Nano Z, beam wavelength = 633 nm, 173° backscatter, Malvern Instruments Ltd., UK).
- Dispersion of bare-QD, core- and shell-doped QDs and shelled QDs, in concentrations of 100 µg/mL.
- Ultrapure water (18.2 MΩ·cm at 25°C, MilliQ®, USA).
- Cell media composed of: RMPI-1640 cell medium (Sigma-Aldrich®, USA) 89.2%, antibiotic antimycotic solution (Sigma-Aldrich®, USA) 9.9%, Foetal Calf Serum (FCS) 0.9%.
- Polyvinylidenefluoride membrane (PVDF 0.20 µm, Graphics Control Ltd., UK).
- Glass cuvette, 10 mm.

Methods

The dynamic light scattering method (DLS) was used to analyse the hydrodynamic diameter of the particles and to show their aggregation behaviour over time.

The samples of bare, shelled, shell-doped and core-doped were analysed in concentration of 100 µg/mL, after 30 seconds of sonication and filtered with a polyvinylidenefluoride membrane. The tests have been conducted at 37°C, fixing the refractive index at 1.338 and 1.330 for QDs dilutions and water respectively. The tests to determine the HDD were held on day 0, 1, 2, 3, 6 and 18 in order to observe the variation of aggregation of the particles over time.

4.3 ASSESSMENT OF CELL VIABILITY

4.3.1 CHO cell line used in the study

The cell line Chinese Hamster Ovary (CHO), was used in this study for flow cytometer analysis. In particular, the host cell line for the used cell line was CHO-K1/SF, a serum free adapted suspension variant of the CHO-K1 (ATCC CLL-61) cell line (Wurm, 2013). This CHO-K1/SF host cell line was indeed used as basis in order to generate the cell bank of CHO-K1/Pool/D1 WCB-160607, via integrating the gene of interest within the Rosa26 locus using the BAC (Bacterial artificial chromosome) system by the Antibody Lab GmbH, Vienna Austria. BAC vectors could be used for cloning parts of DNA, and those which carry entire eukaryotic locus (e.g. Rosa26), beneficial for gene expression, reduce screening efforts and lead to higher production stability (Zboray et al., 2015). The monoclonal recombinant cell line produces a biosimilar of the fully human recombinant monoclonal anti-tumour-necrosis-factor alpha (TNFα) antibody, also known as adalimumab or the trademark Humira.

The CHO-K1/SF WCB was cultured in Dynamis AGT (Gibco) medium, with the addition of 8 mM of L-Gln and 15 mg/L of Phenol red solution, stored at a temperature of 37°C, and at 7% of CO_2.

4.3.2 U937 cell line used in the study

In this study, the cell line used for AlamarBlue® assay analysis was U937 macrophages, human lymphocyte suspension cell line. It was obtained from the American Type Cell Collection (Rockville, MD, ATCC CRL-3253). The cell line has been cultured in RPMI-1640, containing 0.1% of L-glutamine, 10% foetal bovine serum (FBS) and 1% of antibiotic solution and Dulbecco’s phosphate buffered saline (PBS, 10x) purchased from Sigma-Aldrich (Germany), and kept in HERAcell i240 incubator.

4.3.3 Flow cytometry

Material used

The materials used for this test are listed in the following:

- Flow Cytometer (FACSDiva™, BD Bioscience)
- NAC-CdTe QDs, which were dispersed in Dulbecco’s PBS buffer to obtain stock solutions in concentration of 100µg/mL.

- CHO cell line. The initial cell density in the cell suspension was of 7.112 × 10^6 cells/mL, viability 71%. The target concentration prior to the analyses was adjusted to be at 1×10^6 cells/mL.
- Hoechst nucleus stain 33342 (Thermofisher). 1µL from the pre-made stock solution (10 mg/mL in ultrapure water) of Hoechst needed to be mixed in 2 mL of PBS buffer, from this 100 µL to pellet. $\lambda_{ex}/\lambda_{em}$ 361/486 nm.
- Anti-TGN 46: 7-AAD (7-amino-actinomycin D) stain in buffered aqueous solution (~ 1 mg/mL) (Thermofisher). 5 µL of stain are added to 1×10^6 cells with 100 µL FACS buffer. This was left at RT for 10 min. No cell-washing was needed after the staining. $\lambda_{ex}/\lambda_{em}$ 446/650nm.
- PI stain (rnd systems). 5 µL of stain every 1×10^6 cells needed to be mixed in 100 µL FACS buffer (rnd system). $\lambda_{ex}/\lambda_{em}$ 488/617nm.
- Ultrapure water (18.2 MΩ·cm at 25°C, MilliQ®, USA).
- Cell media composed of: RMPI-1640 cell medium (Sigma-Aldrich®, USA) 89.2%, antibiotic antimycotic solution (Sigma-Aldrich®, USA) 9.9%, foetal calf serum (FCS) 0.9%.
- FACS™ buffer (rnd systems).

All samples were prepared in quintuplicates, in CELLSTAR® 12-well transparent flat bottom plate, V_{well}=1000 µL. The well plate was then incubated in the incubator HERAcell24Oi CO_2 (Thermoscientific), at 37°C, (5% CO_2, 95% humidity) for 24 hours.

Sample preparation

As first step, the stock solution containing the NAC-CdTe QDs were prepared. The QDs were provided in powder form, 10 mg of QD powder were redispersed in 1 mL of PBS buffer in order to obtain a stock solution in the concentration of 10 mg/mL. It is important to note that suspended CHO cells were provided by the Vienna Institute of Biotechnology department. Two sets of tests were carried out for this analysis, they are described in the following.

Cell viability analysis with 7-AAD and Hoechst stains – Test 1

In this case, the sample to analyse consisted of treated, untreated, untreated stained and background samples. The first one was composed of bare-QD dispersion (100 µg/mL), CHO suspension (1 × 10^6 cells/mL) and cell media, total volume of 1 mL. The second was prepared with

CHO suspension (1 × 10^6 cells/mL) and cell media only. The untreated stained sample was composed of bare-QD dispersion (100 µg/mL), CHO suspension (1 × 10^6 cells/mL), cell media and the addition of two stains: 7AAD (5 µL from 1 mg/mL solution added to the cell suspension) and Hoechst (1 µL from the 10 mg/mL stock solution in 2 mL PBS solvent, 100 µL of this added to the cell suspension). Finally, the background was made with bare-QD dispersion (100 µg/mL) and cell media. All these were then arranged in a transparent flat bottom 12-wellplate. The quantities, concentration and dilutions steps to prepare the named samples are shown in the Figures 10.1.1, 2 and 3, shown in the Annex. The prepared wellplate was stored in an incubator for 24 hours. After this incubation time length, the samples were centrifuged, the supernatant was discarded and separated from the pellet. The latter needed to undergo to a further process of staining. To note that the background sample was not stained, to attempt detecting the QD-signal only. The steps for dilution and staining are described in the Figure 10.1.4 shown in the Annex. All prepared and stained samples needed to be stored in ice until the measurements were carried out, in order to avoid alterations of the cells' viability. After sample preparation and staining, the samples were ready for flow cytometry analyses. Finally, 400 µL were pipetted into FACS tubes, and positioned in the specific tube-holder.

Cell viability analysis with PI stain – Test 2

An additional attempt using a different stain (PI) was carried out. The samples in this test were untreated unstained, untreated stained, treated and treated stained. The first consisted of native CHO cells suspension (1 × 10^6 cells/mL) and cell media. The second sample was the same as the latter with the addition of PI stain (5 µL every 1 × 10^6 cells in 100 µL), after incubation time length. The treated sample consisted of the incubation of CHO cell suspension (1 × 10^6 cells/mL), with cell media and with bare-QDs (100 µg/mL). Finally, the treated stained sample was prepared as the treated sample, but after the incubation time length it underwent to PI staining process. The samples were incubated for 3, 6, 15, 20 and 24 hours, A further analysis without incubation was carried out as well (simply named as 0 hour incubation). To note that in the results and discussion section the data obtained after 0 and 24h incubation time length are shown. After each different incubation time length, the samples were centrifuged, the supernatant was discarded and separated from the pellet. The latter needed to undergo to a further process: staining. The steps for dilution and staining are described in the Figure 10.1.4 shown in the Annex. All prepared and stained samples needed to be stored in ice until the measurements were carried out, in order to avoid alterations of the cells' viability. After sample preparation and staining, the samples were ready for flow cytometry analyses. Finally, 400 µL were pipetted into FACS tubes, and positioned in the specific tube-holder. The results on flow cytometry are shown and discussed in the Results and Discussion chapter and in the flow cytometry section.

Methods

In the present study flow cytometry was used to assess the viability of CHO cell line. These were treated with QD and stained with 7-AAD, PI and Hoechst stains. The first, 7-AAD, is a red stain, emitting within the range of 560 – 800 nm, peaking at 650 nm, presenting absorbance spectrum within 300 – 660 nm, with maximum at 546 nm. In order to detect its fluorescence signal the channel with laser of 488 nm was selected. The stain was used for non-viable cell exclusion, in order to detect dead/damaged cells. PI is a red fluorescent nuclear and chromosomic counterstain, it binds to double stranded DNA, intercalating between base pairs. However, it does not permeate through living cells, their membranes have the ability to exclude the dye. This one indeed penetrates to damaged or permeable membranes of non-viable cells, therefore it is used to assess cell viability in a population. Its absorbance and emission spectra are 300 – 650 nm and 549 – 800 nm, respectively. The excitation/emission wavelength peak values are 488/617nm, therefore the laser 488 nm has been selected to obtain maximum fluorescence intensity, and according to the PI protocol the PE-A channel was chosen. The nucleus stain with Hoechst 33342 is a blue fluorescent stain, emitting at 486 nm (within the range of 365 – 640 nm), after excitation at 361 nm (within the range of 300 – 430 nm). It is a cell-permeable DNA of living cells and it binds to adenine-thymine (A-T) parts of the DNA, this is why this stain is utilized to enlighten the nuclei of the cells. Each different fluorescent dye was detected in a different fluorescent channel. For example, the FITC channel (Fluorescein Isothiocyanate) detects signal at a wavelength of around 519nm. Or the PE channel (Phycoerythrin) detects light at 575nm wavelength (abcam). In the present study, the channels used were FITC-A and PE-A (both laser at 488 nm), for 7AAD or Hoechst and PI stains, respectively. The settings for the measurements acquiring data were always settled with a medium flow rate and acquisition of 10000 events.

4.3.4 AlamarBlue® assay

Materials

In the following, the materials used for the tests are listed:

- Wellplate reader (Inifinite200PRO® Tecan).
- Dispersions of bare-QD, core- and shell-doped QDs and shelled QDs, initial concentration of 1 mg/mL. Further dilutions were prepared with cell media. The dilution steps are shown in the following scheme, Table 4.3.1.

Table 4.3.1. Schematic representation of dilutions and concentrations of QD dispersion for the conducted test with AlamarBlue® assay.

Test 1	**Initial Concentration**	µg/mL	1000					
	Dilution steps		1:1000	3:4000	1:2000	1:4000	1:10000	1:100000
	Concentration values	**µg/mL**	**1**	**0.75**	**0.5**	**0.25**	**0.1**	**0.01**

Test 2	**Initial Concentration**	µg/mL	1000					
	Dilution steps		1:20	1:40	1:80	1:200	1:2000	1:4000
	Concentration values	**µg/mL**	**50**	**25**	**12.5**	**5**	**0.5**	**0.25**

Test 3.b	**Initial Concentration**	µg/mL	1000					
	Dilution steps		1:10	3:40	1:20	1:40	1:100	1:1000
	Concentration values	**µg/mL**	**100**	**75**	**50**	**25**	**10**	**1**

- Ultrapure water (18.2 MΩ·cm at 25°C, MilliQ®, USA).
- U937 (human lymphocyte suspension) macrophages, cultured in RPMI-1640 media, with 0.1% L-glutamine, 10% FBS (Foetal Bovine Serum) and 1% antibiotic antimicotic and Dulbecco PBS.

  The cell density in method calibration test was 4×10^5 cells/mL and viability 94%, and in the NaN_3 method calibration test of 8.4×10^5 cells/mL and 72%, respectively. The cell density was of 4×10^5 cells/mL and the viability of 94%, for Test 1. In Test 2, the cell density was 4×10^5 cells/mL and the viability of 94%. In Test 3.a the cell density was 9.3×10^5 cells/mL, with viability of 82%. In Test 3.b, the cell density was 4×10^6 cells/mL, viability 85%. The target $c_{well}=5\times10^4$ cells/mL.

- Cell media composed of: RMPI-1640 cell medium (Sigma-Aldrich®, USA) 89.2%, antibiotic antimycotic solution (Sigma-Aldrich®, USA) 9.9%, foetal calf serum (FCS) 0.9%.
- CELLSTAR®96-well transparent flat bottom microplate, V_{well}=200 µL.
- AlamarBlue® reagent, 10% of total volume of the sample (Invitrogen™).
- Sodium azid 2% NaN_3, in Dulbecco PBS solution. The dilution steps are shown in the following Table 4.3.2.

Table 4.3.2. Schematic representation of dilutions and concentrations of NaN_3 solution for the preliminary test with AlamarBlue® assay.

Initial Concentration		2%				
	µg/mL	200				
Dilution steps		1%	0.5%	0.25%	0.1%	0.05%
Concentration values	**µg/mL**	**100**	**50**	**25**	**10**	**5**

- $CdCl_2$ powder in purged N_2 ultrapure water (MilliQ) solution, in concentration of 60 µg/mL, Cadmium referred. The amount in percentage of Cd in QD is ~30%. Further dilutions were created and they are shown in the following Table 4.3.3.

Table 4.3.3. Schematic representation of dilutions and concentrations of $CdCl_2$ solution.

Initial Concentration	µg/mL	60					
Dilution steps		1:2	3:8	1:4	1:10	1:20	1:200
Concentration values	**µg/mL**	**30**	**22.5**	**15**	**6**	**3**	**0.3**

- $FeCl_2$ powder and NAC (N-Acetyl-Cysteine) in purged N_2 MilliQ solution, in initial concentration of 24 µg/mL, Fe referred, and 112 µg/mL, NAC. The amount in percentage of Fe in core-doped QD is ~9%, in shell-doped QD is ~12%. The amount in percentage of NAC in core-doped QD is ~54%, in shell-doped is ~56%. In both cases, the highest value has been chosen for the present study (Fe 12%, NAC 56%). Further dilutions were prepared with MilliQ water, which are shown in the following Tables 4.3.4 and 4.3.5.

Table 4.3.4. Schematic representation of dilutions and concentrations of $FeCl_2$ solution.

Initial Concentration	µg/mL	24					
Dilution steps		1:2	3:8	1:4	1:8	1:20	1:200
Concentration values	**µg/mL**	**12**	**9**	**6**	**3**	**1.2**	**0.12**

Table 4.3.5. Schematic representation of dilutions and concentrations of NAC solution.

Initial Concentration	µg/mL	112					
Dilution steps		1:2	3:8	1:4	1:8	1:20	1:200
Concentration values	**µg/mL**	**56**	**42**	**28**	**14**	**8**	**0.8**

- Trypan Blue staining (Nano EnTek), 50% in volume.
- EVE™ cell counting slide, 2 counts/slide.
- EVE™ automatic cell counter (Nano EnTek, Korea).
- Mega Star 1.6R (VWR) centrifuge.
- Micro Star 17 (VWR) centrifuge.

Sample preparation

The samples prepared consisted of six typologies: treated, control (untreated cells), medium, medium and AlamarBlue®, negative control (cells treated with NaN_3) and background correction. All the samples were prepared in triplicates in a 96-transparent flat bottom well plate. The volume of each well (hence each sample) consisted of 200 µL and the addition of 20 µL of AlamarBlue® stain. A general schematic description of the composition of the mentioned samples is shown in the Figure 10.2.1 in the Annex section. In order to avoid potential measuring errors, the wellplate samples were prepared in the following order:

1. Creation of QD dispersions (or $CdCl_2$, $FeCl_2$ solutions) in separate Eppendorfs.
   The initial dispersions (stock solutions) of QDs were prepared. The QD material was provided in powder form, therefore to obtain the 1 mg/mL concentration the necessary volume of D-PBS buffer or ultrapure water (MilliQ) was added. Once the stock solutions were ready, further dilutions were created. The target concentrations for each of the three tests have been shown in the previous Materials section. For each test, three or six dispersions were prepared in three or six different eppendorf vials. In each of those, a

volume from the stock solution and a volume from the cell media were merged in order to obtain the selected target concentration. This obtained volume was tripled in order to make available a sufficient amount of volume for triplicate samples. The just described procedure is shown in the Figures 10.2.3, 4, 5, 6 and 7 in the Annex section for each test. To note that the powder QDs were stored in dark, at 4°C, sealed with Parafilm (Sigma Aldrich) and protected from UV radiation.

2. Creation of cell suspensions.
   The cell line U937 was cultured in RPMI-1640 and incubated in HERAcell24Oi and provided by the Department of Nanobiotechnology. Prior to the preparation of the samples, the viability and the cell number of the culture needed to be measured. From the culture stored in the incubator, 10 µL of the cell suspension were mixed with other 10 µL of Trypan blue stain (Nano EnTek) in an Eppendorf tube. Consequently, 10 µL of the solution was transferred onto one of the two specific sites of the EVE® Cell counting slide and analysed with the cell counter, obtaining viability and cell number values. Among the usually two cultured passages of cells, the one which presented the highest cell viability was chosen for the following experiments. Thereafter, the chosen cell suspension was centrifuged at 1200 rpm, for 5 minutes and at 20°C in the Mega Star 1.6R centrifuge. The supernatant was discarded and the pellet was ready to be re-dispersed to obtain the target cell density, while adding the necessary cell media. The total number of cells in each well of the microplate (200 µL) was decided to be 10000 cells, which means 5×10^4 cells/mL as cell density. However, due to the further dilution step (1:2) at the wellplate stage, the target cell density to prepare needed to be doubled to 1×10^5 cells/mL. The steps for the cell suspension preparation are described in the Figure 10.2.8 in the Annex section.

3. Merging of the QD dispersion (or NaN_3, $CdCl_2$, $FeCl_2$ solutions) volume with the cell suspension volume. The arrangements of the well plates are shown in the Figures 10.2.9, 10, 11 and 12 in the Annex chapter.

4. Addition of the AlamarBlue® stain, directly to the well plate.

5. Incubation in the HERAcell24Oi incubator at 37°C, 5% CO_2, 95% humidity for the planned incubation times 0, 2, 4, 20 and 24 hours, and after each time analysed with the wellplate reader.

The determination of dose-response relationship using the AlamarBlue® assay occurred in several steps described below.

Method calibration.

Initial preliminary tests were carried out in order to calibrate and to check the validity of the method. To achieve the first goal, five cell densities of U937 macrophages, 3000, 6250, 12500, 25000 and 50000 cells/mL, were incubated with 10% in volume of AlamarBlue® stain for different incubation time lengths, 0, 2, 4, 6, 17.5 and 24 hours. The optimum setting to be selected consisted of the best combination of cell density and incubation time length, hence showing the highest fluorescence intensity value. The optimum cell density selected was incubated with five concentration values of sodium azid (NaN_3, a known cell inhibitor) for incubation time lengths of 0, 2, 4, 6, 21.5 and 24 hours, in order to check the validity of the model. The NaN_3 dilution preparation is shown in Figure 10.2.2 in the Annex section.

Determination of effective concentrations - Test 1

This step consisted of a first attempt in detecting any influence of the QDs on the cells and potential no observable effect level (NOEL). The selected QD was bare-QD in concentrations of 0.05, 0.1, 0.25, 0.5, 0.75 and 1 µg/mL, incubated with the U937 cells (50000 cells/mL) and 10% in volume of AlamarBlue® stain for 18.5 hours and repeated for 24 hours. In the Annex the QD dispersion preparation procedure and the well plate arrangement concerning this test are shown in Figures 10.2.3 and 10.2.9, respectively.

Attempts for method improvement increase of QD concentrations - Test 2

Because of the too low concentrations values to be able to detect any effective influence of the QD on the cells, it was decided to increase the concentration values and to study two additional QD types. Therefore, in this step the QDs tested consisted of bare-, shell-doped and core-doped QDs in concentrations of 0.25, 0.5, 5, 12.5, 25 and 50 µg/mL incubated with the cells U937 (50000 cells/mL) and with 10% in volume of AlamarBlue® stain for 2, 4, 18 and 24 hours. Given the method calibration results, the data are shown only for 24h incubation time length, the fluorescence intensity signals at the remaining incubation time lengths are shown in the Annex section in the Figures 10.4.1 and 2. The QDs dispersion preparation procedure and the well plate arrangement for this test are shown in Figures 10.2.4 and 10.2.9, as well in the Annex section.

Determination of dose-response curve and IC_{50} values and $CdCl_2$ and $FeCl_2$•H_20 samples - Test 3.a-b

Due to uncertain results obtained from the previous step, two further tests were carried out using an additional QD type and increasing the concentration values. The test 3.a consisted of the evaluation of bare, shelled, shell-doped and core-doped QDs at concentrations of 1, 10, 25, 50 and 100 µg/mL incubated with U937 cells (50000 cells/mL) and 10% in volume of AlamarBlue® for 0, 2, 4, 20 and 24 hours. To have more specific information about the behaviour of the viability (fluorescence intensity signal) between the concentration samples of 50 and 100 µg/mL, in Test 3.b an additional concentration step was added, 75 µg/mL. Therefore, in this attempt the concentration of bare, shelled, shell-doped and core-doped QDs were 1, 10, 25, 50, 75 and 100 µg/mL, always incubated with 50000 cells/mL and 10% in volume of AlamarBlue® stain for 0, 2, 4, 20 and 24 hours. To note that different batches of shelled-QDs powder were used for Test 3.a and b, in the first an old synthetisation crystal batch of the QDs was used, which was replaced in the following test by a fresher one. The histograms presenting the fluorescence intensity detected at lower incubation time lengths than 24h are shown in Figures 10.4.3 - 13 in the Annex section. Here, the QDs dispersion preparation procedure and the well plate arrangements are shown in the Figures 10.2.5 and 10.2.10 and 11. Dissolved $CdCl_2$ and $FeCl_2$ samples were used in order to examine differences between (nanoparticulate) QDs and their potential dissolved counterparts. For this reason, samples composed of cells treated with $CdCl_2$ and $FeCl_2$ solutions have been analysed as well. The procedure of how to obtain the mass of the Cd and Fe counterparts (from $CdCl_2$ and $FeCl_2$) and the dilution stage are shown in the Figure 10.2.6 and 7 in the Annex section. To note that the dilution values of Cd^{2+} and Fe^{2+} have been chosen to recreate the identical Cd and Fe concentrations as contained in the QD dispersion in Test 3.a and b. The initial solution in the case of iron counterparts has been created through merging the dilutions of $FeCl_2$ and NAC, in order to obtain information of potential effects to the cells from the organic ligand as well. CdCl2 solution was incubated in concentration of 0.3, 3, 6, 15 and 30 µg/mL in Test 3.a, and of 0.3, 3, 6, 15, 22.5 and 30 µg/mL in Test 3.b, with cells (U937 50000 cells/mL) and 10% in volume of AlamarBlue®. The solution composed of iron chloride and NAC was studied only in Test 3.b, using concentration of 0.12, 1.2, 3, 6, 9 and 12 µg/mL. The well plate arrangements are shown in the Figures 10.2.12, in the Annex section.

Fluorescence intensity signals and background corrections

After the evaluation of the data of the Test 2, it was necessary to include in the well plate arrangement samples composed of media, AlamarBlue® stain and only QDs (in respective concentrations and types), called background correction. In this way it was possible to subtract the background signal and obtain the fluorescence intensity only of the cells.

Methods

AlamarBlue® assay is a method used in order to assess the viability or proliferation of a specific cell line. This occurs by measuring the metabolic activity of the cells through the fluorescence or absorbance signals of samples contained in a well plate reader. The AlamarBlue® is a blue coloured, water soluble, non-toxic and ready-to-use stain, which is added to the cell suspension to be analysed. The main component of the dye is a colorimetric growth indicator, resazurin, which is reduced to resorufin, a bright red fluorescent indicator, during the metabolic activity of a cell. Usually a continuous growth induces a reduced environment and on the other hand when the cell proliferation is inhibited the environment is oxidized. Hence, the higher the signal of the detected fluorescence and absorbance, the higher the viability of the cell culture (Invitrogen; Scientific).

The main scope of the objective study was to adapt this assay while using a microplate reader of Tecan Infinte200® Pro in order to assess the viability of the U937 macrophages after incubation with QDs. The resulted and optimized protocols for cytotoxicity assessment are shown in the section Determined dose-response relationship by using AlamarBlue® assay, for the obtained results.

Data evaluation

The well plates were prepared with the target samples to be studied, and after incubation at 37°C, 5% of CO_2 and 95% of humidity for different optional time lengths, it was ready to be analysed with the well plate reader (Inifite200PRO® Tecan). The samples prepared consisted of six types: treated, control (untreated cells), medium, medium and AlamarBlue®, negative control (cells treated with NaN_3) and background correction.

The software i-control 1.9 was used as the respective data collection software with the well plate reader analysis. For each new test the following settings were defined. Firstly, the well plate type needed to be selected, in this case it was NUNC-96 flat transparent with cover. In the displayed well plate layout, the wells to be checked needed to be selected. The first measurement consisted of absorbance signal detection at 595nm. This was accomplished inserting the specific yellow filter, directly in the device. Consequently, a new absorbance measurement window needed to be created, and the excitation wavelength of 595 nm was chosen. The settings for the first step were ready, therefore the sample measurements were then started and the data values were saved in a new excel file. Afterwards, the yellow filter was substituted with the red one, in order to measure the absorbance value for excitation at 560nm. Afterwards to detect the fluorescence signal of the sample this red filter was used again. The fluorescence measurement window was created: the fluorescence intensity values were selected as combination of excitation/emission 560/595nm, the gain was chosen as optimal. The measurements were then ready to be started, but in this case the data were saved in a new sheet of the same excel file.

According to the AlamarBlue® assay protocol, the fluorescence intensity, as the absorbance, represents the quantity of reduced AlamarBlue®, hence the quantity of viable cells. Therefore, the data collected showed indeed the viability of the cells incubated with the different quantum dots types and dilutions at different incubation lengths. Nevertheless, some data evaluation needed to be done. Along with the AlamarBlue® assay protocol, the raw data obtained after the well plate reading, needed to be corrected with more complex calculations than the basic ones. This is made if the sample are known to be not completely reduced or not completely oxidized, which is supposed to occur in all of the considered samples.

The steps which have been followed in order to obtain the final absorbance data are presented in Table 4.3.6. They are based on the template provided by the protocol for AlamarBlue®, as general optical-filter case. The first step consisted of calculating the average values of the absorbance signal measured for each of the sample analysed from both wavelength values. Secondly, the absorbance of oxidized form (AO) needed to be calculated for both the highest and lowest wavelength measurements: the average value of the triplicates for the medium sample was subtracted from the average value of the triplicates of the Medium-AlamarBlue® sample. Afterwards, the ratio among these two obtained values, AO_{560} ratio AO_{595}, was calculated and defined as correction factor, R_o. Finally, the corrected absorbance intensity, therefore the percentage of reduced AlamarBlue®, was calculated. The product between the correction factor, R_o, and the absorbance mean value at 595nm for each treated sample, A_{i595}, was subtracted from the absorbance mean value at 560nm for the correspondent treated sample, A_{i560}. This value then was always divided ratio the subtraction referred to the control sample. Therefore, the product among the correction factor, R_o, and the absorbance mean value at 595nm of the control sample, Ac_{595}, was subtracted from the absorbance mean value of the control sample, A_{i560}. The number obtained from the ratio was multiplied to 100 in order to obtain the percentage values. This described indeed the reduced amount of AlamarBlue® for the specific treated case, or for the same control case, when it was divided ratio itself.

Table 4.3.6. Calculation steps for raw data correction of Absorbance intensity signal.

Steps		Specific	Symbols		Equations	
			560nm	595nm	560nm	595nm
1	Average values calculation	Media	M_{560}	M_{595}	$\frac{\sum AbsMedia@560nm}{3}$	$\frac{\sum AbsMedia@595nm}{3}$
		AlamarBlue + media	AB_{560}	AB_{595}	$\frac{\sum AbsAB@560nm}{3}$	$\frac{\sum AbsAB@595nm}{3}$
		Control sample	Ac_{560}	Ac_{595}	$\frac{\sum AbsAc@560nm}{3}$	$\frac{\sum AbsAc@595nm}{3}$
		Treated samples i	A_{i560}	A_{i595}	$\frac{\sum AbsAi@560nm}{3}$	$\frac{\sum AbsAi@595nm}{3}$
2	Subtraction of media from the AlamarBlue® in average values	Absorbance of oxidized form	AO_{560}	AO_{595}	$AB_{560} - M_{560}$	$AB_{595} - M_{595}$
3	Correction Factor Calculation		R_o		$\frac{AO_{560}}{AO_{595}}$	
4	Percentage of reduced AlamarBlue calculation	Absorbance intensity %	Reduction %		$\frac{Ai_{560} - (Ai_{595} \times Ro)}{Ac_{560} - (Ac_{595} \times Ro)} \times 100$	

In general, concerning the fluorescence evaluation, the average value of the fluorescence signal of media and AlamarBlue® sample was subtracted from the one of treated or the control sample. Nevertheless, in this way, the result obtained corresponded to the fluorescence intensity of both the cells and the QDs. Therefore, differently, as it can be observed in Figures 5.2.15 and 16 in

Fluorescence intensity signals and background corrections, in Results and discussion chapter, in order to obtain the fluorescence signal only from the cells, the fluorescence signal also coming from the quantum dots needed to be subtracted from the total one. Hence, the fluorescence average values of the background correction samples needed to be subtracted from the total treated one. These values corresponded to the absolute fluorescence intensity representing the cell viability of the test. Afterwards, in order to obtain information about the reduction of the cell viability, all the treated samples' results were normalized considering the control value as reference: the absolute values were divided ratio the value of the control sample and transformed into a percentage result. The three phases to obtain the corrected fluorescence data are presented in the following Table 4.3.7.

Table 4.3.7. Calculation steps for raw data correction, absolute and normalized fluorescence intensity.

560/595 nm				
Step		Specific	Symbol	Calculation
1	Average values calculation	Treated Samples	T	$\frac{\sum TreatedSampleRawData}{3}$
		QDs and AlamarBlue samples	QDs+AB	$\frac{\sum QDs+ABRawData}{3}$
		Control sample	CTL	$\frac{\sum ControlSampleRawData}{3}$
		Media and AlamarBlue	AB	$\frac{\sum M+ABRawData}{3}$
2	Subtraction of QDs, Media and AlamarBlue signal	from average values	FL_absolute_T	$\mathrm{T} - (\mathrm{QDs} + \mathrm{AB})$
			FL_absolute_CTL	$CTL - AB$
3.a	Fluorescence Intensity - Absolute Values	*values from subtraction step*	FL absolute	
3.b	Fluorescence Intensity - Normalized Values		FL normalized	$\frac{FL\_absolute\_T(CTL)}{FL\_absolute\_CTL} \times 100$

Concerning both the absorbance and the fluorescence data, standard deviation was calculated related to the mean values of the triplicates, which were then corrected to obtain an error lower than 15%. When the average values were subtracted, the related errors were then summed up.

Determination of dose-response and IC_{50} values

The inhibition concentration values (IC_{50}) have been calculated after the data fitting using a sigmoidal function regression. The dose-response fitting function used was:

$$Y = Y_1 + \frac{Y_2 - Y_1}{1 + 10^{(LogX_0 - X)p}}$$

Where Y is the response and X is the Log of the concentration, Y_1 and Y_2 are the value of Y at bottom plateau and top plateau respectively, p is the hillslope of the curve. $LogX_0$ is the value when the response is halfway between the bottom and the top plateaux. Therefore, it is possible to compute the IC_{50} value as:

$$IC_{50} = LogX_0$$

The results are shown in the Results and Discussion chapter.

Statistical analysis of data

In the AlamarBlue® assay method many samples were measured and analysed, in particular for each new set of experiment a new control sample (U937 native cells) was studied as well, producing six different fluorescence intensity data about it. Therefore, in order to obtain information about the significant differences or analogies among those samples, some statistics analysis was made.

In this study the Student t-test used was the Welch's test, for two samples assuming unequal variances. It was used to define the significant difference among the samples analysed. The t-test allows to state if two samples are statistically different from each other, comparing their means in relation to their variability of their scores. When the distribution of two samples varies considerably among one another (low overlapping among the distribution), significant difference between the samples occurs. The formula for Welch's test to calculate the statistic t is:

$$t = \frac{\bar{X}_1 - \bar{X}_2}{\sqrt{\frac{s_1^2}{N_1} + \frac{s_2^2}{N_2}}}$$

Where $\bar{X}_1$, s_1^2 and N_1 are mean, variance and number of events in the group one, respectively (same for group 2). Usually, the larger the t statistic, the higher difference there is between the groups. The formula to calculate the degree of freedom of the variance is $\nu = \frac{(\frac{s_1^2}{N_1}+\frac{s_2^2}{N_2})^2}{\frac{s_1^4}{N_1^2\nu_1}+\frac{s_2^4}{N_2^2\nu_2}}$, with $\nu_1 = N_1 - 1$ and $\nu_2 = N_2 - 1$. In order to test the significant difference of the groups, it is necessary to firstly state a so-called alpha level, representing the probability that the results obtained in the samples occurred by chance. The alpha level chosen in the present study was of 0.05, which means that only the 5% of the results in the samples happened by chance. These three values are used in a table of significance, necessary in order to assess the value of the t, if large enough to define the significant difference. In this study, it was used an automated self-made program, which computed the t-value and the alpha values and printing the significance test results. Initially, the null hypothesis of no difference in the means of the samples compared was selected. In order to define rejection or acceptance of this hypothesis the alpha value initially stated and alpha value calculated needed to be compared. If the alpha value given as output was lower than the alpha value initially stated the hypothesis was not valid, hence significant difference may be detected.

4.4 QD LOCALIZATION IN CELLS

In order to obtain a more detailed idea about how the nanoparticles may have interacted with the cells, some tests have been conducted with the confocal laser scanner microscope.

4.4.1 Confocal laser scanner microscope

Materials used

- Confocal Laser Scanner Microscope (CLSM, TCS SP8 Leica Microsystems, 487 Mannheim, Germany)
- Dispersions of bare-QD, core- and shell-doped QDs and shelled QDs, initial concentration of 1 mg/mL. Further dilutions were prepared with cell media. The dilution steps are shown in the following scheme, Table 4.4.1.

Table 4.4.1. Schematic representation of dilutions and concentrations of QD dispersion for the conducted test with CLSM.

Test 3	**Initial Concentration**	µg/mL	1000					
	Dilution steps		1:10	3:40	1:20	1:40	1:100	1:1000
	Concentration values	**µg/mL**	**100**	**75**	**50**	**25**	**10**	**1**

- Ultrapure water (18.2 MΩ·cm at 25°C, MilliQ®, USA).
- U937 (human lymphocyte suspension) macrophages, cultured in RPMI-1640 media, with 0.1% L-Glutamine, 10% FBS (Foetal Bovine Serum) and 1% antibiotic antimicotic and Dulbecco PBS.

  The cell density was of 1.7×10^6 cells/mL and the viability of 83%. The target $c_{well}=5\times10^4$cells/mL.
- Cell media composed of: RMPI-1640 cell medium (Sigma-Aldrich®, USA) 89.2%, antibiotic antimycotic solution (Sigma-Aldrich®, USA) 9.9%, foetal calf serum (FCS) 0.9%.
- Hoechst nucleus stain 33342. 1µL from the pre-made stock solution (10 mg/mL in ultrapure water) of Hoechst needed to be mixed in 2 mL of PBS buffer. From this 100 µL to the pellet. $\lambda_{ex}/\lambda_{em}$ 361/486 nm.
- 4% formaldehyde.
- Fluoroshield™ (Sigma-Aldrich, Austria).
- Glass slides, 5 mm (Hampton Research).
- Glass covers, diameter 22 mm (Hampton Research).

Sample preparation

The samples were prepared with U937 macrophages, and the cell density was of 50000 cells/mL. The concentration values of the quantum dots were the same as in the Test 3.b (i.e. 100, 75, 50, 25, 10 and 1 µg/mL). The analysed incubation time was just after 24 hours. The procedure to prepare the sample was similar to the AlamarBlue® assay procedure. However, in this case the only samples made were the treated and the control ones. Prior to the CLSM analyses, all samples needed to be fixed. The fixation of cell should guarantee the possibility of long-term storage of the samples at 4°C without any negative effect on their integrity. In addition, cell fixation allowed to increase the resolving power of the microscope. In order to be able to enlighten the nucleus from the rest of the cell, a staining step was necessary prior the microscope analysis. The chosen stain was a nucleus stain, Hoechst 33342 exciting and emitting at 361 nm and 486 nm, respectively. The procedure of samples preparation for the CLSM analysis is shown in the Figure 10.3.1 in the Annex section.

Methods

The confocal laser scanner microscope (CLSM, TCS SP8 Leica Microsystems, 487 Mannheim, Germany) was used in order to obtained confocal measurements of the treated samples. The excitation source in the microscope as a pulsed white light laser (WLL 2) and a 405 nm diode laser. For the collection of the fluorescence emission instead, a HyD spectral detector in the range of 520-590 nm was used.

5 RESULTS AND DISCUSSIONS

5.1 QD CHARACTERIZATION

The results obtain from the UV/VIS and fluorescence spectrometry measurements are shown in the graph below, Figure 5.1.1 from the study of Part et al. (*submitted*). The absorbance and emission spectra of the QD are displayed in broken and solid lines, respectively.

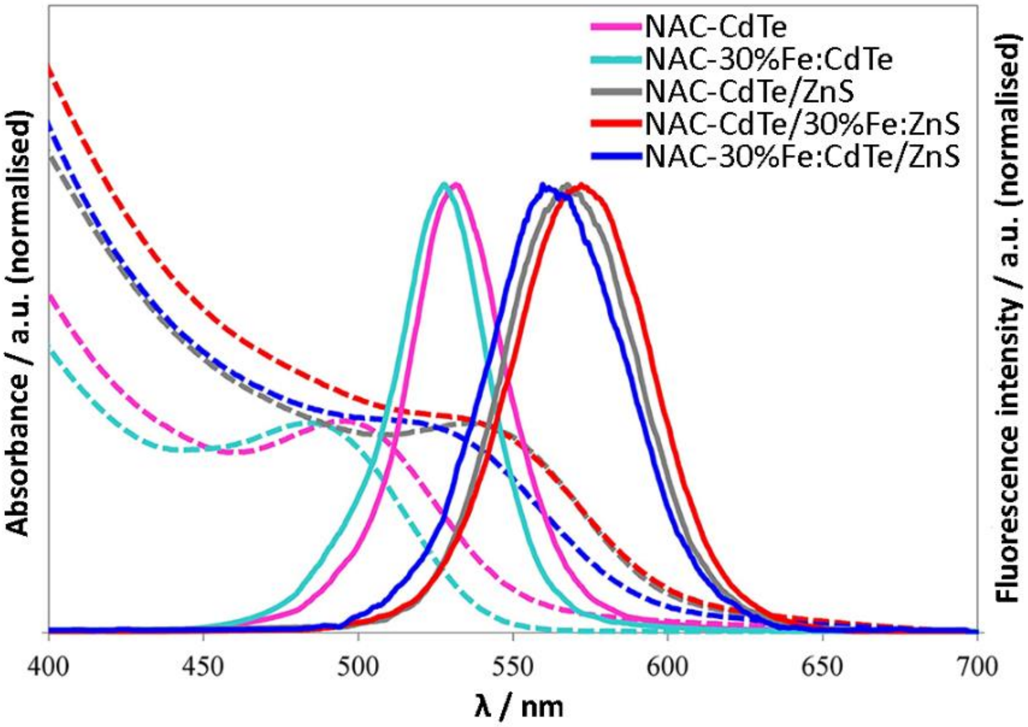

Figure 5.1.1. Absorbance and normalized fluorescence spectra (broken and solid lines) of bare-, shelled, shell-doped, core-doped QDs according to Part et al. (submitted).

The bare-QD (purple and light blue lines) show characteristic wavelengths of first excitonic absorption and fluorescence maxima of 537±1 and 568±1 nm, respectively (Part et al., *submitted*). The iron dopants did not particularly influence the characteristic wavelengths of first excitonic absorption and fluorescence maxima, being 521±1 and 562±1 nm respectively for the core-doped

QD, and 540±1 and 573±1 nm respectively for the shell-doped QD (Part et al., *submitted*). As well the full width half maximum (FWHM) does not display huge variations: 51, 54 and 53 nm for the bare-/shelled-, core-doped and shell-doped QD respectively (Part et al., *submitted*). The main difference was in their photoluminescence quantum yield (PL QY). The value for the core-doped and shell-doped QD decreases of -63% and -38% respectively, compared to the bare- and shelled-QD one (8±0.5 %) (Part et al., *submitted*).

The behaviour of the HDD of the four QD types is shown in the Figure 5.1.2 below from Part et al. (*submitted*): it shows how the HDD of the particles increases over time. This is a phenomenon called aggregation: QDs tend to bind together due to electrostatic forces, forming bigger clusters, which may induce problems in the further imaging application.

From the study of Part et al. (2016), the geometric radius of a single NAC-coated QD was measured to be ~ 2.7 nm and the correspondent HDD of ~ 16 nm and ~ 91 nm, presenting a bimodal distribution, the NAC ligands presented ~0.9 nm thickness value (Part et al., 2016b). from the XRD measurements of the study of Part et al. (*submitted*) showed the sizes of bare-QD and shell-coated QDs to be 2.02 and 2.23 nm, respectively, concerning core-doped QDs the size could not be detected with this method. The TEM measurements however confirmed the previous findings: 2.9±0.3 nm of shell-doped QD (Part et al., *submitted*).

Usually, when dispersed QDs show higher size values due to hydrophilic ligands and water interaction, hence the hydrodynamic diameter. Usually, when let in dispersion for long periods, QDs tend to agglomerate. From the measurements displayed in the Figure 5.1.2 below, at day 0 the HDD of bare- and shelled QDs present the lowest value, 8.3 ± 2.5 nm (polydispersity index, PdI = 0.24) compared to 37.0 ± 13.0 nm (PdI = 0.20) and 17.4 ± 6.7 nm (PdI = 0.22) of core-doped and shell-doped QD, respectively. Over time, after 18 days, the HDD of the bare-/shelled- and shell-doped QD considerably increased, showing a higher tendency of aggregation than the core-doped ones: 24.5 ± 9.5 nm (PdI = 0.29) for the bare-QD, 31.9 ± 13.5 nm (PdI = 0.21) the shell-doped, compared to 39.9 ± 13.3 nm (PdI = 0.19) of the core-doped QD. To note that QD were all dispersed in ultrapure water (MilliQ) (Part et al., *submitted*).

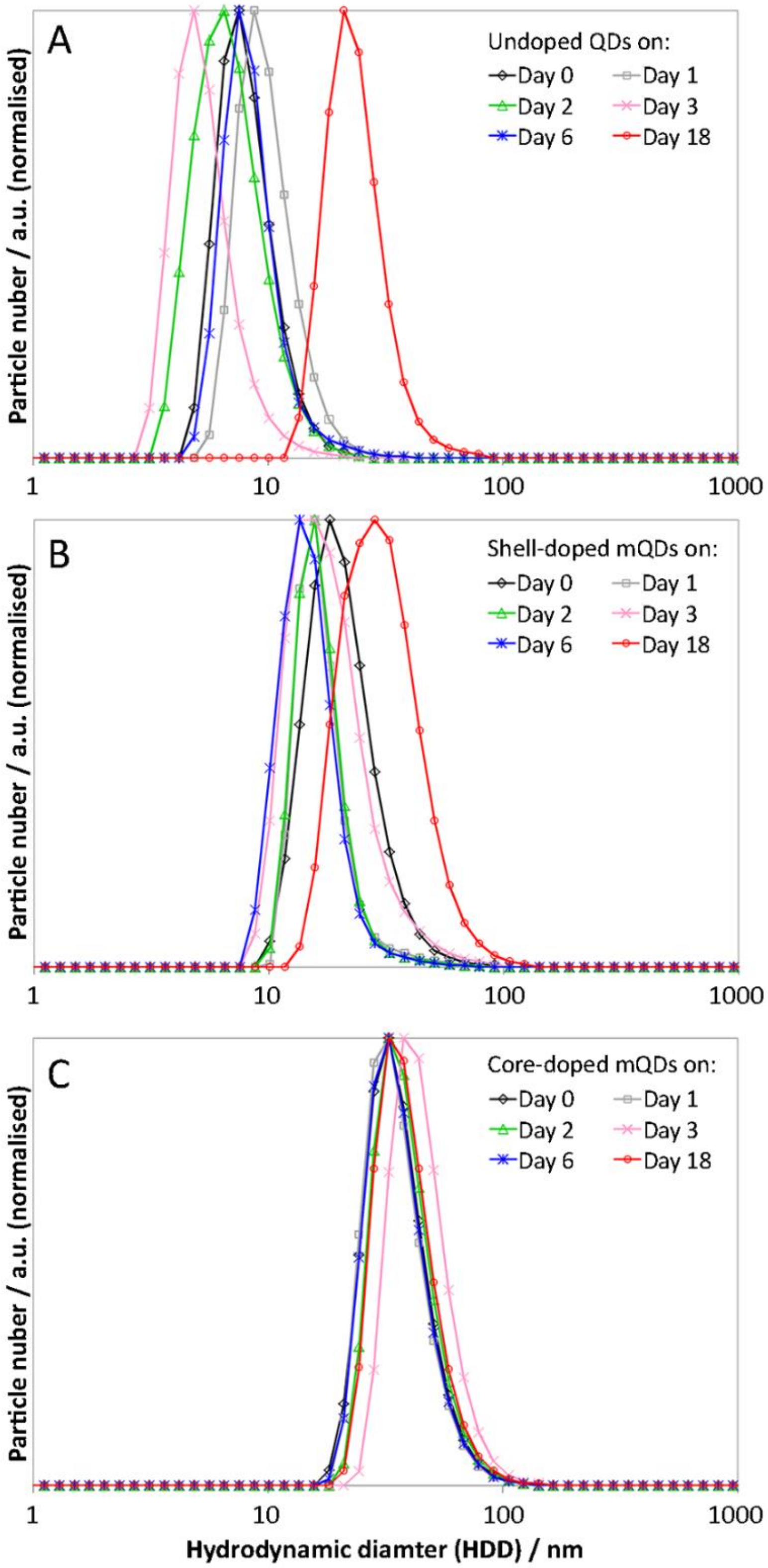

Figure 5.1.2. Comparison of particle number vs HDD distributions over time (0 – 18 days) of bare-QD (A), shell-doped QD (B) and core-doped QD (C) (taken from Part et al., submitted).

5.2 CELL VIABILITY

5.2.1 Flow Cytometry

Flow cytometry was applied to untreated and treated CHO cells, which were incubated with NAC-CdTe, bare- QDs.

__Cell viability analysis with 7-AAD and Hoechst stains – Test 1__

Tests using different dyes have been conducted with the flow cytometer method. The dot-plots and the single-parameter histograms obtained after the analysis of CHO untreated, CHO treated with NAC-CdTe (100 µg/mL) and CHO treated with bare-QDs and stained with 7-AAD and Hoechst samples are shown in the Figure 5.2.1.

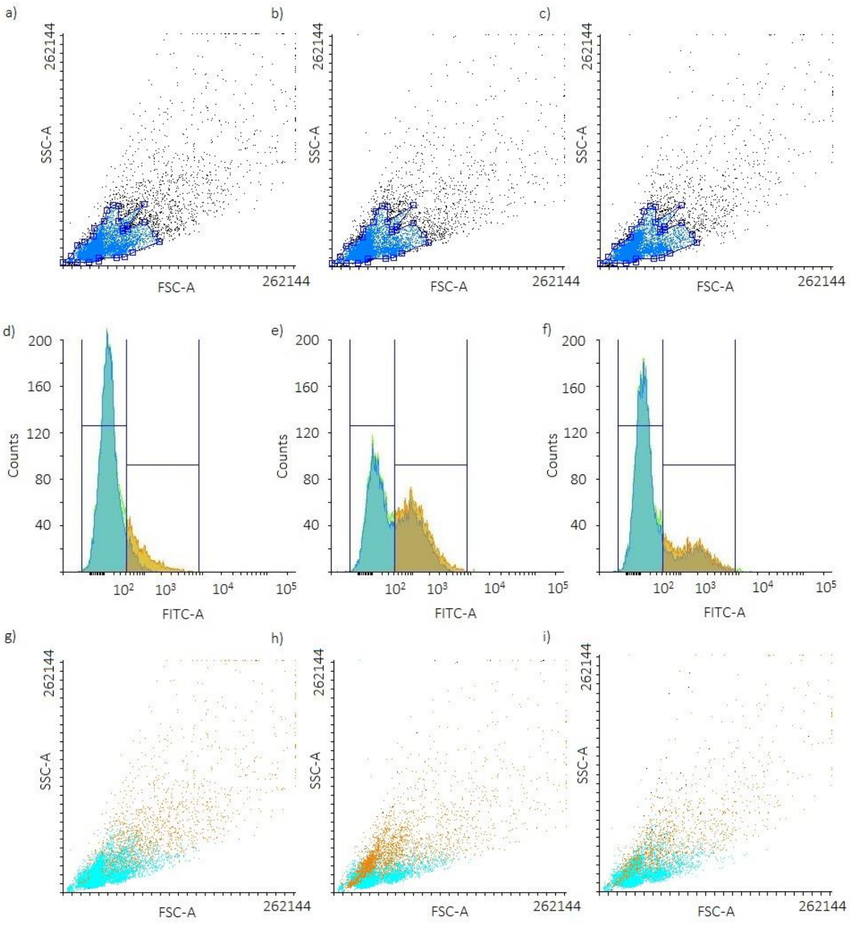

Figure 5.2.1. From flow cytometry analysis dot-plots (side scatter signal on y-axis, forward scatter signal on the x-axis) show the gated population (blue) for a) untreated cells, b) treated cells (100 µg/mL of NAC-CdTe QDs), c) treated cells that additionally contain Hoechst and 7-AAD stains. Single-parameter histograms from flow cytometry analysis using fluorescence channel FITC-A d)

represents untreated cells, e) treated cells, and f) displays stained-treated cells. Dot-plots at the bottom of the Figure show the two populations created from the analysis of the histograms for g) untreated cells, h) treated cells, i) stained-treated cells.

The single parameter histograms display the number of counts, such as the number of events or number of detected cells, as a function of the respective fluorescence intensity by using a specific different filter set. The three histograms in Figure 5.2.1 show: the unstained untreated sample, media and cells only, d); the unstained treated sample, media, cells and QD, e); and of the stained and treated sample, media, cells, QD, 7-AAD and Hoechst stains, f). The number of events has been previously gated in the dot plot SSC-A versus FSC-A, obtaining the main population of the sample. This one is then possible to observe as the blue colour part in each of the histograms. On the other hand, the green colour is related to the whole number of events detected. Finally, the orange part to the gating made to highlight the second peak appeared in the unstained and treated sample. In addition, a further sample composed of only ultrapure water (MilliQ) and diluted QD (NAC-CdTe) was analysed. However, no signal could be detected, due to the very small size of the nanoparticles, below the threshold triggering value.

The dot-plots a, b, c, g, h and i in Figure 5.2.1 show the distribution of the events detected from the untreated cells, treated cells and stained-untreated cells, respectively. No significant difference can be noted after QD-treatment or after staining. The dot-plots a, b and c were gated, to show the principle population of the sample (blue), highlighted as well in the following histograms (light blue). On the contrary, the dot-plots g, h and i display the populations created during the histograms analysis: the light blue dots reflect the population with very low fluorescence intensity, and the orange dots correspond to the events presenting higher fluorescence intensity.

The single-parameter histograms in Figure 5.2.1 show a clear difference in unstained-untreated sample and of QD-treated samples. Considering the results from these tests, the characteristic QD signal was possible to be detected, but only when associated with the cell suspension. The single histogram 5.2.1.d shows how the native cells display very low fluorescence intensity. It is important to note that QD dispersions without any cells were also analysed as a reference to treated cells, at which no fluorescence QD-specific signals could be detected. Due to this and the low fluorescence intensity in the untreated sample, it could be possible to assume that the second peak, which rises in the unstained and treated samples (e), represents the characteristic emission signal of the QDs associated with the cells. The size of the cells is high enough to be detected, and their fluorescence has been shown to be low, therefore a higher intensity of the fluorescence in the treated sample could be explained assuming that the QDs penetrated the cells and in this way their fluorescence could be detected.

The two stains Hoechst and 7-AAD had the purpose of trying to differentiate the nuclei of living cells and the damaged/dead cells respectively in the sample. The results from these stained tests show a weak signal in the higher fluorescence intensity part of the graph (low number of counts). This could be explained assuming that there were no damaged or dead cells and therefore no fluorescence from the 7-AAD stain could be detected. At the same time, the stain Hoechst was not excited at its maximum: the laser used was of 488 nm wavelength and the excitation peak or Hoechst is at 361 nm. Finally, the results could be also interpreted as a potential overlapping interference between the spectra of the two stains and the QDs. However, in this case compensation process could not really be effective due to the non-fluorophore nature of the QD.

Cell viability analysis with PI stain – Test 2

Further analysis has been carried out with a different stain: propium iodide. Figures 5.2.2 shows flow cytometry analysis of untreated cells and PI-stained cells with no incubation time. In specific Figure 5.2.2 displays: gated dot-plots of untreated and PI-stained untreated cells (a and b); single-parameters histograms displaying events counted and the fluorescence intensity detected in the channel PE-A of untreated CHO cells (c), and PI-stained untreated cells (d), highlighting the populations gated in the previous dot-plots; dot-plots of untreated and PI-stained untreated cells (e and f), displaying the populations created during the analysis of the histograms.

The following Figures 5.2.3, 4 and 5 present the same structure as Figure 5.2.2, but showing untreated and PI-stained untreated cells after 24h of incubation (Figure 5.2.3), QD treated and PI-stained QD treated cells with no incubation time (Figure 5.2.4), and finally showing QD treated and PI-stained QD treated cells after 24h of incubation (Figure 5.2.5).

In general, the dot-plots a, b, e and f show the distribution of the events detected from the unstained cells, stained cells, respectively, with no incubation storage and after 24h of incubation and of untreated or treated cells, depending on the figure. No significant difference can be noted after QD-treatment or after staining. In all the Figures (5.2.2, 3, 4 and 5) the dot-plots a and b were gated to show the principle populations (blue and orange), highlighted as well in the following histograms. On the contrary, the dot-plots at the bottom of the Figures show the population created after the analysis of the histograms. In this case, the visible events correspond mainly to the population having very low fluorescence intensity.

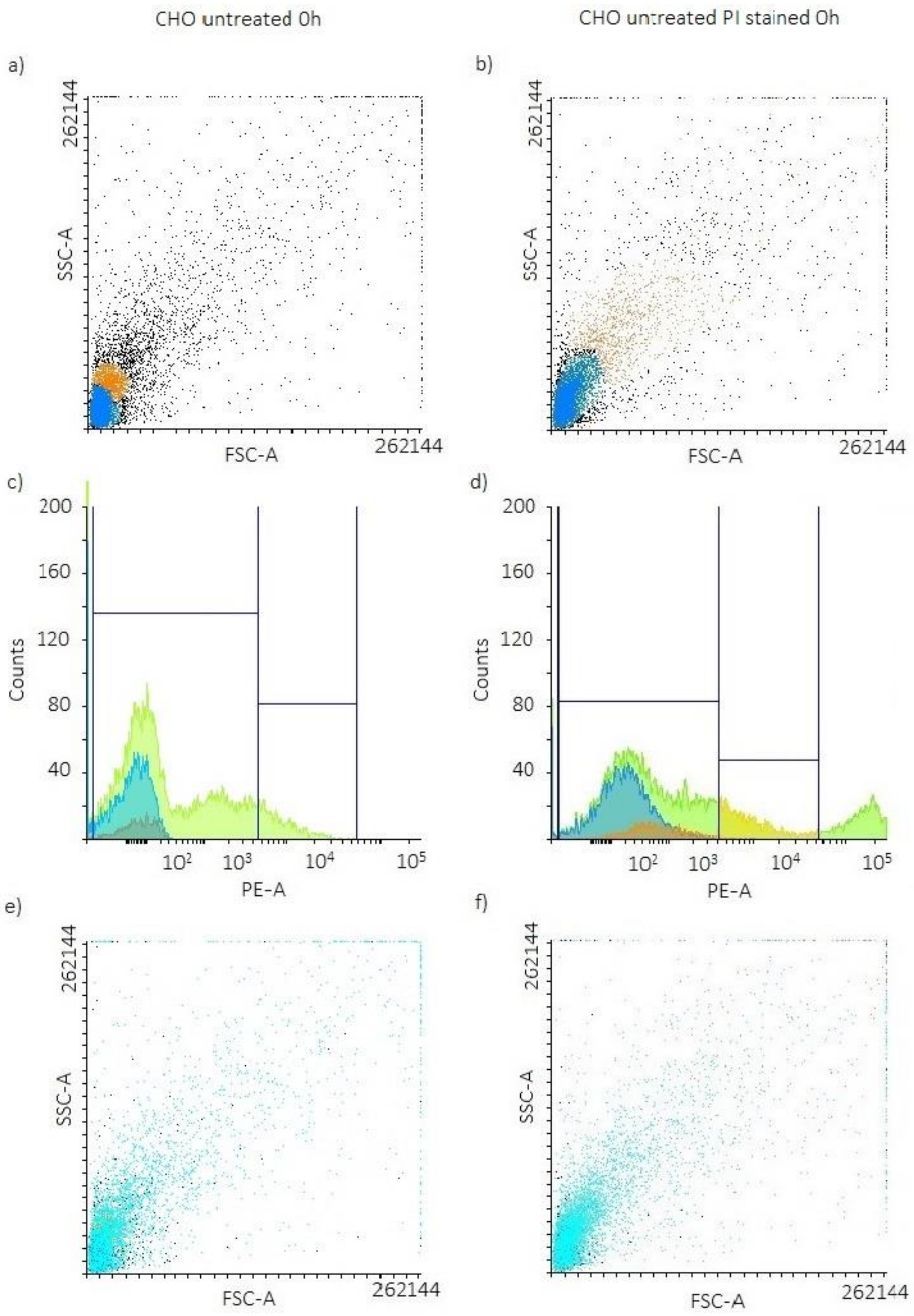

Figure 5.2.2. From flow cytometry analysis after no incubation. The dot-plots (side scatter signal on y-axis, forward scatter signal on the x-axis) show the gated populations (blue and orange) for a) untreated cells, 1×10^6 cells/mL, b) PI-stained-untreated cells, 1×10^6 cells/mL. Single-parameter histograms show fluorescence intensity detected in the channel PE-A. Histograms c) is untreated cells, and d) is PI-stained-untreated cells. Dot-plots at the bottom of the Figure show the populations created during the analysis of the histograms c and d, for e) untreated cells, f) PI-stained-untreated cells.

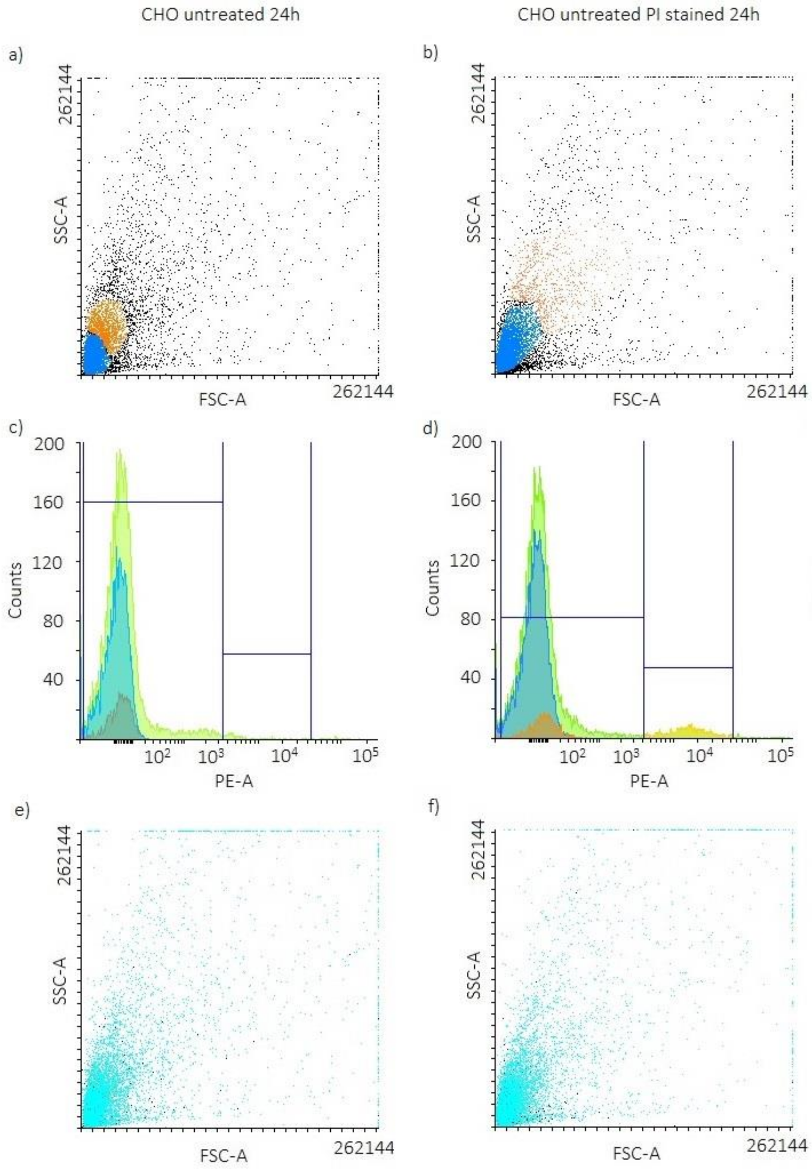

Figure 5.2.3. From flow cytometry analysis after 24h of incubation. The dot-plots (side scatter signal on y-axis, forward scatter signal on the x-axis) show the gated populations (blue and orange) for a) untreated cells, 1×10^6 cells/mL, b) PI-stained-untreated cells, 1×10^6 cells/mL. Single-parameter histograms show fluorescence intensity detected in the channel PE-A. Histograms c) is untreated cells, and d) is PI-stained-untreated cells. Dot-plots at the bottom of the Figure show the populations created during the analysis of the histograms c and d, for e) untreated cells, f) PI-stained-untreated cells.

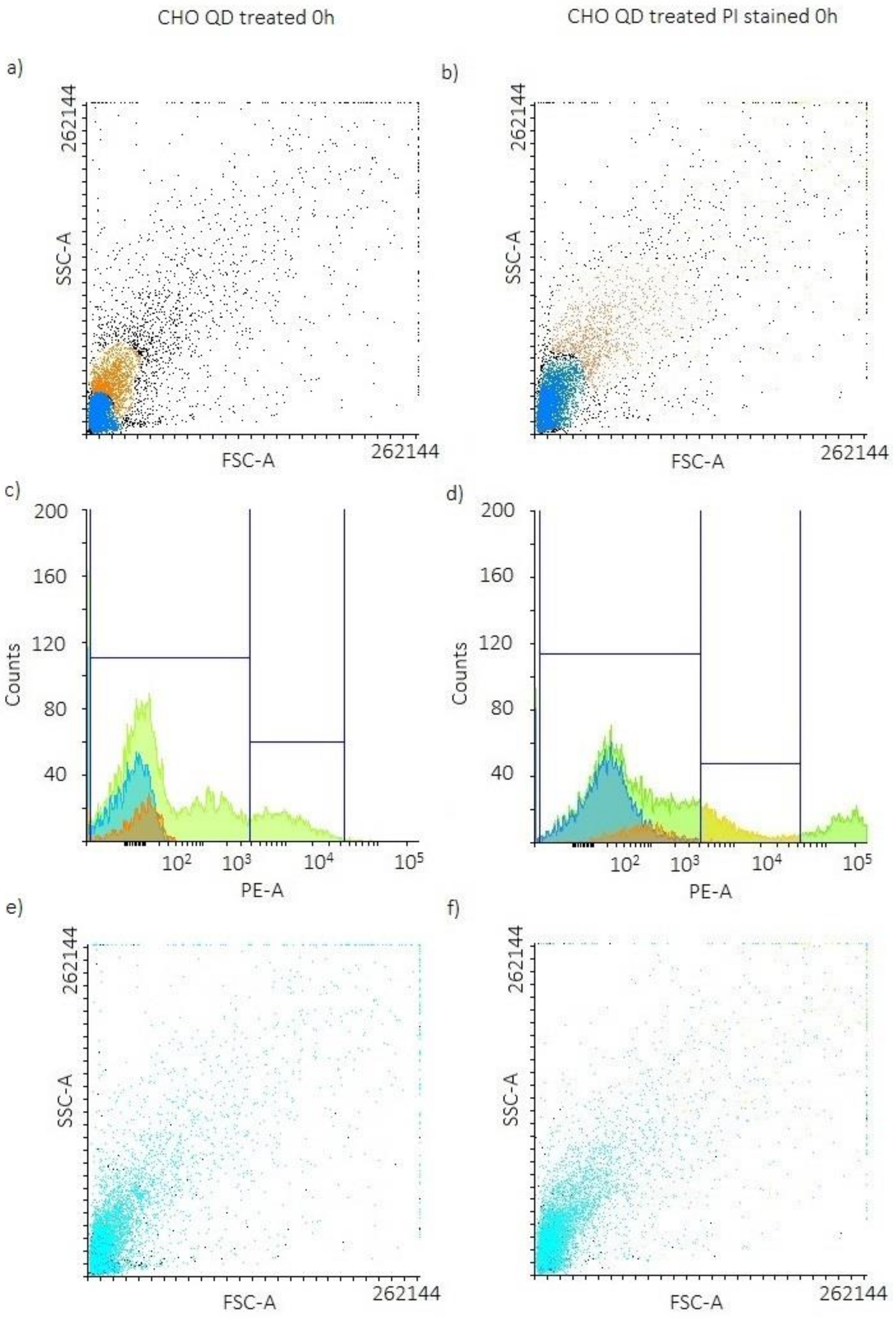
CHO QD treated 0h

CHO QD treated PI stained 0h

Figure 5.2.4. From flow cytometry analysis after no incubation. The dot-plots (side scatter signal on y-axis, forward scatter signal on the x-axis) show the gated populations (blue and orange) for a) treated cells, 1×10^6 cells/mL, 100µg/mL NAC-CdTe, b) PI-stained-treated cells. Single-parameter histograms show fluorescence intensity detected in the channel PE-A. Histograms c) is treated cells, and d) is PI-stained-treated cells. Dot-plots at the bottom of the Figure show the populations created during the analysis of the histograms c and d, for e) treated cells, f) PI-stained-treated cells.

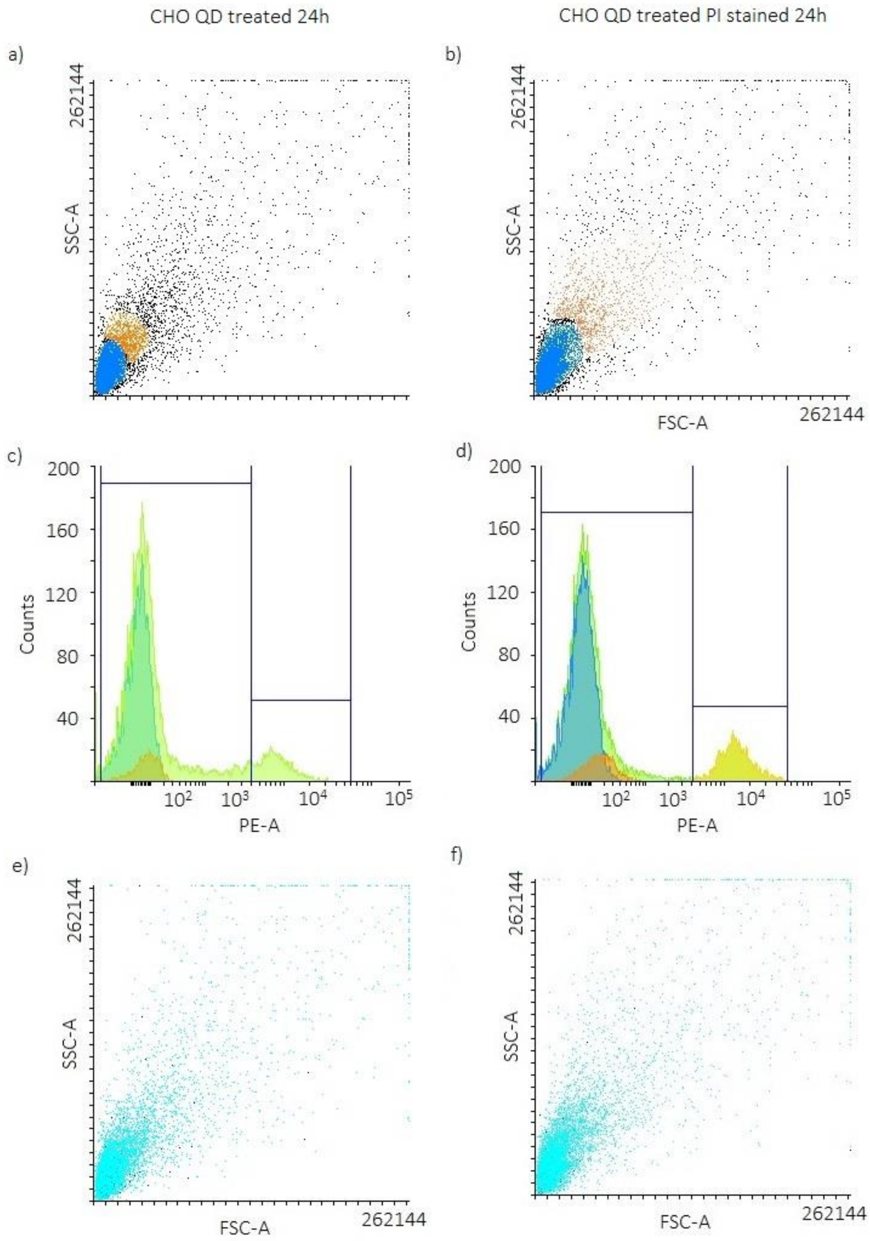

Figure 5.2.5. Flow cytometry analysis after 24h incubation. The dot-plots (side scatter signal on y-axis, forward scatter signal on the x-axis) show the gated populations (blue and orange) for a) treated cells, 1×10^6 cells/mL, 100µg/mL NAC-CdTe, b) PI-stained-treated cells. Single-parameter histograms show fluorescence intensity detected in the channel PE-A. Histograms c) is treated cells, and d) is PI-stained-treated cells. Dot-plots at the bottom of the Figure show the populations created during the analysis of the histograms c and d, for e) treated cells, f) PI-stained-treated cells.

Comparing the histograms created during the analysis of both the untreated and treated sample without any incubation time, no significant variation in detected number of events and fluorescence intensity is noted. Nevertheless, concerning the stained samples a small difference is the appearance of a new low peak at very high fluorescence intensity. This may be explained by possible damage of part of the cells due to initial cell stress: the PI stain may have managed to penetrate through their membranes. On the contrary, the analysis of untreated, treated and both stained with PI samples after 24h of incubation show substantial variations in the histograms pattern. In all those graphs, the number of events emitting at very low fluorescence intensity increased of four times, compared to the non-incubated samples, possibly showing more stable cells than the initial analysis. Nevertheless, the significant observed change is among the untreated and treated graphs: in the latter (both in unstained and stained) a second clear peak at higher fluorescence intensity appears. Consequently, it was assumed that QD were visible and they were internalized into the cells. Due to the fact that the PI stain can penetrate only damaged or dead cell membranes, it was assumed that the appearance of the high fluorescence intensity peak in the QD-treated PI-stained sample graph could be linked to the presence of the QDs. These may have requested some time to associate to the cells, inducing some harm or damage to the membrane and therefore allowing the PI stain to permeate into them, and afterwards be detected during the FACS analysis. The assumption of internalization may be confirmed by the similar peak visible in the histogram of treated unstained sample, by the impossibility of detecting any event from samples composed of only QDs and the comparison among treated unstained histogram with the related untreated unstained one. The appearance of the small peak at high fluorescence only in the treated cells data and not in the untreated one may reflect the internalization of the QD into the cells, being the only difference among those two samples. Moreover, QD were not detected by flow cytometry analysis, hence the only way that they could have been detected was association or internalization to bigger particles, in this case cells, therefore as it may have happened in the treated case. Finally, the presence of the high fluorescence intensity peak in the stained-treated sample allows to assume that the QD not simply associate to the cells, but they internalized. As already explained PI stain penetrates only through damaged membranes, therefore observing a very similar peak in stained and unstained sample lead to the assumption that those cells which have been dyed by the PI have been penetrated and therefore damaged by the QDs.

Nevertheless, overlapping interference between the PI stain and the QD spectra needs to be taken into consideration as in the previous analysis, as the emission peaks are very close to each other: the ex/em values for NAC-CdTe according to the fluorescence spectrometry data are 537/568 nm, and the ex/em values for PI stain are 535/617 nm. As in the previous analysis no compensation was possible due to the non-fluorophore nature of the QD. Because of this overlapping phenomenon, it was decided to proceed via using different methods to test the toxicity of the QD, e.g. AlamarBlue® assay. This allows to distinguish among the stain and the nanoparticles spectra, besides to assess the viability of the cell line.

5.2.2 Determined dose-response relationship by using AlamarBlue® assay

The AlamarBlue® assay was adapted to QD-spiked cells in order to develop a rapid screening method that allowed to assess cell cytotoxicity in large sample numbers. In the following paragraphs, the already elaborated data obtained with the AlamarBlue® assay are presented.

Method calibration

As suggested from the protocol of the AlamarBlue® assay, it was firstly necessary to calibrate the model. The optimum length of incubation time and density of the cells needed to be found out. Five different cell densities were considered: 3000, 6250, 12500, 25000 and 50000 cells/mL. The cells were incubated with 10% in volume of AlamarBlue® for 2, 4, 17.5 and 20 hours. The Figure 5.2.6 shows the results obtained.

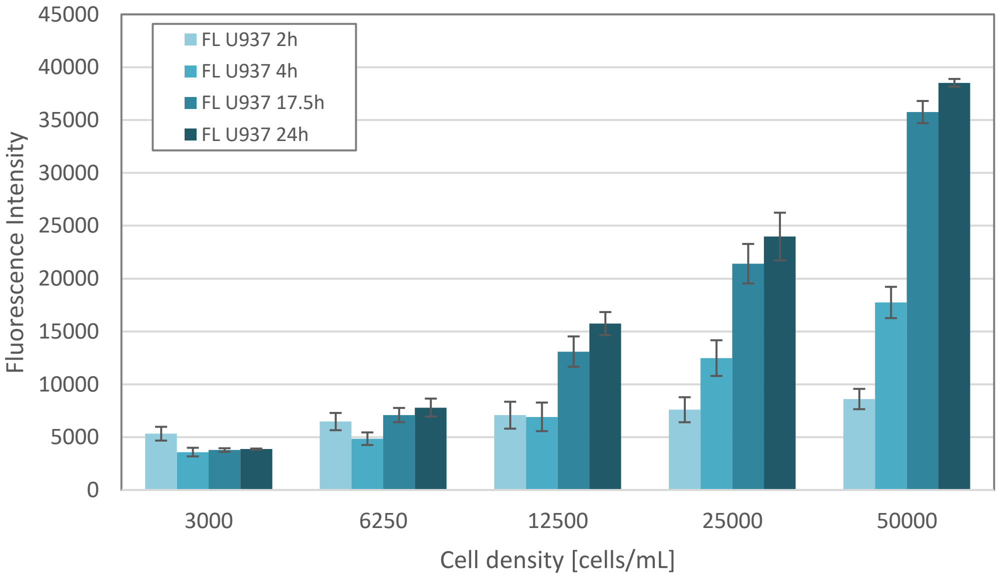

Figure 5.2.6. Change of fluorescence intensity of different U937 cells density as a function of incubation time.

For each cell density, the four time lengths are grouped and coloured with different shades of petrol-green (the darker, the longer time). As a general consideration, with the increasing of cell density values the fluorescence intensity increased too. Parallelly, the longer the incubation time, the higher the fluorescence intensity. The shortest time length of 2 hours does not present any significant change in fluorescence intensity. On the contrary, all other time spans showed increased fluorescence intensity values with increasing QD concentration. In conclusion, the optimum values or highest fluorescence intensities (including the lowest standard deviation) were found to be at 24 hours and 50000 cells/mL. To note that t-test statistical analysis was carried out for this test, showing significant difference among the longer incubation times (17.5 and 24 hours) at highest cell density (25000 and 50000 cells/mL) and the rest of the incubation times and concentrations, confirming the decided optimum setting.

Figure 5.2.7 shows fluorescence intensity detected from samples composed of U937 cells (50000 cells/mL) merged with the sodium azid solution in different concentrations, 0 (control), 5, 10, 25, 50 and 100 µg/mL, after 0, 2, 4, 6, 21.5 and 24h of incubation.

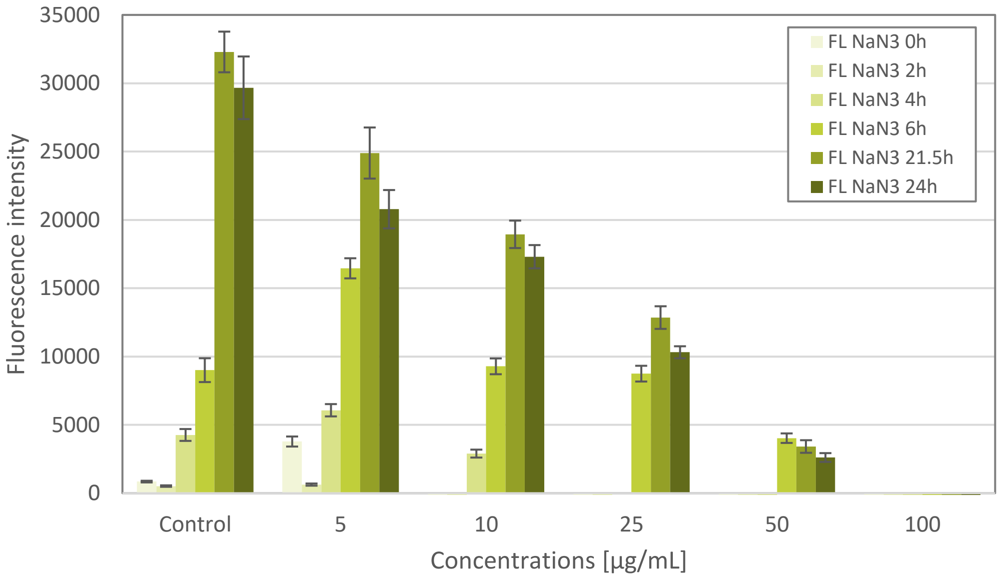

Figure 5.2.7. Change of fluorescence intensity of U937 cells treated with NaN_3 as a function of NaN_3 concentration and incubation time.

The purpose of this further analysis was to counter check the validity of the method via measuring the fluorescence intensity of supposed dying cells. Positive results were obtained: increasing the concentration of NaN_3, the fluorescence, therefore the viability of the cells, decreases, as expected. To note that the control sample at early incubation times analysis shows very low viability, confirming the decision of selecting the 24h time lapse to proceed with the studies. Concerning the data of concentration 100 µg/mL of NaN_3 and of several incubation times are not visible in the histogram, due to negative values obtained after the data evaluation, meaning that no metabolic activity occurred. This is the reason why it was imposed a limit of detection at ~100 counts of fluorescence intensity (see Figure 5.2.15, the fluorescence intensity of the sample composed of media was detected at 113 counts). The statistical evaluation of those data confirmed the differences among the highest concentrations of NaN_3 and the longest incubation times with the rest of the samples.

In order to know whether the control sample (U937 cells native and the addition of AlamarBlue® dye) showed similar results at each new measurement, some statistical analysis was faced. All the control fluorescence intensity detected in the following tests were compared using the t-test, showing no significant different among each other except for two cases (the control of the well plate containing core-doped QDs in Test 2 and the case of the well plate containing $CdCl_2$ and $FeCl_2$ in Test 3.b), which had values lower than the average of the rest. In the present study the control samples considered range within 25000 and 35000 counts of fluorescence intensity.

Determination of effective concentrations - Test 1

The first set of experiments consisted of the evaluation of potential cytotoxicity incubating NAC-CdTe QDs for 24 hours and repeated for 18.5 hours while using a fixed cell density of 50000 cells/mL. In this first step, the concentration values were 0.05, 0.1, 0.25, 0.5 and 0.75 µg/mL, as shown in the Figure 5.2.8.

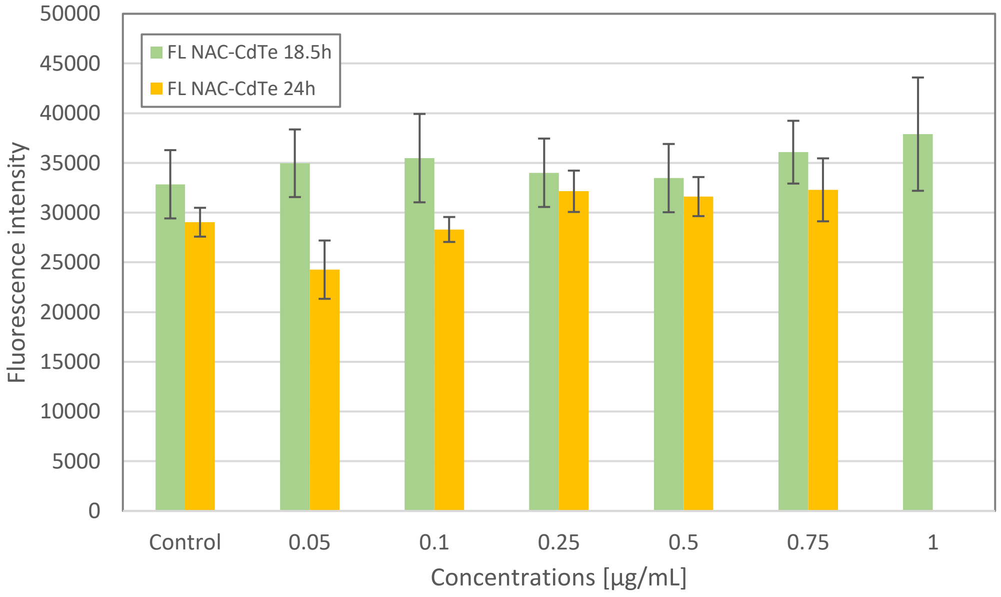

Figure 5.2.8. Dose-response relationship of U937 cells incubated with NAC-CdTe QDs after 18.5 and 24 hours (green and yellow bars, respectively). The fluorescence intensity was normalized related to the control (untreated) sample.

It is important to note that all samples need to be background corrected, which is described in more detail in Material and Methods chapter, AlamarBlue® assay section. However, for this first set of experiments the fluorescence signal of the sample composed of QD, media and AlamarBlue® could not be detected as those samples were not included in the preparation of the Test 1. The background correction in this very case consisted of the subtraction of the signal of the sample composed of AlamarBlue® and media from the total detected signal. The Figure 5.2.8 shows that it would be possible to state that there is no influence on the viability from the Quantum Dots presence. Even if the concentration values of the QDs increases, the fluorescence signal does not vary significantly from the control reference. After evaluation with statistical tool, t-test (see section in Material and Method, Statistical data analysis), significant difference has been found between the sample of bare-QD after 24h at 0.05μg/mL and the rest of the data. Significant difference is found also among the control and the 0.75, 0.5 and 0.25 μg/mL, after 24h. on the contrary, difference between the control and the 0.1 and 0.05 μg/mL samples after 18.5h is found. Despite those differences observed, it would be possible to assume that those concentrations of QD did not induce toxicity to the cells: the lowest value of fluorescence detected (at 0.05 μg/mL) corresponds to 83.6% and of the respective controls, within the limits of variation of the control sample. It could be therefore assumed that the No Observable Effect Level (NOEL) value for QD is above 1 μg/mL.

Attempts for method improvement increase of QD concentrations - Test 2

In this second set of experiments the potential toxicity of three types of QDs was evaluated: NAC-CdTe NAC-CdTe/30%Fe:ZnS and NAC-30%Fe:CdTe/ZnS QDs. Considering the results from the first set of experiments, in order to be able to detect any influence of the QD on the viability of the selected cells, the concentration values of the QD needed to be increased. Therefore, for each QD type, six new different concentration values have been chosen for this test: 0 (control sample), 0.25, 0.5, 5, 12.5, 25 and 50 μg/mL. The QDs were incubated for 2, 4, 17.5 and 24 hours while using a cell density of 50000 cells/mL and adding the AlamarBlue® stain (10% v/v), as shown in Figure 5.2.9.

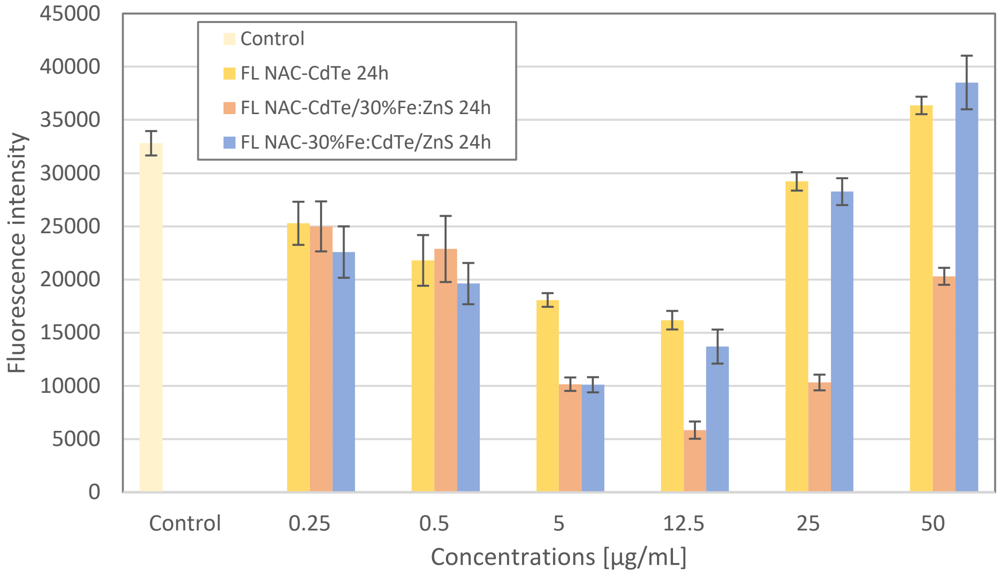

Figure 5.2.9. Comparison of fluorescence intensity of the U937 cells, incubated with NAC-CdTe (yellow), NAC-CdTe/30%Fe:ZnS (orange) and NAC-30%Fe:CdTe/ZnS (blue) and 20% in volume AlamarBlue® stain.

As in the previous step, the background correction consisted of the subtraction of the signal of just AlamarBlue® and media sample from the total detected signal. Figure 5.2.9 shows the comparison among the three QD types after 24h of incubation. The fluorescence intensity detected in this set of tests, which directly reflects cell viability, shows a non-expected behaviour: with the increasing of the concentrations, the viability decreases and after a turning point it constantly increases. The expected result was of an increasing-decreasing dose-response behaviour. From the statistical evaluation of these samples overall almost all the samples are significantly different among each other, confirming the behaviour observable in the Figure. An explanation for this unexpected fluctuation could lie in possible dilution or pipetting errors. Therefore, further experiments were necessary to carry out.

Concerning the evaluation of the other four incubation times (shown in Annex, Figures 10.4.1 and 2) for each QD type the behaviour of the viability of the cells does not show significant and reproducible results. Because of this and because of the results obtained with the method calibration analysis, the results shown in this study represent the fluorescence intensity detected after 24h of incubation of samples composed of QD dilutions and 50000 cells/mL. Nevertheless, an example displaying the fluorescence intensity of shelled-doped QD and U937 cells detected after each incubation time is shown in Figure 5.2.10 to confirm the data selection of this study.

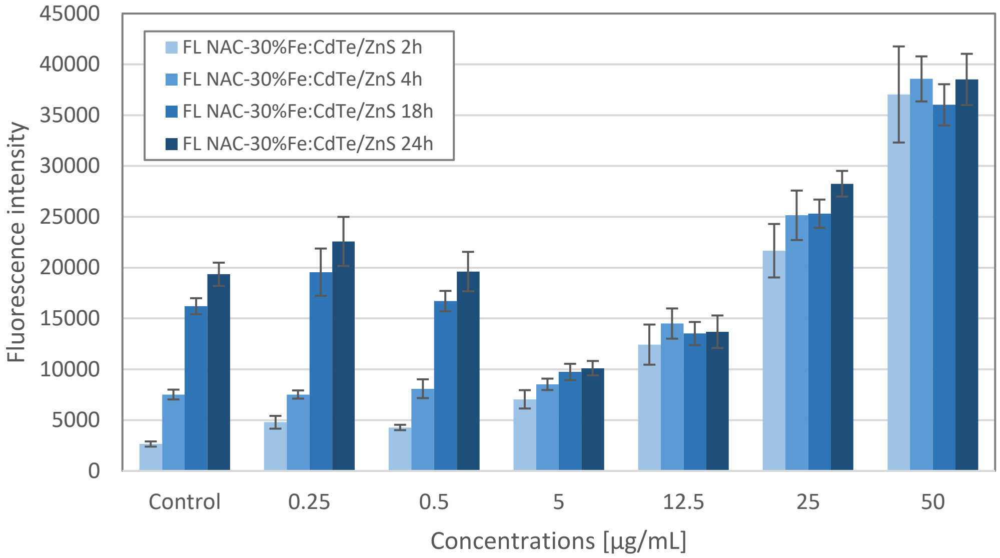

Figure 5.2.10. Fluorescence intensity of U937 incubated with NAC-30%Fe:CdTe/ZnS and 20% volume AlamarBlue® stain for 2, 4, 18 an 24h. For each concentration value, the incubation times are grouped, from the shortest to the longest.

As shown in Figure 5.2.10, for very short incubation times (2 and 4h) the fluorescence detected reached very high values with the increasing of the concentrations. This could be potentially related to the initial cell stress and the possibility of detection of only QD signal. To note that the data of fluorescence detected right after the sample preparation always showed negative and fluctuating results, possibly cause by initial cell stress. Moreover, no trend could have been described as dependence among concentration and incubation time. On the other hand, the 20h incubation time usually reflects the behaviour of the viability assessed in the 24h case. Thanks to the t-test evaluation, to significant difference was detected within the samples measured at difference incubation times composed of the same concentration of the QD, for values of 12.5, 25 and 50 µg/mL. For lower concentration samples significant difference was observed among the two longer and the two shorter incubation times (18, 24 h and 2, 4h). The concentration samples at 50 µg/mL is significant different form the rest of the data. The incubation times 18 and 24h samples for the control and for the concentration samples at 0.25 and 0.5 µg/mL differ significantly from the samples at concentration of 5 and 12.5 µg/mL.

Determination of dose-response curve and IC_{50} values and $CdCl_2$ and $FeCl_2$•H_20 samples – Test 3.a-b

At the second set of experiments bare-QD, shelled-QD, shell-doped and core-doped QDs were tested, whereby the optimized and previously described protocol was used. The concentration values considered in Test 3.a were initially of 1, 10, 25, 50 and 100 µg/mL, and later in Test 3.b with the addition of 75 µg/mL dilution. They were then incubated with 5 × 10^4 cells/mL of U937 cell suspension and 20 µL of AlamarBlue® stain for 0, 2, 4, 20 and 24 hours. Figure 5.2.11 shows the reduction in fluorescence intensity after 24 hours incubation with the four types of QDs and with $CdCl_2$ for comparison, for Test 3.a.

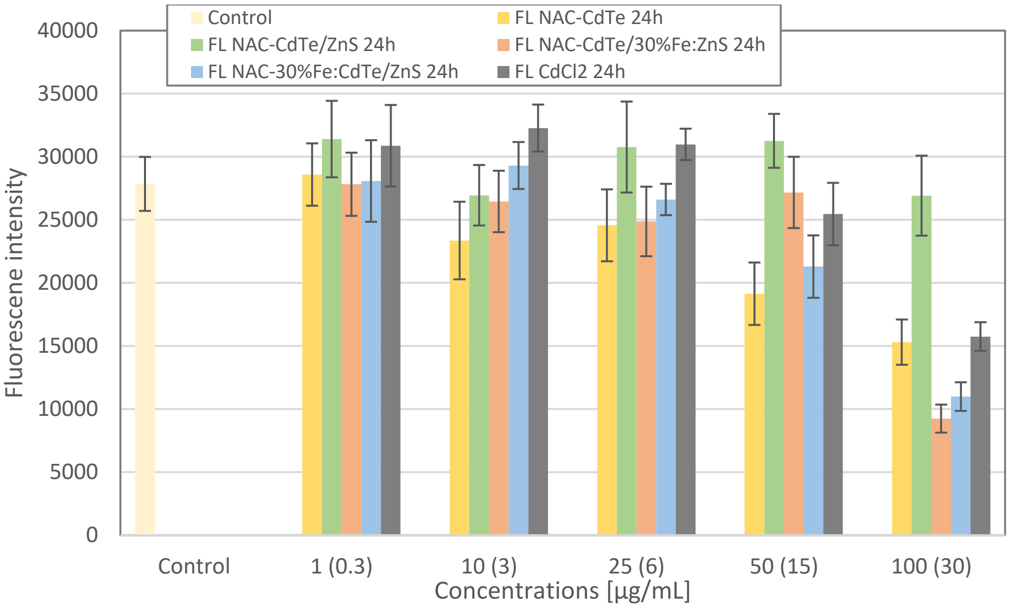

Figure 5.2.11. Comparison of fluorescence intensity of U937 incubated with AlamarBlue® stain and with NAC-CdTe, NAC-CdTe/ZnS, NAC-CdTe/30%Fe:ZnS, NAC-30%Fe:CdTe/ZnS and $CdCl_2$ (concentration values of $CdCl_2$ are shown in brackets).

To compare QD-specific effects with those from their ionic counterparts, dissolved Cd^{2+} and Fe^{2+} in form of $CdCl_2$ and $FeCl_2$, respectively, were studied. The $CdCl_2$ solution, in concentration values of 0.3, 3, 6, 15 and 30 µg/mL and the $FeCl_2$ in concentration values of 0.12, 1.2, 3, 6, 9 and 12 µg/mL. These concentrations correspond to the elemental concentration contained in the QDs, as described in the Material and Methods chapter. The solutions were incubated as well with 5 × 10^4 cells/mL of U937 cell suspension and with 20 µL of AlamarBlue® for 0, 2, 4, 20 and 24 hours.

Generally, it is assumed that cell viability reduces with increasing QD (mass) concentration, with exception of the shelled-QD case which caused almost no decrease in viability of the cells. This behaviour could be explained by the use of an old batch of NAC-CdTe/ZnS powder, therefore not properly dissolving after dilution. For all the rest of QD types, cell viability shows a clear drop after the concentration step of 50 µg/mL, 15µg/mL for $CdCl_2$. At 100 µg/mL all the QDs and $CdCl_2$ except for the QDs NAC-CdTe/ZnS, present a reduction of the fluorescence greater than 40%. Because of this significant drop in fluorescence detection (viability of the cells) between the values 50 and 100 µg/mL, a further concentration value needed to be evaluated, which results are displayed in Figure 5.2.12. As well for this test (3.a) statistical evaluations were made. The t-test showed significant difference between the control sample and the concentration of 100 µg/mL for the QDs and the Cd except the shelled type. Further statistical analysis was made among each concentration samples. Within the concentrations of 100 and 50 µg/mL, no significant difference is observable among the shelled-QD sample at 100 µg/mL and all the samples at 50 µg/mL, the rest is all significant different. At 50 µg/mL just the two samples of bare and core-doped QDs differ significantly from the control and the shelled, shell-doped and Cd samples at the same concentration. Comparing the 50 and the 25 µg/mL concentrations, it is important to note that the bare-QDs for the first are significantly different form the rest of the samples at the second, and the Cd between those two concentrations differs as well. Within the concentration of 25 µg/mL Cd and bare, shell-doped and core-doped QDs show significant difference, the only sample showing difference with the control sample is the Cd solution one. After the comparison between the concentrations of 10 and 25 µg/mL, it was visible a significant difference among the Cd sample of the first and the bare, shell- and core-doped QDs samples of the second. Moreover, the bare QDs sample at 10 µg/mL are significantly different form the Cd and the shelled QDs at 25 µg/mL. The sample of Cd at concentration 10 µg/mL results significant different from the bare, shell-doped QDs and the control samples. Among the lower two concentrations the Cd sample at 10 µg/mL is significantly different from the bare, shell-doped, core doped QDs samples at 1 µg/mL. however, in general the samples at 1, 10 and 25 µg/mL do not present many significant differences cases. The final samples at 1 µg/mL do not show any difference among each other.

As mentioned in the Materials and Methods chapter, in the sample preparation section, according to the results obtained in the previous test, an additional concentration step had to be analysed. From the fluorescence intensity detection (Figure 5.2.11) and from its statistical evaluation it was possible to assume that the major influence started happening at 50 µg/mL and in particular at 100 µg/mL. Consequently, the following test was carried out to observe if a further concentration in between would show higher viability reduction than the previous step or still no observable significant influence. Moreover, after having analysed potential influence of the Cd counterparts, it was decided to study the potential effects showed by the Fe counterparts, present in the doped-QDs. To note that for this test (3.b) a fresher batch of powder shelled-QDs was used for the QDs dispersions. Figure 5.2.12 shows the reduction in fluorescence intensity after 24 hours incubation with the four types of QDs and with $CdCl_2$ and $FeCl_2$ for comparison, and the additional concentration value of 75 µg/mL (Test 3.b). The cells U937 (50000 cells/mL) were incubated with 1, 10, 25, 50, 75 and 100 µg/mL of the four types of QDs. They were additionally incubated with $CdCl_2$ in Cd-based concentrations of 0.3, 3, 6, 15, 22.5 and 30 µg/mL, and with $FeCl_2$ in Fe-based concentrations of 0.12, 1.2, 3, 6, 9 and 12 µg/mL.

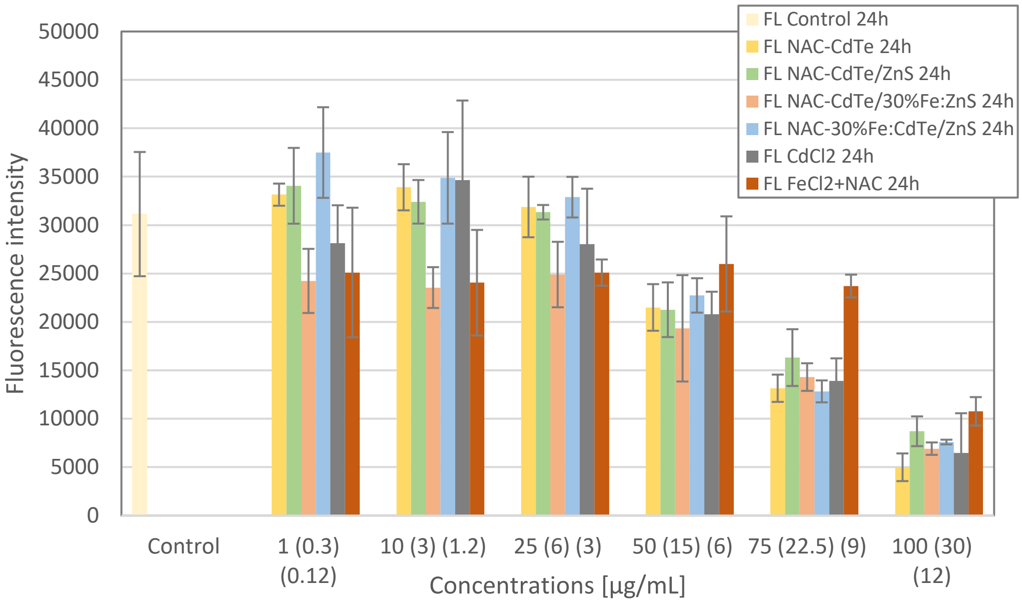

Figure 5.2.12. Comparison of fluorescence intensity of U937 incubated with NAC-CdTe, NAC-CdTe/ZnS, NAC-CdTe/30%Fe:ZnS, NAC-30%Fe:CdTe/ZnS, $CdCl_2$ and $FeCl_2$ (concentration values of $CdCl_2$ and then of $FeCl_2$ are shown in brackets).

Generally, it is assumed that cell viability reduces with increasing QD (mass) concentration. For all QD types, cell viability shows a clear drop after the concentration step of 50 µg/mL, and 15µg/mL for $CdCl_2$. At 100 µg/mL all the QDs and $CdCl_2$, present a reduction of the fluorescence greater than 40%. To note that in this new test set, the viability of the cells incubated with the shelled-QD is not almost constant as in the previous test set, but it decreases. This may be explained due to the use of a fresher batch of QD powder, which tends less to aggregation after dispersion. Overall, the QDs may be toxic at concentrations higher than 50 µg/mL: also at the concentration of 75 µg/mL the viability of the cells is influenced by the presence of the QDs and $CdCl_2$ solution. Finally, for this test the statistical Welch t-test was run. It is important to note that there was significant difference between all the samples types at 100 µg/mL and all the rest of the concentrations and the control samples, confirming the assumption of toxicity at high concentrations. Comparing the samples at 100 µg/mL with the samples at 75 µg/mL, it was found that the fluorescence intensity of iron at 75 µg/mL is significantly different from all the samples at 100 µg/mL. The only exceptions of no difference found are among the iron samples at 100 µg/mL and the samples at 75 µg/mL; and the shelled and shell-doped QDs at 100 µg/mL among the bare, shell, core-doped QDs and Cd counterparts. The comparison with the concentration value of 75 µg/mL the significant difference is observable among the QD types or $CdCl_2$ and the $FeCl_2$ and the control sample. Comparing the fluorescence intensity of the samples at 75 µg/mL and the rest it was observed always significant difference, confirming that also at this concentration value the QD may influence negatively the cell viability. The only fluorescence intensity at 50 µg/which differs significantly from the control sample is the one related to the shell-doped QDs, the rest odes not. No significant difference was detected between the shell-doped, cd, Fe samples at 25 µg/mL and the samples at 50 µg/mL, the rest significantly differ. The same is valid comparing the 50 µg/mL samples with the ones at 10 and 1 µg/mL, excluding the Cd samples. Within the concentration of 25 µg/mL the bare, shelled and core-doped QDs are significantly different form the iron fluorescence, but not form the Cd or from the shell-doped QDs. Samples of shell-doped QD and iron counterparts at concentrations of 1, 10 and 25 µg/mL do not differ from the samples at 50 µg/mL. Concerning these low concentration samples, the only significant differences found were among the shell-doped QDs and the iron counterparts.

As already shown in Figure 5.2.12, in Test 3.b in order to observe potential further influence, $FeCl_2$ in concentration of 0.12, 1.2, 3, 6, 9 and 12 µg/mL were incubated with the U937 cells and tested as well, beside the $CdCl_2$ solution assessment. The Figure 5.2.13 shows the comparison among the fluorescence intensity detected after 24h of incubation of $FeCl_2$ (orange) and of $CdCl_2$. The fluorescence intensity of the Fe ions shows as well variation in viability of the cells compared to the control sample.

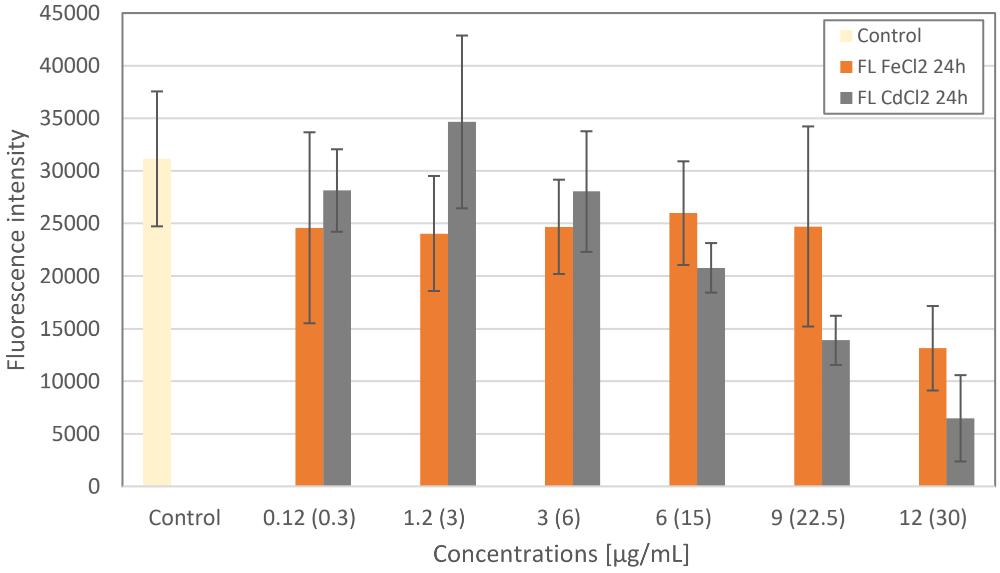

Figure 5.2.13. Comparison of fluorescence intensity of U937 incubated with $FeCl_2$ (concentrations in brackets) and $CdCl_2$.

The viability of the cells is reduced of ~20% when incubated with Fe counterparts' concentrations within 0.12 – 9 µg/mL, therefore showing a certain influence but still within the level of npn-toxicity. On the contrary, Cd counterparts show toxicity influence when incubated at 22.5 µg/mL (9 µg/mL Fe respective concentration). However, a significant drop occurs at the highest concentration of Fe counterparts (12 µg/mL), which could be explained by a potential inhibition of the metabolic activity of the cells. Statistical evaluation was carried out to show that the samples at high concentration values (15/6, 22.5/9 and 30/12 µg/mL) present significant difference among each other, which does not occur at the low concentrations (0.3/0.12, 3/1.2 and 6/3 µg/mL). Moreover, the samples incubated with $CdCl_2$ and with $FeCl_2$ were statistically compared with the control sample. Concerning the Cd case significant difference was found among the concentration samples at 22.5 and 30 µg/mL, confirming a similar behaviour as the QDs of important influence on the viability of the cells from 22.5 µg/mL on. According to the t-test made on the Fe sample the only case of significant difference with the control occurred at the 12 µg/mL sample, showing that potentially also the iron counterpart may induce some negative effects to the cells when their concentration is high.

Calculation of IC_{50} values

The IC_{50} values express the concentration at which half of the total population has been inhibited by the substance under analysis. These values give further information concerning the toxicity of the QD. Figure 5.2.14 below shows the sigmoidal function regression calculated with the data from obtained after Test 2 analysis. The calculated IC_{50} values were 62.5 µg/mL for bare-QD, 66.3 µg/mL for shelled-QD, 79.5 µg/mL for shell-doped QD, 57.9 µg/mL for core-doped QD and 21.5 µg/mL for Cd ions in $CdCl_2$. The value of R^2 are very near the maximum value of 1, which means a good fitting regression to the original available data. The calculated concentrations are shown in the Table 5.2.1.

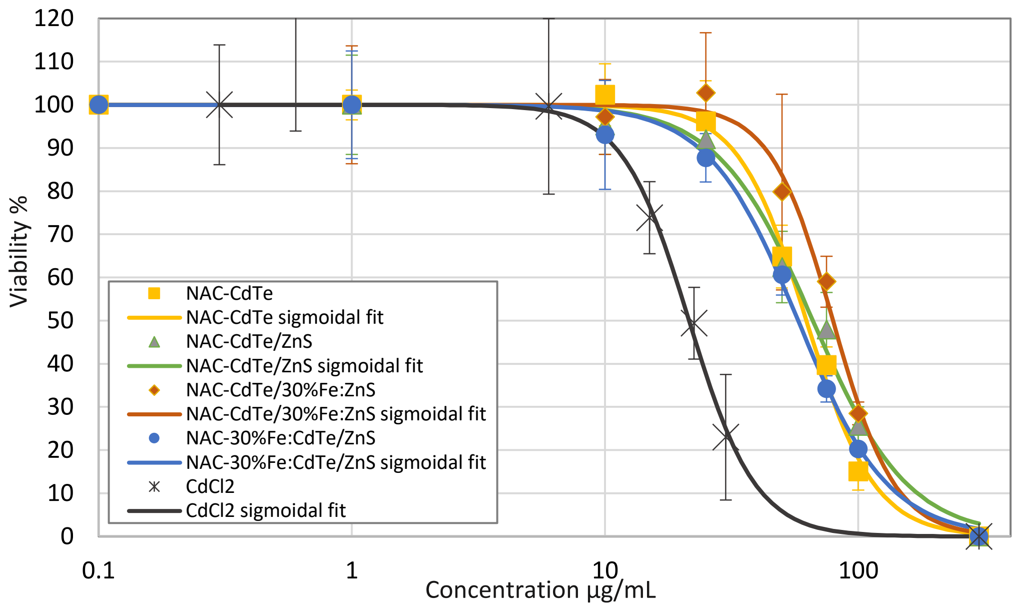

Figure 5.2.14. Sigmoidal function for curve fitting, exposure-concentration graph, with QDs concentrations from the second set of experiments, in logarithmic scale, % fluorescence signal for viability (inhibition of the cells), calculation of IC$_{50}$ values for each different QDs type.

Table 5.2.1. IC$_{50}$ values, with standard error R^2 from sigmoidal curve fitting after 24h incubation of QDs/Cd and U937 cells.

IC$_{50}$ values - 24h incubation		
QD type	IC$_{50}$ St. Error	R^2
NAC-CdTe	62.5 ± 1.03 µg/mL	0.99571
NAC-CdTe/ZnS	66.3 ± 1.04 µg/mL	0.99111
NAC-CdTe/30%Fe:ZnS	79.5 ± 1.03 µg/mL	0.99199
NAC-30%Fe:CdTe/ZnS	57.9 ± 1.03 µg/mL	0.99489
$CdCl_2$	21.5 ± 1.09 µg/mL	0.9438

The IC$_{50}$ for cadmium is 21.5 µg/mL, three times higher than the IC$_{50}$ values for the QD, it shows higher toxicity compared to the nanoparticulate counterparts. This confirms how the decomposition of QDs and the consequent leaching of Cd ions could be avoided by the presence of the coating layer (organic ligands, NAC layer). Moreover, from these data two possibilities may explain the trigger of adverse toxic effects. The first one is the release of Cd^{2+} and other toxic heavy metals from the inorganic core/shell materials. Additionally, some QD may present HDD values of about 5.5 nm, and therefore they may be able to penetrate into cells, leading to oxidative stress.

Fluorescence intensity signals and background corrections

In this study, and in specific in Test 1 and 2, background correction was the subtraction of the signal of AlamarBlue® and media from the fluorescence intensity detected from the samples composed of same QD type and concentration incubated with cell culture U937 in media and the addition of AlamarBlue® (treated sample). After the first attempts and the related analysis of the data, a further subtraction of fluorescence intensity signal of the QD themselves appeared to be necessary. Therefore, in Test 3 (a and b), the background correction consisted of the subtraction of the fluorescence intensity of QD dispersed in media with the addition of AlamarBlue® from the treated sample. In this way the signal of only the metabolic activity of the cells is obtained. In order to understand the influence of each different sample on the detected fluorescence intensity, the Figure 5.2.15 shows the fluorescence values of media, of AlamarBlue® and media, of QD dispersed in media and the addition of AlamarBlue®, of only QD, of before and after the background correction.

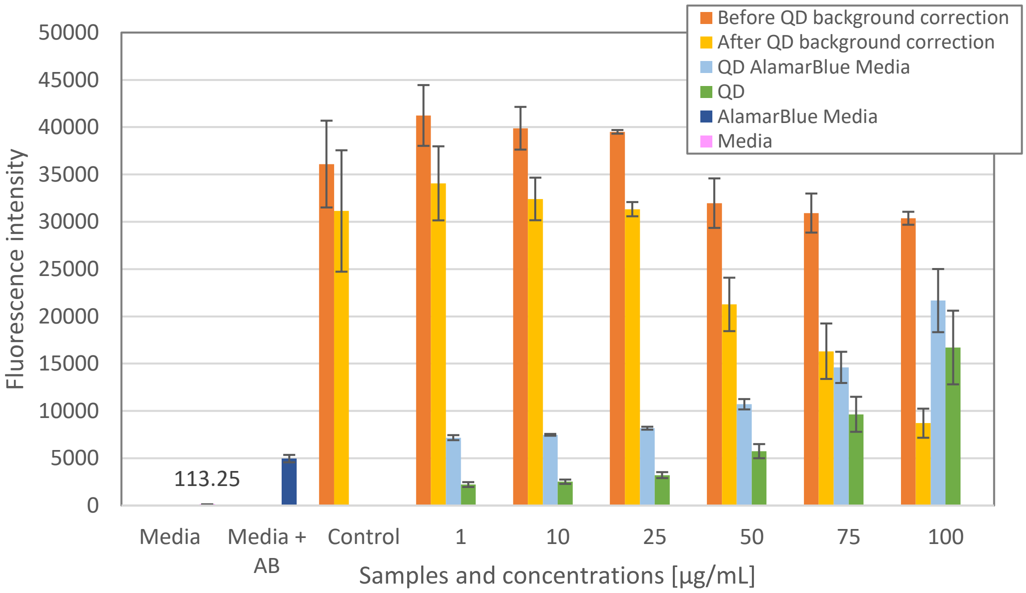

Figure 5.2.15. Comparison of fluorescence intensity values of media, media and AlamarBlue®, background correction, QD, and of before and after background correction samples. Data from shelled-QD incubated with U937 for 24h.

To note that the signal of only QD was obtained subtracting the intensity of AlamarBlue® and media from the sample composed of QD dispersed in media and the addition of AlamarBlue®. To note that data from the fluorescence detection of shelled-QD incubated with U937 cells for 24h was considered as a general example. As expected, the fluorescence intensity of these (and consequently of the QD dispersed in media with the addition of AlamarBlue®) increases with the increasing of the selected concentration values. To note that the signal of the sample composed of only media is very low, and almost negligible compared to the other samples. From this Figure it is important to observe that the background correction is fundamental in order to obtain realistic results: without any background correction the viability would not significantly vary and would not display any QD influence.

Figure 5.2.16 allows to compare the fluorescence intensity signals of not corrected samples, of background correction results, and of AlamarBlue® and media correction. The correction of the treated sample with the signal of AlamarBlue® and media only shows the same pattern as if no correction were made. On the contrary, subtracting the QD signal as well reveals the effective variation of the metabolic activity (hence, the viability) of the cells, allowing to observe the effects caused by the incubation with the QDs.

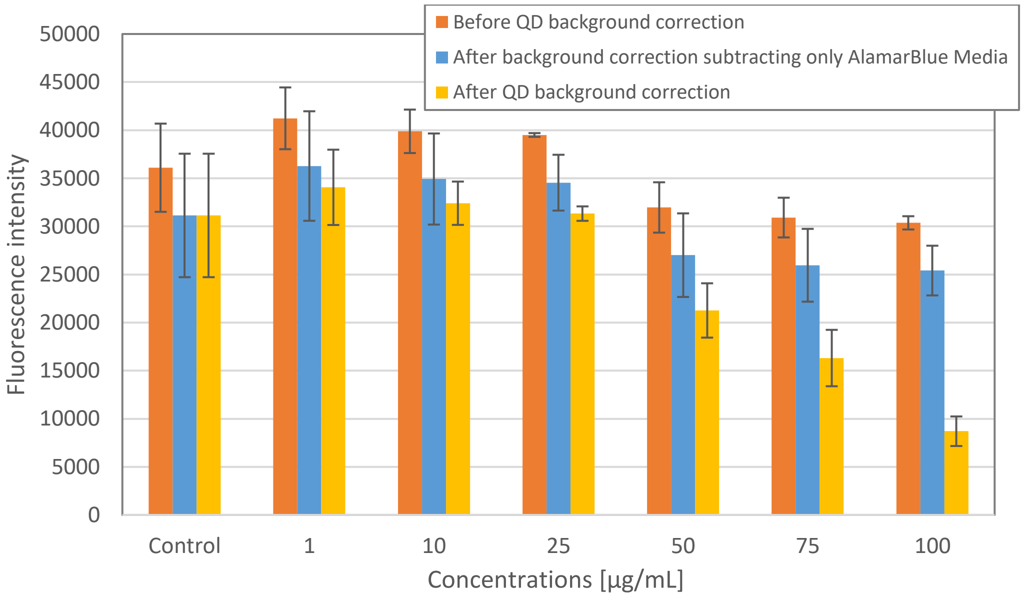

Figure 5.2.16. Comparison of background correction with only AlamarBlue® and media and background correction comprehending the QD fluorescence intensity.

5.2.3 Localization of quantum dots

Further analysis with the CLSM have been conducted in order to attempt to localize the QDs in U937 cells. The aim was to better understand the potential uptake and interactions of the QDs with the cells. The studied sample was composed of 5 × 10^4 cells/mL incubated with the four QD types for 24 hours.

After fixation, the samples have been analysed using CLSM (see also Material and Methods chapter). Figure 5.2.17 shows a representative CLSM image of localized NAC-CdTe/ZnS Quantum Dots (as red dots), in a relatively low concentration of 1 µg/ml and after 24 hours of incubation.

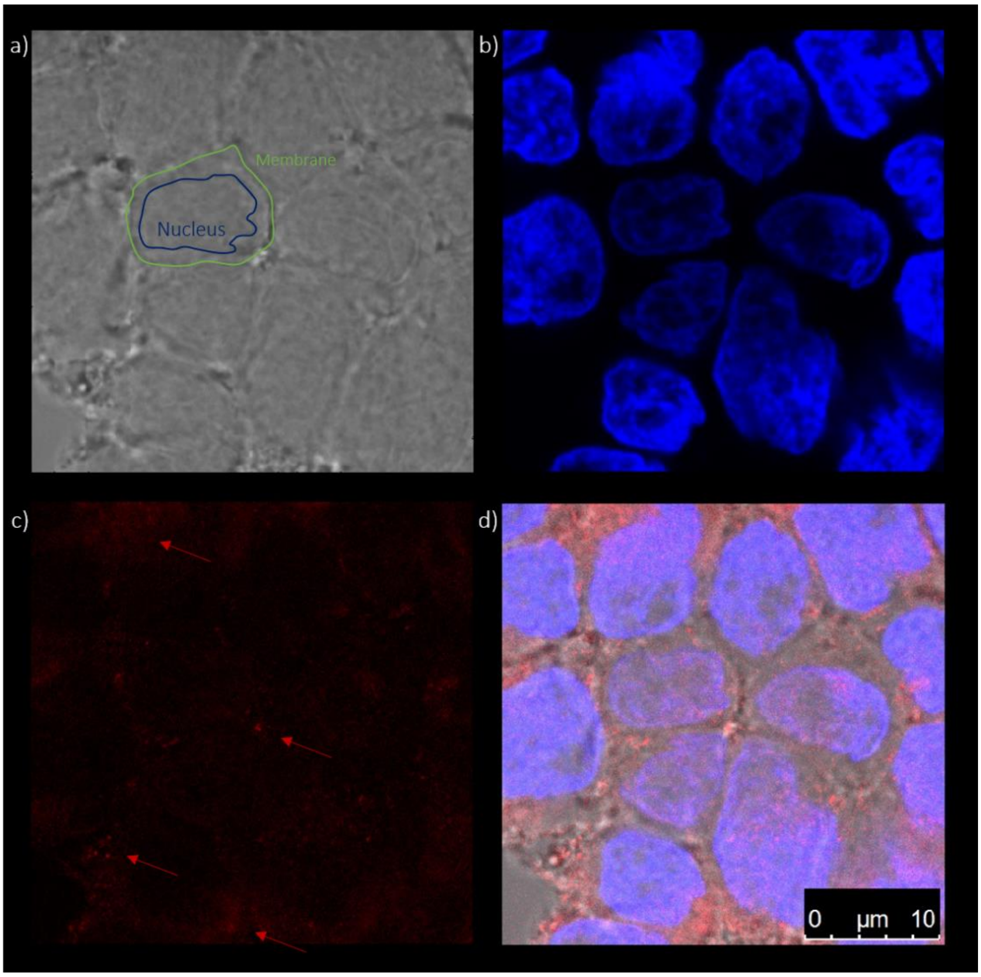

Figure 5.2.17. Localization of NAC-CdTe/ZnS Quantum Dots, 1 µg/mL, after 24 hours of incubation, using confocal laser scanning microscopy. Bright field image of U937 macorphages(nucleus and membrane depited) (a). Fluorescent image of illuminated nuclei (stained with Hoechst) with DAPI filter channel (b). Fluorescent image of illuminated quantum dots (red arrows) (c). Overlay of the three micrographs (d).

Inset (a) the bright field image of QDs, where it is possible to see the cell morphology including cell membranes and nuclei are visible. DAPI filter channel was used to illuminate the nucleus, previously stained with Hoechst 33342 (see Material and Methods chapter). In inlet (b), it is possible to clearly see the nuclei (blue) of the cells from the previous picture. As the figure shows, the macrophages are composed mainly of nucleus. Inlet (c) reveals the presence of the QDs which tend to form small aggregates. Finally, the three fields have been overlaid (d) to visualize better the correlated position of nuclei and quantum dots.

Based on the 2D Figure a clear accumulation of QD in the cytoplasm can be observed, and it could be preliminary assumed that QDs also penetrated the cell nuclei. To ensure if the internalization of the QD in the nuclei occurred or not, z-stacks have been taken. The 3D visualization, Figure 5.2.18, based on these z-stacks allowed to verify that the QDs were internalized inside the cells but not inside the nuclei.

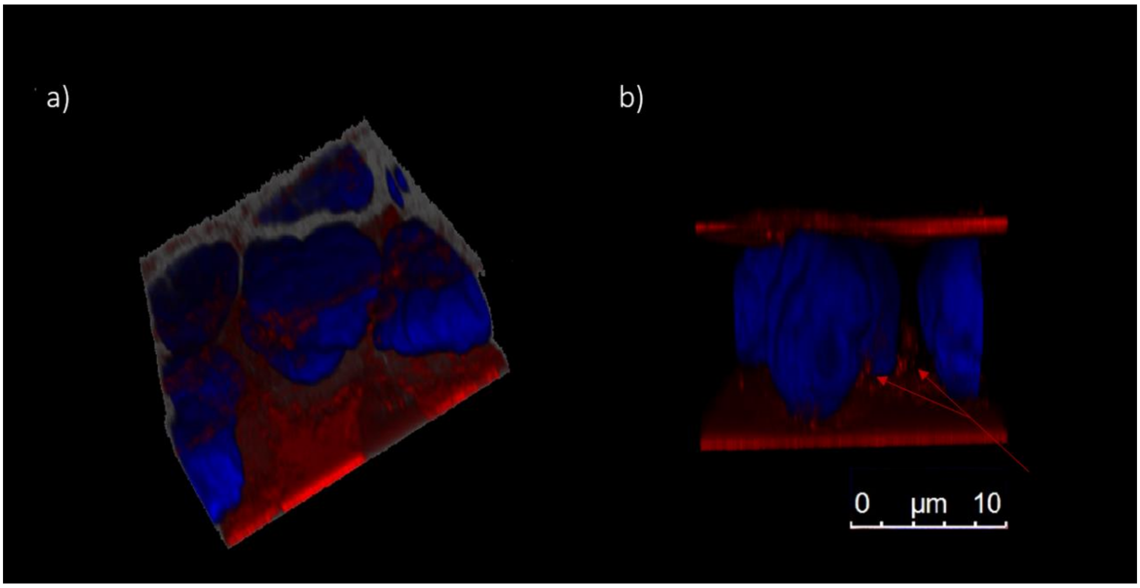

Figure 5.2.18. Localization of NAC-CdTe/ZnS QD 1 µg/mL inside the U937 samples after 24 hours of incubation, 3D visualization. NAC-CdTe/ZnS red dots, figure a). NAC-CdTe/30%Fe:ZnS red dots, figure b). Nuclei of the macrophages are enlightened in blue colour. Quantum dots are not localized inside the nuclei, but on the bottom and top layer of the sample and between the cells, probably inside their cytoplasm.

Figure 5.2.18 reveals that the majority of the QDs, indicated as red dots, are grouped on the bottom and top layer of the sample. This means that only a small part of QDs was internalized into the cells, which is highlighted with arrows in red. Therefore, it could be assumed that larger QD aggregates do not penetrate the cell membrane, whereas smaller aggregates are able to be internalize. However, the uptake mechanisms are still not fully understood and needs to be examined in future studies.

Both the previous two Figures 5.2.17 and 18 show that even at very low concentrations (1 µg/mL), the QDs were uptaken by the cells. Despite no relevant reduction in viability could be observed based on the AlamarBlue® assay results, this new finding leads to the assumption that QD exposure rather lead to chronic than to acute toxicity.

5.3 DISCUSSION OF OBTAINED RESULTS

The results obtained from the optical analysis show that the QD used in this study (100 µg/mL, dispersed in ultrapure water) tend to importantly aggregate after 18 days. Further aggregation phenomena may occur very likely also previous the measured time. An example is shown in the inter-laboratory study of Piret et al. (2016), who compared the mean diameter of Ag and CuO nanoparticles (100 µg/mL) measured with DLS and CLS right after the dispersion in ultrapure water media and after 24 h. Ag NP showed mean diameter values of 20 and 116 nm at 0h and 24h, respectively. CuO increased the diameter from 41 nm at 0h to 68 nm after 24h. Moreover, the measured mean diameter of the same nanoparticles merged with cell culture before and after incubation. The results did not show significant difference in the size of the particles, agreeing with the results obtained in this study: the higher toxicity was assessed after 24 hours of incubation, therefore the QD stayed unaggregated and penetrated inside the cell damaging it. From this it may be assumed that also the QD in this study would aggregate more after longer time if left in stock solution, but they would potentially less after merging with cell suspension. As a matter of fact, the results from both the flow cytometry and the AlamarBlue® assay analysis in the present research show potential toxicity after 24h of incubation of cells with QDs. If all the QDs did aggregate as well when merged with cell suspension and incubated, no variation of the viability and high and low values of fluorescence intensity would have been expected via AlamarBlue® assay and flow cytometry, respectively. The latter case showed the appearance of a secondary peak with increased fluorescence intensity after treatment with QDs (bare-QD, 100 µg/mL) of the CHO cells. This was not present in the data of untreated CHO cells. Moreover, also after staining the untreated sample with PI, a very similar result as for the unstained treated one was obtained: a secondary peak at higher fluorescence intensity was created. The PI stain could penetrate only through damaged cell membranes, therefore this allowed to hypothesize that QD internalized inside the cells. The presence of the QDs may have harmed the membranes of the cells and the cells themselves, while being uptaken by them, consequently the stain was enabled to penetrate through the damaged membranes. Moreover, it was not possible to detect samples composed of only QD and ultrapure water, because of the small size of the particles, below the threshold limit of event-detection in flow cytometry. Therefore, if usually QD cannot be spotted, if a secondary peak at higher fluorescence occurred when cells were incubated with QDs and if the PI stain could be clearly measured when the cells were treated with QDs, it was consequently assumed that QDs managed to internalize into the QDs in the cells. The results from flow cytometry of the present study find confirmation in the results of Lai et al. (2013) research. They analysed the toxicity of CdTe QD coated with either NAC, MPA or GSH. Among the several methods used they analysed with flow cytometry the membrane permeability of *E. coli* untreated and treated with GSH-CdTe (hydrodynamic radius of 5.22±0.07 nm, 0.6 and 1.2 µmol/L), stained with PI dye. They analysed the samples after 4h of incubation and obtained very similar results to the present study: in the treated sample a secondary peak at higher fluorescence signal was detected. They concluded that the membrane permeability was significantly affected by the QDs themselves, and because of this the PI stain penetrate trough the harmed membranes (Lai et al., 2013). However, due to difficulties in obtaining the optimum parameter settings and due to potential overlapping of the stains used and the QDs spectra, in this study it has been decided to proceed the evaluation of toxicity and the establishment of a method to accomplish this via using the AlamarBlue® assay. Several attempts were necessary in order to reach expected results. Comparable results were obtained in the study of Ulusoy et al. (2014), in which they examined with CellTiter Blue assay (same principle as AlamarBlue® assay) the toxicity of Cd-based QD, CdTe/CdS (mean diameter of 3.68±0.74 nm), CdTe/CdS/ZnS (mean diameter of 4.31±0.76 nm), at concentrations within 0.002 – 600 µg/mL, on A549 carcinoma lung cancer cells. They observe no influence after only 2h of incubation, on the contrary after 24h of incubation at higher concentration values the viability decreased. Between 100 – 600 µg/mL concentrations the viability reduced of more 70% for the ZnS shelled QDs and for the thin shelled QDs, the thick shelled-QDs reduced the viability of ~50%. Small non-shelled QDs at 70 µg/mL reduced the viability of ~40%, the rest of QDs at 70 µg/mL and at the remaining concentrations induced <30% viability reduction. (Ulusoy et al., 2014). Another study from Derfus et al. (2004) assessed the viability of hepatocytes incubated with MAA-CdSe or TOPO-CdSe QDs (λ_{em} = 582 nm) at 0.25 and 0.0625 mg/mL with MTT assay (Derfus et al., 2004). They evaluated three cases: standard conditions (inert atmosphere QD storage), exposure of QD to air for 30 minutes, exposure to UV light within 1 and 8h, showing toxic influence, decrease of the viability from 98 to 21% (for 0.0625 mg/mL) and decreasing of 6% after 1h, 42% after 2h, 83% after 4h and 97% after 8h in viability, for the three cases respectively (Derfus et al., 2004). The QD in the present study were synthetized in inert atmosphere, stored in dark and closed environment but not in N_2 atmosphere. The results from the AlamarBlue® assay could be compared then to the second case of the Derfus study: at similar concentration, 75 µg/mL, the viability decreased to around 45%. Nevertheless, to note that the QD in the present study were coated with NAC ligands, antioxidant and biocompatible, and shelled by ZnS, inorganic layer, allowing therefore potentially slower degradation rate. Both the studies, from Ulusoy et al. (2014) and from Derfus (2003), hypothesized that the reason of toxicity was the release of Cd ions from the core of the QDs. However, just the latter study confirmed their assumption via measuring the Cd concentrations with ICP-OES for the three cases, obtaining: 6 ppm of Cd ions at standard conditions, 82 ppm after air exposure and 126 ppm after UV-light exposure. This confirmed that oxidant environment (e.g. air, light) induce the oxidation of selenide or sulphur, and therefore expose the core of the QD to further degradation, with the consequent release of the Cd ions. Those are likely to bind to sulfhydryl proteins in mitochondria, deactivating the thiol group, causing cell disfunction and possible cell death (Derfus et al., 2004). In the present study as well, it has been assumed that the principle reason of cell viability decrease could possibly lay on the release of Cd ions: the comparison among the viability of cells incubated with the four types of QDs, with the $CdCl_2$ solution and with $FeCl_2$, shows how the latter has partly lower influence on the metabolic activity of the cells (cell viability was reduced of ~65% only when incubated with 12 µg/mL, highest concentration, lower concentrations showed ~20% reduction). On the contrary, $CdCl_2$ shows viability reduction of ~30% already when incubated at 15 µg/mL (6 µg/mL respective Fe concentration) and reduction of ~45% already at 22.5 µg/mL (9 µg/mL for Fe). From the IC_{50} calculation $CdCl_2$ shows an important influence on the reduction of the viability of the U937 cells, its half inhibition concentration value (21.5± 1.09 µg/mL) is three times higher compared to the QDs ones, showing consequently more significant toxicity than the particulate counterparts. Moreover, the behaviour of viability reduction detected with the AlamarBlue® assay for all the four types of QD studied presents the same pattern as when cells were incubated with cadmium solution only. This allowed to assume that the cytotoxicity of the first case may have been caused by the presence of released Cd ions. Furthermore, the hypothesis of Cd^{2+} release as reason of cytotoxicity of the QD is given as well in the study of Kirchner et al. (2005), in which they incubated CdSe, CdSe/ZnS and Au QD (coated with MPA, silica shell or amphiphilic shell) with

MDA-MB-4355 breast cancer cells for 18h (Kirchner et al., 2005). Through studying the behaviour of adherent cells per labelled region on cell culture substrate, they measured the cytotoxicity of the samples and they managed to measure the concentration of Se, Zn and Cd ions of 40 µM and 0.48 µM, respectively. Even though the concentration of Se or Zn ions was higher they showed relative higher viability than in the case of Cd ions, confirming the assumption of Cd ions cytotoxicity as the reason (Kirchner et al., 2005). According to them not only the concentration of Cd^{2+} influence the viability of the cells, but as well the location where those were released: if the QDs were ingested by the cells, Cd^{2+} being already inside the biological system may cause far more sever toxicity, than if present only in the outer environment (phos-silica coated QD showed higher viability reduction and more internalization than the PEG-silica coated QD, which thanks to the different outer coating less nanoparticles penetrated) (Kirchner et al., 2005). The assumption of internalization proposed with the flow cytometry data analysis in our study found confirmation with CLSM detection. The images captured show the localization of NAC-CdTe/ZnS and NAC-CdTe/30%Fe:ZnS Quantum Dots, 1 µg/mL, after 24 hours of incubation with U937 cells. The combination of the 2D and he 3D visualizations allows to state that the QD internalized inside the cells but did not penetrate through the nuclei barrier. Kirchner et al. (2005) found as well how MPA, PEG-silane or amphilphillic coated CdSe/ZnS incubated with MDA-MB-435S for 18h were by them ingested. They analysed the samples with fluorescence microscope and differential interference contrast (DIC), observing internalized QD in the cells, adherent to the nucleus membrane, as in the case of the present study (Kirchner et al., 2005). However, the study of Lai et al. (2012) showed that MPA-CdTe (hydrodynamic raidus of 5.17±0.21 nm) in concentration of 0.5 and 1 µmol/L did not penetrate through *E. coli* cells, but just attached to their membranes damaging them. Via ICP-AES they calculated the amount of Cd ions attached to the surface and the amount in the suspension obtaining that only the 20% of the Cd ions were bound to the bacteria (Lai et al., 2013). Those examples confirmed how not only the nature of the QDs may induce toxicity, but the natural environment as the chosen cell line may partly influence it. One of the main key factors which influence cytotoxicity is the QD size: in general, the smaller the QD the higher the toxicity induced. This has been shown in the study of Zhang (2008). They compared the time of internalization of CdTe QD in spherical shape (11.2±2 nm of diameter) and CdTe in cylindrical form (20±2 nm diameter and 180±120 nm long, and larger with 30±2 nm diameter and 970±900 nm long) incubated with CHO cell line at 37°C for 1 h. The results from CLSM analysis showed that despite the higher surface to volume ratio of the cylinder QDs these were not ingested by the CHO cells, as occurred instead for the spherical ones (Zhang et al., 2008). The study of Ulusoy et al. (2014) as well confirmed that smaller QDs (CdTe/CdS, 3.68±0.74 nm) showed higher toxicity (IC_{50} of 83±1.2 µg/mL) than the bigger ones (CdTe/CdS/ZnS, 4.31±0.76 nm) showing lower toxicity (IC_{50} of 150.8±1.1 µg/mL) (Ulusoy et al., 2014). In this study, the measured HDD for bare-QDs was around 8.3±2.5 nm, the HDD of shell-doped 17.4±6.7 nm and the one of core-doped QDs was of 37.0±13.0 nm. The hypothesis of smaller QDs – higher toxicity may be valid in the case of undoped QDs, but not for the doped ones, causing a very similar viability reduction behaviour. However, it is important to note that the QDs of this research were coated with NAC ligands, which are biocompatible, hydrophilic and antioxidant. Hence, those characteristics may have allowed the QDs to penetrate through biological systems anyway.

Overall, the methods used in the different studies presented were always combination of viability assessment, as CellTiter Blue or MTT assay (as the AlamarBlue®) or counting of number of living cells, and the analysis of the samples through microscope images, as CLSM or TEM, to observe potential QDs internalization.

The study of Murray et al. (2017) presents common issues or mistakes when labelling NPs with fluorophores in order to localize them with e.g. CLSM or flow cytometry in intracellular environment (Murray et al., 2017). Even though, the NPs in the present study are QDs, hence already self-emitting fluorescence, some of the cases may be considered for this study as well, for example, non-specific binding of the fluorophores (in both flow cytometry and AlamarBlue® assay) (Murray et al., 2017). The stains used may have bound to buffer components or other molecules, therefore showing fluorescence signal mistaken for QDs influence on the cells or no viability reduction. They also listed as potential interference the interaction between fluorophores and noble metal NPs with strong magnetic field: the labels may interact with the field of the NPs. Fluorophores fluorescence could be enhanced by large NPs (> 30 nm) and be quenched by smaller NPs (<20 nm) (Murray et al., 2017). Despite the different nature of metal in the QDs, something similar may also occur in the present study concerning Fe doped-QDs, even though no reliable data can confirm this. Core-doped QDs having a HDD > 30 nm may enhance the fluorescence intensity of the reduced AlamarBlue® stain and therefore show higher values. On the contrary, shell-doped may quench the fluorescence intensity of the resazurin, showing lower values. In the Test 3.b of AlamarBlue® assay, lower fluorescence intensity of the shell-doped compared to the rest of the QDs were detected at low concentrations values (1, 10 and 25 µg/m L), which could be assumed as magnetic field quenching effect. However, further and more detailed are necessary.

6 SUMMARY

QDs are fluorescent semiconductors, characterized by very small size, that range from 2 to 10 nm. They are more and more utilized in different application fields due to their unique optical properties, such as high photostability and wide range of excitation and a very narrow emission wavelength. QDs are used in the biomedical field as, for example, fluorescent dyes – as photostable alternatives to organic dyes – for bioimaging. QDs are also mainly applied to electrical devices, specifically the QDs can be used as components in LED screens. However, their potential adverse effects on the environment are not fully understood.

The goal of this study was to evaluate the potential toxicity of four different types of Cd-based QDs. Each type was equipped with a CdTe core and a capping agent comprising of N-acetyl-L-cysteine. These organic ligands improve biocompatibility and show stabilizing effects. The QDs, which were provided in powder form, were additionally modified with magnetic agents. In particular, either the QD's core or the shell was doped with ferrous ions in order to obtain both fluorescent and magnetic properties, which would allow for fluorescence as well as magnetic resonance analyses. The additional goal of this thesis was to verify if there is a significant difference in toxicity effects of undoped and iron-doped QDs. For cytotoxicity assessment, two different mammalian cell lines were selected: CHO cells and U937 macrophages. A further goal was to develop a fast-screening and reproducible method to assess such ENMs. For this, flow cytometry and the AlamarBlue® assay, were used to assess the viability of QD-treated cells.

Flow cytometry analysis was conducted in order to detect fluorescence signal from a sample prepared with CHO cells incubated with NAC-CdTe QDs for various time lengths, and stained with 7AAD, Hoechst and propium iodide dyes. This last organic dye is able to penetrate only through the membrane of damaged or dead cells. Therefore, if a high fluorescence signal was detected, it could have been assumed that damaged/dead cells were present. The goal was to assess the potential cytotoxicity of the nanoparticles, through spotting some difference of the fluorescence signal among the treated (with QDs) and untreated (without QDs) samples.

From the results obtained with the flow cytometer, it was possible to notice some differences among the single parameter histograms of untreated, treated and stained treated. The second showed the appearance of a secondary peak in fluorescence intensity which may be explained by the internalization of the QDs by the cells (the signal of the sample of only bare-QD could not be detected). Moreover, it was possible to notice some differences between the PI stained untreated (without QDs) and the stained-QD-treated samples after 24 hours incubation. In the histogram of the untreated sample the fluorescence was detected only at very low intensity values. On the other hand, concerning the treated one a clear QD-specific fluorescence peak was visible. The appearance of this new peak may be caused by the detection of dead/damaged cells and/or associated QDs. This increase in fluorescence intensity may be explained by the following two effects. The PI stain penetrates only into damaged/dead cells and because the higher fluorescence intensity peak was observed only in the treated sample after 24 hours of incubation. Hence, it could be assumed that the QDs may have damaged the membrane and consequently let the stain penetrate through the cells and therefore this characteristic fluorescence signal could be detected. It is also possible that QD association and/or uptake occurred after a couple of hours and led to such increase (note that pristine QD dispersions without the presence of cells triggered no fluorescence signals during flow cytometry analysis).

The viability of U937 human macrophages incubated with various increasing concentration values of Cd-based QDs, namely NAC-CdTe, NAC-CdTe/ZnS, NAC-CdTe/30%Fe:ZnS and NAC-30%Fe:CdTe/ZnS QDs was tested with the AlamarBlue® assay.

Based on the AlamarBlue® assay analysis, it was possible to have more detailed information regarding the dose-response relationship between QDs and U937 cells. The no observable effects level (NOEL) value for QDs was above 1 µg/mL, after incubation of U937 with NAC-CdTe at 0.05, 0.1, 0.25, 0.5, 0.75 and 1 µg/mL. A second test was carried out, exposing the macrophages to bare, shell and core-doped QDs, in concentrations of 0.25, 0.5, 5, 12.5, 25 and 50 µg/mL. However, no expected dose-response behaviour was observed. Therefore, a final set of experiments was held, incubating bare, shelled, core and shell-doped QDs with U937 macrophages. The QD concentration values, which were tested, ranged between 100, 50, 25, 10 and 1 µg/mL and in a second case 100, 75, 50, 25, 10 and 1 µg/mL. The results showed a clear relationship between the increasing concentration values of the QDs present in the samples and the decreasing viability. According to the ISO 10993-5 (2009) cytotoxicity standards a substance is considered not biocompatible when the reduction in cell viability is ≥ 30%. The obtained dose-response curves revealed that cell viability significantly decreased of more than 30% above concentrations of 75 µg/mL. This allowed to state that the QDs may cause acute toxicity towards living cells at concentrations higher than 75 µg/mL. Parallelly to the QDs, adverse effects of dissolved cadmium ions have been studied. The chosen concentration of Cd is related to the amount present in a (nanoparticulate) QD. The results of the AlamarBlue® assay showed a very similar behaviour regarding cell viability: with increasing amount of cadmium, the viability decreases. Despite the known toxicity of the dissolved Cd species, these results led to the assumption that the potential reason of negative effects by QDs are very likely to be caused by the release/liberation of the Cd ions from the QD's inorganic materials, and at very high concentrations (100 µg/mL) by potential release of Fe ions concerning the doped-QDs. From these viability data, a sigmoidal regression function was used to calculate the inhibition concentration (IC_{50}), at which 50% of cell viability is reduced. These values showed that, in case of all tested QD types, below the average value of 66.6 µg/mL the viability dropped to half of the initial value. The IC_{50} value of Cd ions was 3 times lower than for their nanoparticulate counterparts (21.5 µg/mL), showing then much higher toxicity than the QDs. These different values also show how the presence of capping agent NAC may sufficiently retard the liberation of toxic heavy metals.

In order to localize the QDs in U937 cells, fluorescence microscopy analysis was carried out. The sample prepared with U937 and incubated with 1 µg/mL of NAC-CdTe/ZnS for 24 hours was studied.

The images obtained from the CLSM analysis showed that the QDs were internalized into the cells even at very low concentrations. This led to the assumption that QD exposure is likely to induce chronic toxicity: the viability of the cells at this low concentration was as high as the control sample, therefore no acute toxicity could have been induced. Nevertheless, if the QDs are present inside the cells, this may cause on the long-run organelles damages and/or potential oxidative stress after the formation of ROS. Finally, the three-dimensional image based on z-stacking confirmed that the QDs were not able to penetrate inside the nuclei of the cells, but they were distributed inside the cytoplasm in small aggregates.

7 CONCLUSIONS

The goal of this study was to evaluate the potential toxicity of four different types of Cd-based QDs, verifying significant differences in effects of undoped and iron-doped QDs. Additionally, a parallel goal was to develop a fast-screening and reproducible method to assess such ENMs.

From the flow cytometry and AlamarBlue® assay analysis, it is possible to assume that the QDs trigger toxic effects on CHO cells as well as on U937 macrophages. The results from the flow cytometry showed increase of fluorescence intensity when the CHO cells were incubated with QDs. It was assumed that QDs may have been internalized by the cells (no detection of QDs only was possible with method), potentially causing membrane/cell damage. As matter of fact, when the treated sample was as well stained with PI, the same peak presenting high fluorescence intensity occurred. Furthermore, the IC_{50} calculated from the AlamarBlue® assay data showed a critical value of the QDs incubated with the cells of around 66.6 µg/mL. The dose-response relationship showed a similar behaviour for the four types of QDs and for the ionic counterparts, even if the IC_{50} value of Cd ions was 3 times lower. However, significant negative effects on the cells were caused by the presence of Fe counterparts as well, but only when incubated at the highest concentration (12 µg/mL). Therefore, it could be assumed then that one of the main reason for the cell damage/death or viability reduction may be found in the release of the Cd ions and of the Fe ions (in doped-QDs case) from the core (or shell) of the nanoparticles. However, further and more detailed test need to be conducted in order to have more results to possibly confirm this assumption. Potential chronic toxicity effects cannot be excluded, as from CLSM images QDs were localized and distributed in the cytoplasm of the cells even at very low concentrations (1 µg/mL, 24h of incubation). However, many QDs were observed outside the intracellular environment as well, therefore further analysis is necessary to understand the triggering mechanism of the cell uptake. Finally, despite the very small size of the used QDs, they could be used as toxicity model to test the harmful effects of other similar ENMs. In some of the results obtained from fluorescence intensity detection from AlamarBlue® assay, significant difference was observed among the types of QDs, in particular shell-doped QDs in Test 2 and Test

3.b (12.5 – 50 µg/mL and 1 – 25 µg/mL, respectively) and for bare-QDs in Test 3.b (100 µg/mL). However, no constant evidence of this assumption was observed among the different tests, therefore further tests will be needed to carry out to obtain more detailed information.

Finally, concerning the method development goal, despite the positive results obtained from the flow cytometer tests (potential visible QDs influence), the suggested protocol in order to detect the effect of the quantum dots is the AlamarBlue® assay in combination with analysis with CLSM. The preparation process requires more expertise than the AlamarBlue® assay regarding the sample preparation (in specific staining process) and regarding the optimum settings establishment. On the contrary, the optimized protocol for the AlamarBlue® assay enabled time-efficient analyses and large sample sizes. The AlamarBlue® stain is ready-to-use and included in the wells since the beginning, making it fast-screening and reproducible cell viability assessment method.

8 OUTLOOK

This study presented positive results concerning the evaluation of QD cytotoxicity. However, some further test need to be carried out in order to clarify in more detail the behaviour, fate and uptake mechanisms of QDs when they are exposed cells.

More specifically, other AlamarBlue® assay tests need to be held with others cell lines, which may better simulate potential end-points of human beings. An example is the HepG2 cell line, which are human liver cells. This is because it is known that cadmium species tend to accumulate and target specifically organs as the liver in humans. Further analysis assessing the cell viability are needed also in order to evaluate effective differences among the influence of the different QD types, and obtain more detailed information concerning Cd and Fe ions release and reduced cell viability influence.

The fluorescence microscope image showed how even at very low QD concentrations those ENMs were uptaken by the cells and distributed in the cytoplasm. This opened another assumption of not only acute toxicity induction, but as well of chronic toxicity occurs. This long-term toxicity may be observed after a longer period of time than the 24 hours of the experiment. For this, it is necessary to additionally test the two potential negative consequences of the penetration of QD inside the cells: potential formation of Reactive Oxidative Species (ROS), therefore cell oxidative stress; and potential damage to the organelles (mitochondria). Finally, the mechanisms how QDs penetrate cell membrane are still needed to be investigated in more detail. Therefore, supplementary analysis concerning the interaction of cells and QDs are necessary.

9 REFERENCES

abcam, 2018. Introduction to flow cytometry. abcam discover more, http://www.abcam.com/protocols/introduction-to-flow-cytometry.

AbDSerotec, 2017. Flow Cytometry Basic Guide, in: abdserotec.com/flowguide, V. (Ed.). BIO-RAD, www.abdserotec.com/flowguide.

Bassi, M., Santinello, I., Bevilacqua, A., Bassi, P., Nanotechnology: a big revolution from the small world. Nanotecnologie: una grande rivoluzione che parte dal piccolo 80, 46.

Bassi, M., Santinello, I., Bevilacqua, A., Bassi, P., 2013. [Nanotechnology: a big revolution from the small world.].

Bilan, R., Fleury, F., Nabiev, I., Sukhanova, A., 2015. Quantum dot surface chemistry and functionalization for cell targeting and imaging.

Bimberg, D., Pohl, U.W., 2011. Quantum dots: promises and accomplishments. Materials Today 14, 388-397.

Bioscience, B., 2000. Introduction to Flow Cytometry: A Learning Guide. © 2000 Becton, Dickinson and Company, 2350 Qume Drive, San Jose, CA 95131-1807, United States of America.

Bonilla, J.C., Bozkurt, F., Ansari, S., Sozer, N., Kokini, J.L., 2016. Applications of quantum dots in Food Science and biology. Trends in Food Science & Technology 53, 75-89.

Boxberg, F., Tulkki, J., 2018. Quantum Dots: Phenomenology, Photonic and Electronic Properties, Modeling and Technology.

Chanput, W., Peters, V., Wichers, H., 2015. THP-1 and U937 Cells, in: Verhoeckx, K., Cotter, P., López-Expósito, I., Kleiveland, C., Lea, T., Mackie, A., Requena, T., Swiatecka, D., Wichers, H. (Eds.), The Impact of Food Bioactives on Health: in vitro and ex vivo models. Springer International Publishing, Cham, pp. 147-159.

Chiang, H.-m., Xia, Q., Zou, X., Wang, C., Wang, S., Miller, B.J., Howard, P.C., Yin, J.J., Beland, F.A., Yu, H., Fu, P.P., 2012. Nanoscale ZnO Induces Cytotoxicity and DNA Damage in Human Cell Lines and Rat Primary Neuronal Cells. Journal of Nanoscience and Nanotechnology 12, 2126-2135.

Derfus, A.M., Chan, W.C.W., Bhatia, S.N., 2004. Probing the Cytotoxicity of Semiconductor Quantum Dots. Nano Letters 4, 11-18.

EC, 2011. Commission recommendation of 18 October 2011 on the definition of nanomaterial, in: Commission, E. (Ed.), L 275/38. Official Journal of the European Union, Brussels, p. 3.

Elsaesser, A., Howard, C.V., 2012. Toxicology of nanoparticles. Advanced Drug Delivery Reviews 64, 129-137.

European Union: communication from the commission to the council. The combination effects of chemicals. COM/2012/0252 final, 31/05/2012, pp. 1–10.

Foss Hansen, S., Heggelund, L.R., Revilla Besora, P., Mackevica, A., Boldrin, A., Baun, A., 2016. Nanoproducts - what is actually available to European consumers? Environmental Science: Nano 3, 169-180.

Fu, P.P., Xia, Q., Hwang, H.-M., Ray, P.C., Yu, H., 2014. Mechanisms of nanotoxicity: Generation of reactive oxygen species. Journal of Food and Drug Analysis 22, 64-75.

Hardman, R., 2006. A Toxicologic Review of Quantum Dots: Toxicity Depends on Physicochemical and Environmental Factors. Environmental Health Perspectives 114, 165-172.

Hauck, T.S., Anderson, R.E., Fischer, H.C., Newbigging, S., Chan, W.C.W., 2010. In vivo Quantum-Dot Toxicity Assessment. Small 6, 138-144.

Hoskins, C., Cuschieri, A., Wang, L., 2012. The cytotoxicity of polycationic iron oxide nanoparticles: Common endpoint assays and alternative approaches for improved understanding of cellular response mechanism. Journal of Nanobiotechnology 10, 15-15.

Invitrogen, AlamarBlue ® Cell Viability Reagent. Biosource invitrogen cytokines & singaling.

ISO, 2015. ISO TS 80004-1:2015, Nanotechnologies - Vocabulary Part 1 - Core terms.

Kirchner, C., Liedl, T., Kudera, S., Pellegrino, T., Muñoz Javier, A., Gaub, H.E., Stölzle, S., Fertig, N., Parak, W.J., 2005. Cytotoxicity of Colloidal CdSe and CdSe/ZnS Nanoparticles. Nano Letters 5, 331-338.

Lai, L., Lin, C., Xiao, C.-Q., Xu, Z.-Q., Han, X.-L., Fu, L., Li, D.-W., Mei, P., Jiang, F.-L., Guo, Q.-L., Liu, Y., 2013. Adhesion of quantum dots-induced membrane damage of Escherichia coli. Journal of colloid and interface science 389, 61-70.

Mahto, S.K., Yoon, T.H., Rhee, S.W., 2010. A new perspective on in vitro assessment method for evaluating quantum dot toxicity by using microfluidics technology. Biomicrofluidics 4, 034111.

Midha, K., Kalra, S., Nagpal, M., 2015. Quantum Dots in Cancer Therapy. International Journal of Current Science and Technology 3, 84-89.

Murray, R., Escobar, A., Bastús, N., Andreozzi, P., Puntes, V., Moya, S., 2017. Fluorescently labelled nanomaterials in nanosafety research: Practical advice to avoid artefacts and trace unbound dye.

Müller, K.H., Motskin, M., Philpott, A.J., Routh, A.F., Shanahan, C.M., Duer, M.J., Skepper, J.N., 2014. The effect of particle agglomeration on the formation of a surface-connected compartment induced by hydroxyapatite nanoparticles in human monocyte-derived macrophages. Biomaterials 35, 1074-1088.

Oh, E., Liu, R., Nel, A., Gemill, K.B., Bilal, M., Cohen, Y., Medintz, I.L., 2016. Meta-analysis of cellular toxicity for cadmium-containing quantum dots. Nature Nanotechnology 11, 479.

Panuganti, S.J., 2015. Principles Involved in Bioassay by different Methods: A Mini-Review. Research and Reviews: Research Journal of Biology.

Part, F., Huber-Humer, M., Berge, N.D., 2016a. Engineered nanomaterials in waste streams. Waste Management 51, 1-2.

Part, F., Zaba, C., Bixner, O., Grünewald, T., Michor, H., Küpcü, S., Debreczeny, M., De Vito-Francesco, E., Lassenberger, A., Schrittwieser, S., Hann, S., Lichtenegger, H., Sinner, E., *submitted*. The doping method determines para- or superparamagnetic properties of photostable and surface midifiable quantum dots for multimodal bioimaging, p. 29.

Part, F., Zaba, C., Bixner, O., Zafiu, C., Hann, S., Sinner, E.-K., Huber-Humer, M., 2016b. Traceability of fluorescent engineered nanomaterials and their fate in complex liquid waste matrices. Environmental Pollution 214, 795-805.

Piccinno, F., Gottschalk, F., Seeger, S., Nowack, B., 2012. Industrial production quantities and uses of ten engineered nanomaterials in Europe and the world. Journal of Nanoparticle Research 14, 1109.

Piperigkou, Z., Karamanou, K., Engin, A.B., Gialeli, C., Docea, A.O., Vynios, D.H., Pavão, M.S.G., Golokhvast, K.S., Shtilman, M.I., Argiris, A., Shishatskaya, E., Tsatsakis, A.M., 2016. Emerging aspects of nanotoxicology in health and disease: From agriculture and food sector to cancer therapeutics. Food and Chemical Toxicology 91, 42-57.

Piret, J.-P., Bondarenko, O.M., Boyles, M.S.P., Himly, M., Ribeiro, A.R., Benetti, F., Smal, C., Lima, B., Potthoff, A., Simion, M., Dumortier, E., Leite, P.E.C., Balottin, L.B., Granjeiro, J.M., Ivask, A., Kahru, A., Radauer-Preiml, I., Tischler, U., Duschl, A., Saout, C., Anguissola, S., Haase, A., Jacobs, A., Nelissen, I., Misra, S.K., Toussaint, O., 2017. Pan-European inter-laboratory studies on a panel of in vitro cytotoxicity and pro-inflammation assays for nanoparticles. Archives of Toxicology 91, 2315-2330.

Scientific, T.F., AlamrBlue ® - Rapid and Accurate Cell Health Indicator. Thermo Fisher Sientific, Austria.

Semonin, O.E., Luther, J.M., Beard, M.C., 2012. Quantum dots for next-generation photovoltaics. Materials Today 15, 508-515.

Serotec, A., Flow Cytometry Basic Guide, in: abdserotec.com/flowguide, V. (Ed.).

SigmaAldrich, 2017. Quantum Dots. Sigma Aldrich, http://www.sigmaaldrich.com/technical-documents/articles/materials-science/nanomaterials/quantum-dots.html.

Sozer, N., Kokini, J., 2014. Use of quantum nanodot crystals as imaging probes for cereal proteins.

THEMESHAKER, 2017. CHO line general information and resources. WORDPRESS.

Ulusoy, M., Bongartz, R., Walter, J., Springer, S., Lavrentieva, A., Stahl, F., A Green, M., Scheper, T., 2015. Aqueous Synthesis of PEGylated Quantum Dots with Increased Colloidal Stability and Reduced Cytotoxicity.

Ulusoy, M., Walter, J., Lavrentieva, A., Kretschmer, I., Sandiford, L., Le Marois, A., Bongartz, R., Aliuos, P., Suhling, K., Stahl, F., Green, M., Scheper, T., 2014. One-pot aqueous synthesis of highly strained CdTe/CdS/ZnS nanocrystals and their interactions with cells.

Verhoeckx, K., Cotter, P., Lòpez-Expòsito, I., Kleiveland, C., Lea, T., Mackie, A., Requena, T., Swiatecka, D., Wichers, H., 2015. The Impact of Food Bioactives on Health

in vitro and ex vivo models. Springer International Publishing.

Wang, H., Li, Y., Wang, A., Slavik, M., 2011. Rapid, Sensitive, and Simultaneous Detection of Three Foodborne Pathogens Using Magnetic Nanobead-Based Immunoseparation and Quantum Dot-Based Multiplex Immunoassay.

Wernersson, A.-S., Carere, M., Maggi, C., Tusil, P., Soldan, P., James, A., Sanchez, W., Dulio, V., Broeg, K., Reifferscheid, G., Buchinger, S., Maas, H., Van Der Grinten, E., O'Toole, S., Ausili, A., Manfra, L., Marziali, L., Polesello, S., Lacchetti, I., Mancini, L., Lilja, K., Linderoth, M., Lundeberg, T., Fjällborg, B., Porsbring, T., Larsson, D.G.J., Bengtsson-Palme, J., Förlin, L., Kienle, C., Kunz, P., Vermeirssen, E., Werner, I., Robinson, C.D., Lyons, B., Katsiadaki, I., Whalley, C., den Haan, K., Messiaen, M., Clayton, H., Lettieri, T., Carvalho, R.N., Gawlik, B.M., Hollert, H., Di Paolo, C., Brack, W., Kammann, U., Kase, R., 2015. The European technical report on aquatic effect-based monitoring tools under the water framework directive. Environmental Sciences Europe 27, 7.

Wurm, M.F., 2013. CHO Quasispecies—Implications for Manufacturing Processes. Processes 1.

Xu, M., Deng, G., Liu, S., Chen, S., Cui, D., Yang, L., Wang, Q., 2010. Free cadmium ions released from CdTe-based nanoparticles and their cytotoxicity on.

Zboray, K., Sommeregger, W., Bogner, E., Gili, A., Sterovsky, T., Fauland, K., Grabner, B., Stiedl, P., Moll, H.P., Bauer, A., Kunert, R., Casanova, E., 2015. Heterologous protein production using euchromatin-containing expression vectors in mammalian cells. Nucleic Acids Research 43, e102-e102.

Zhang, K., Fang, H., Chen, Z., Taylor, J.-S.A., Wooley, K.L., 2008. Shape effects of nanoparticles conjugated with cell-penetrating peptides (HIV Tat PTD) on CHO cell uptake. Bioconjugate chemistry 19, 1880-1887.

Zhu, J.-J., Li, J.-J., Huang, H.-P., Cheng, F.-F., 2013. Quantum Dots for DNA Biosensing, p. 91.

Zhu, L., Ang, S., Liu, W.-T., 2004. Quantum Dots as a Novel Immunofluorescent Detection System for Cryptosporidium parvum and Giardia lamblia.

10 ANNEX

10.1 SAMPLE PREPARATION FOR FLOW CYTOMETRY

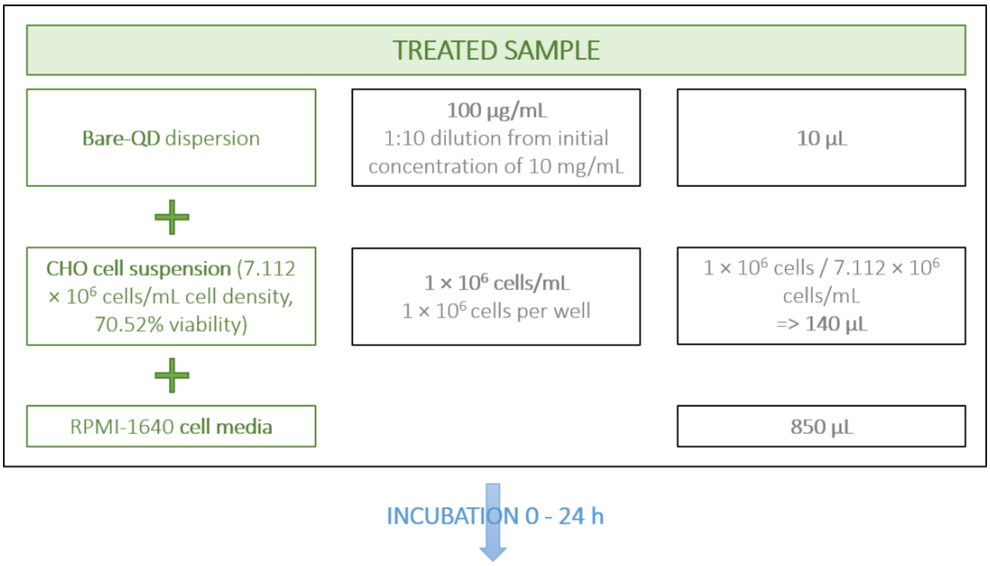

TREATED SAMPLE		
Bare-QD dispersion	100 µg/mL 1:10 dilution from initial concentration of 10 mg/mL	10 µL
+		
CHO cell suspension (7.112 × 10^6 cells/mL cell density, 70.52% viability)	1 × 10^6 cells/mL 1 × 10^6 cells per well	1 × 10^6 cells / 7.112 × 10^6 cells/mL => 140 µL
+		
RPMI-1640 cell media		850 µL

INCUBATION 0 - 24 h

Figure 10.1.1. Schematic description of treated sample preparation, for following flow cytometry analysis.

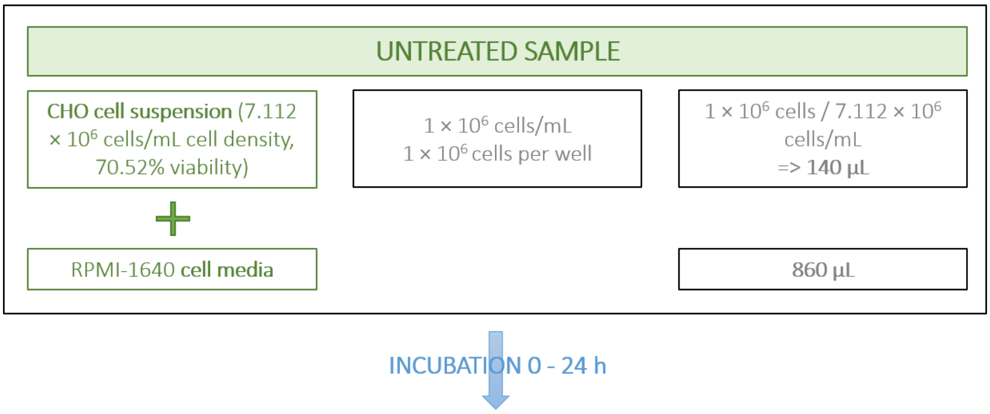

UNTREATED SAMPLE		
CHO cell suspension (7.112 × 10^6 cells/mL cell density, 70.52% viability)	1 × 10^6 cells/mL 1 × 10^6 cells per well	1 × 10^6 cells / 7.112 × 10^6 cells/mL => 140 µL
+		
RPMI-1640 cell media		860 µL

INCUBATION 0 - 24 h

Figure 10.1.2. Schematic description of untreated sample preparation, for the following flow cytometry analysis.

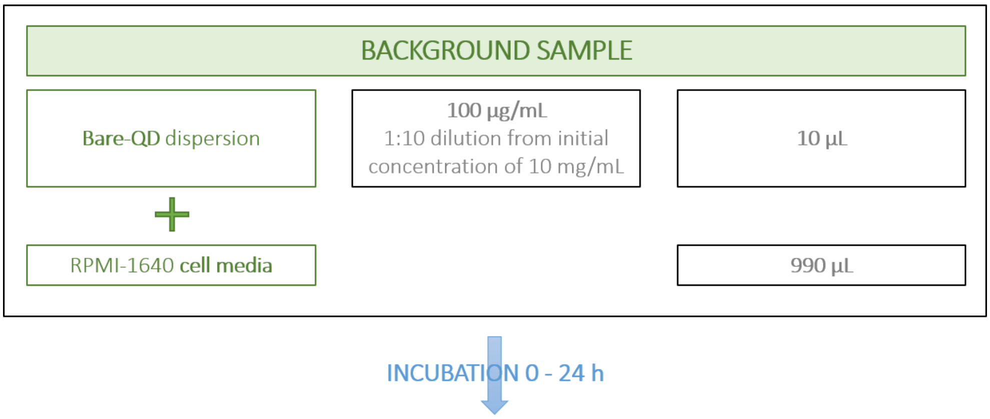
BACKGROUND SAMPLE
Bare-QD dispersion
100 µg/mL
1:10 dilution from initial concentration of 10 mg/mL
10 µL
RPMI-1640 cell media
990 µL
INCUBATION 0 - 24 h

Figure 10.1.3. Schematic representation of background sample preparation, for the following flow cytometry analysis.

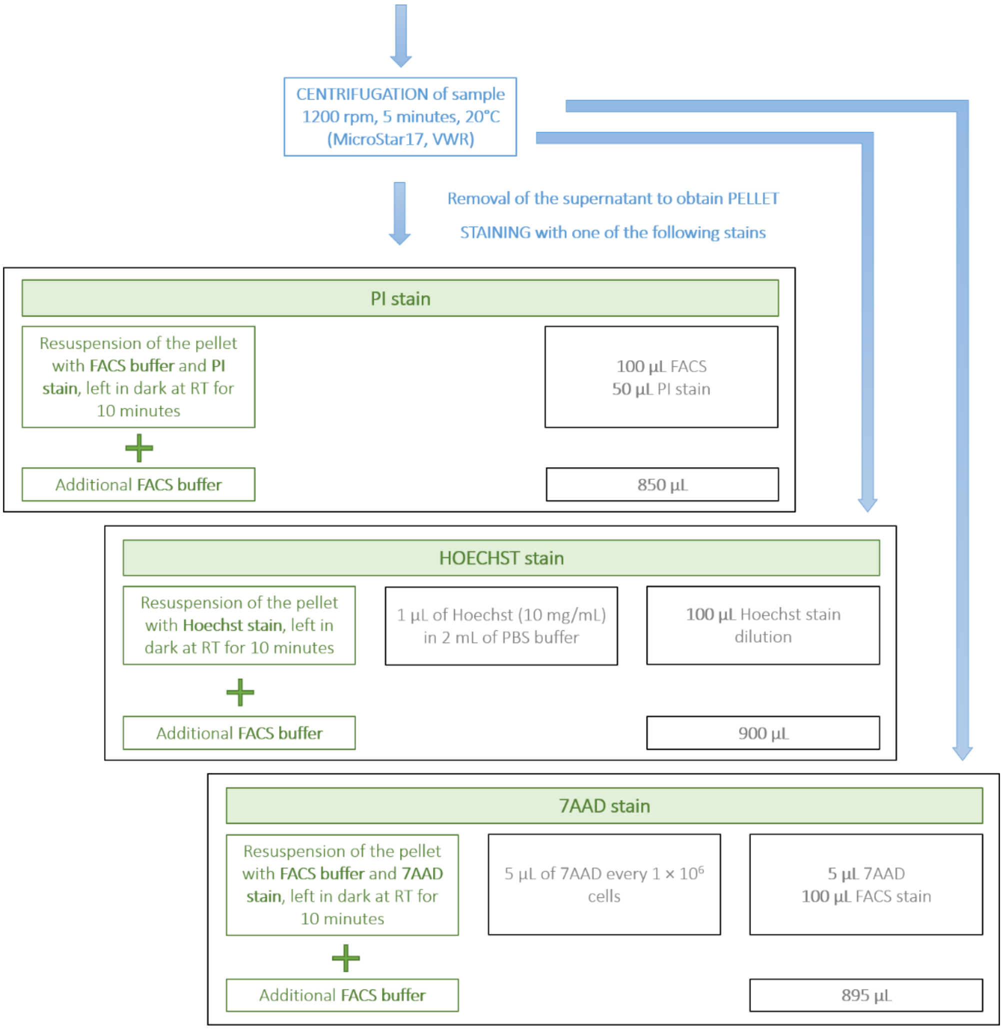
CENTRIFUGATION of sample
1200 rpm, 5 minutes, 20°C
(MicroStar17, VWR)
Removal of the supernatant to obtain PELLET
STAINING with one of the following stains
PI stain
Resuspension of the pellet with FACS buffer and PI stain, left in dark at RT for 10 minutes
100 µL FACS
50 µL PI stain
Additional FACS buffer
850 µL
HOECHST stain
Resuspension of the pellet with Hoechst stain, left in dark at RT for 10 minutes
1 µL of Hoechst (10 mg/mL) in 2 mL of PBS buffer
100 µL Hoechst stain dilution
Additional FACS buffer
900 µL
7AAD stain
Resuspension of the pellet with FACS buffer and 7AAD stain, left in dark at RT for 10 minutes
5 µL of 7AAD every 1 × 10⁶ cells
5 µL 7AAD
100 µL FACS stain
Additional FACS buffer
895 µL

Figure 10.1.4. Schematic description of the staining steps, after the incubation for the following flow cytometry analysis.

10.2 SAMPLE PREPATATION FOR ALAMARBLUE® ASSAY

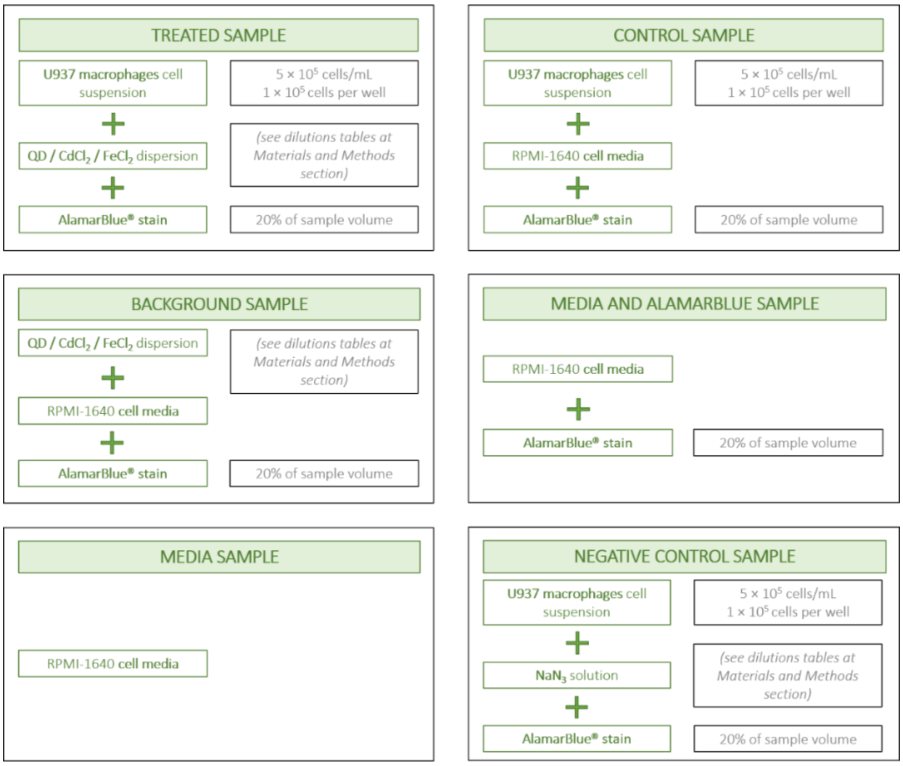
TREATED SAMPLE
U937 macrophages cell suspension
5 × 10⁵ cells/mL
1 × 10⁵ cells per well
+
QD / $CdCl_2$ / $FeCl_2$ dispersion
(see dilutions tables at Materials and Methods section)
+
AlamarBlue® stain
20% of sample volume
CONTROL SAMPLE
U937 macrophages cell suspension
5 × 10⁵ cells/mL
1 × 10⁵ cells per well
+
RPMI-1640 cell media
+
AlamarBlue® stain
20% of sample volume
BACKGROUND SAMPLE
QD / $CdCl_2$ / $FeCl_2$ dispersion
(see dilutions tables at Materials and Methods section)
+
RPMI-1640 cell media
+
AlamarBlue® stain
20% of sample volume
MEDIA AND ALAMARBLUE SAMPLE
RPMI-1640 cell media
+
AlamarBlue® stain
20% of sample volume
MEDIA SAMPLE
RPMI-1640 cell media
NEGATIVE CONTROL SAMPLE
U937 macrophages cell suspension
5 × 10⁵ cells/mL
1 × 10⁵ cells per well
+
NaN_3 solution
(see dilutions tables at Materials and Methods section)
+
AlamarBlue® stain
20% of sample volume

Figure 10.2.1. Schematic description of the composition of samples to be analysed with the AlamarBlue® assay.

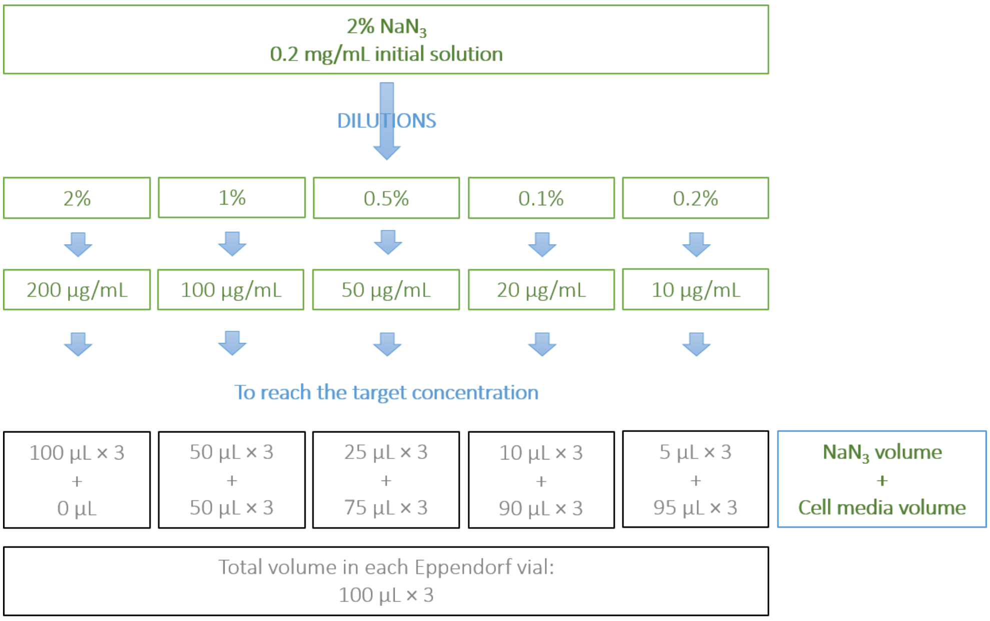
2% NaN_3
0.2 mg/mL initial solution
DILUTIONS
2%
1%
0.5%
0.1%
0.2%
200 µg/mL
100 µg/mL
50 µg/mL
20 µg/mL
10 µg/mL
To reach the target concentration
100 µL × 3 + 0 µL
50 µL × 3 + 50 µL × 3
25 µL × 3 + 75 µL × 3
10 µL × 3 + 90 µL × 3
5 µL × 3 + 95 µL × 3
NaN_3 volume + Cell media volume
Total volume in each Eppendorf vial: 100 µL × 3

Figure 10.2.2. Schematic procedure to prepare the NaN_3 dilutions for preliminary analysis with AlamarBlue® assay.

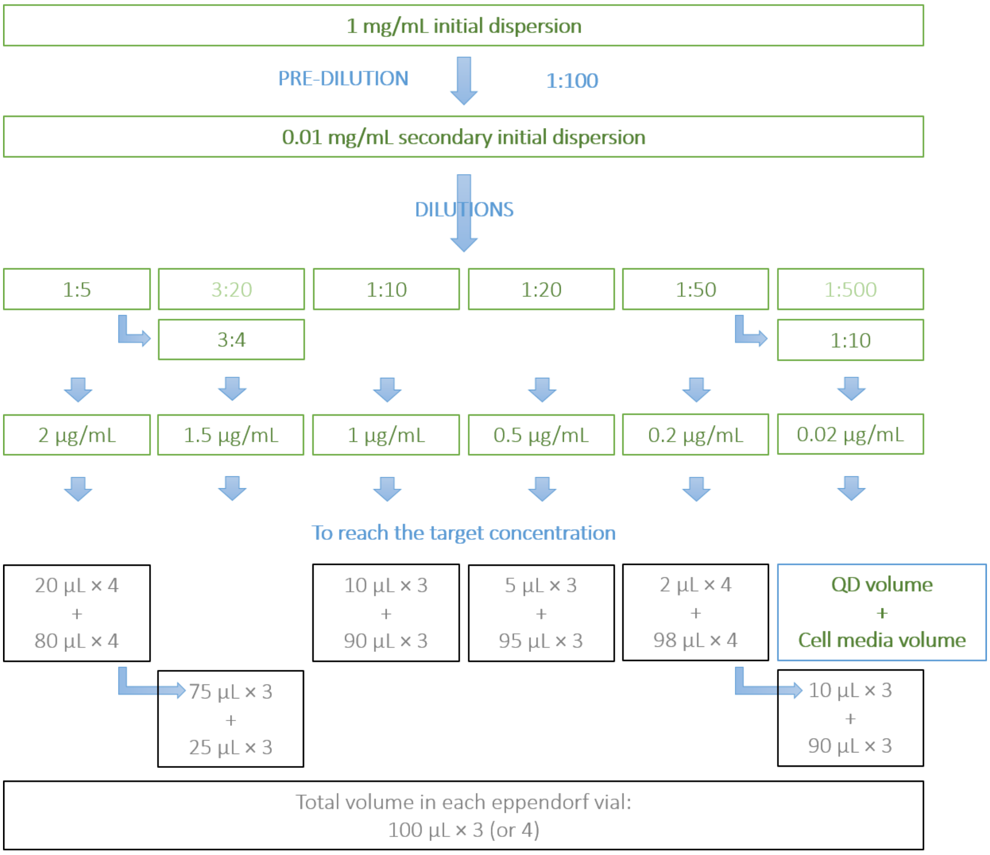
1 mg/mL initial dispersion
PRE-DILUTION
1:100
0.01 mg/mL secondary initial dispersion
DILUTIONS
1:5
3:20
1:10
1:20
1:50
1:500
3:4
1:10
2 µg/mL
1.5 µg/mL
1 µg/mL
0.5 µg/mL
0.2 µg/mL
0.02 µg/mL
To reach the target concentration
20 µL × 4 + 80 µL × 4
10 µL × 3 + 90 µL × 3
5 µL × 3 + 95 µL × 3
2 µL × 4 + 98 µL × 4
QD volume + Cell media volume
75 µL × 3 + 25 µL × 3
10 µL × 3 + 90 µL × 3
Total volume in each eppendorf vial:
100 µL × 3 (or 4)

Figure 10.2.3. Schematic procedure to prepare the QD dispersions in Test 1, for further analysis with AlamarBlue® assay.

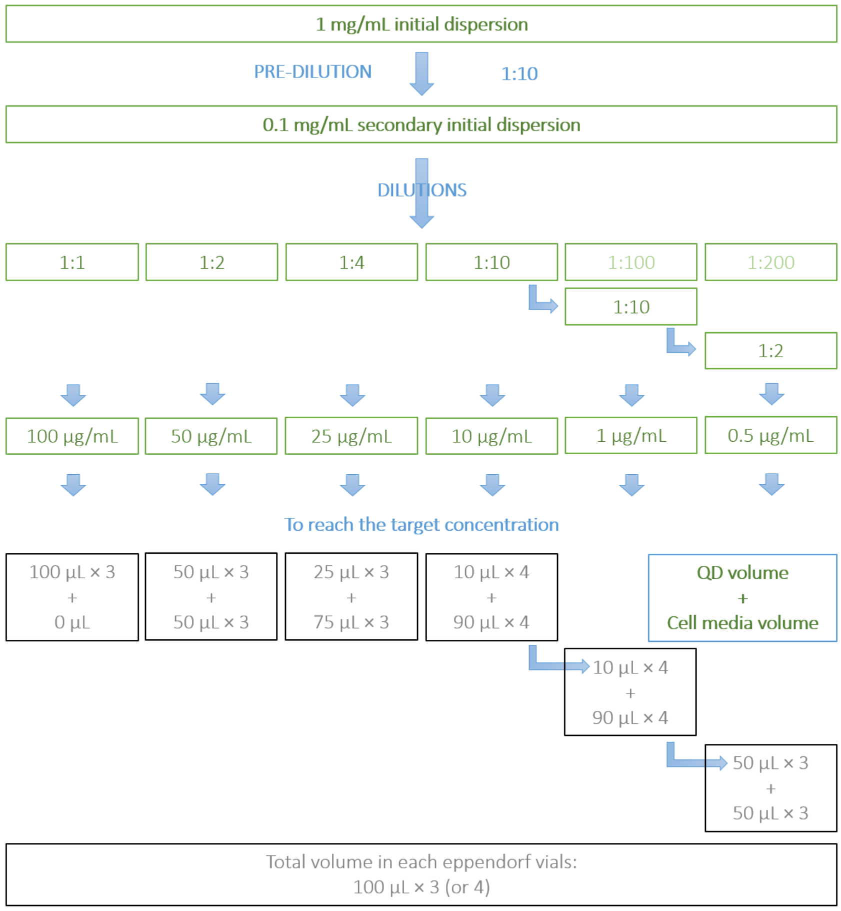
1 mg/mL initial dispersion
PRE-DILUTION
1:10
0.1 mg/mL secondary initial dispersion
DILUTIONS
1:1
1:2
1:4
1:10
1:100
1:200
1:10
1:2
100 µg/mL
50 µg/mL
25 µg/mL
10 µg/mL
1 µg/mL
0.5 µg/mL
To reach the target concentration
100 µL × 3 + 0 µL
50 µL × 3 + 50 µL × 3
25 µL × 3 + 75 µL × 3
10 µL × 4 + 90 µL × 4
QD volume + Cell media volume
10 µL × 4 + 90 µL × 4
50 µL × 3 + 50 µL × 3
Total volume in each eppendorf vials:
100 µL × 3 (or 4)

Figure 10.2.4. Schematic procedure to prepare the QD dispersions in Test 2, for further analysis with AlamarBlue® assay.

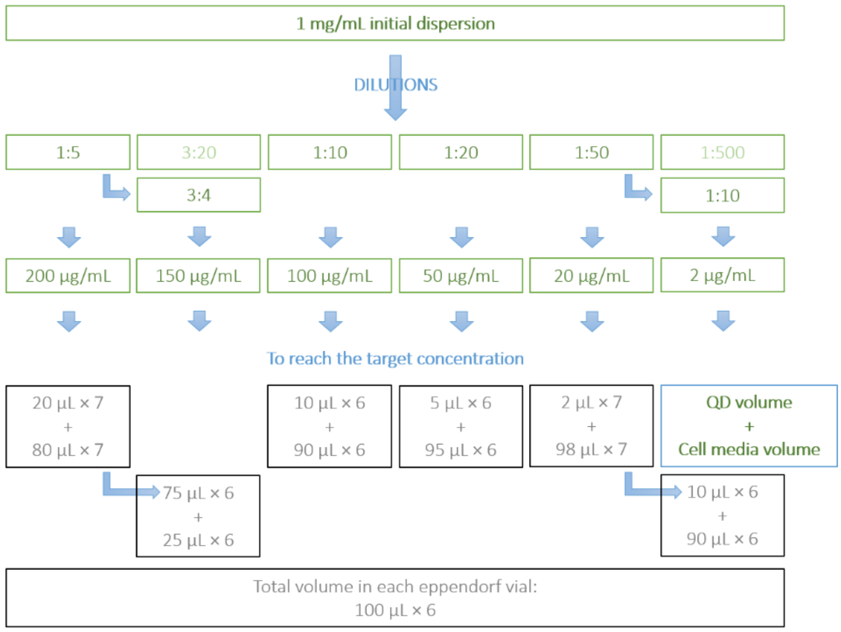
1 mg/mL initial dispersion
DILUTIONS
1:5
3:20
1:10
1:20
1:50
1:500
3:4
1:10
200 µg/mL
150 µg/mL
100 µg/mL
50 µg/mL
20 µg/mL
2 µg/mL
To reach the target concentration
20 µL × 7 + 80 µL × 7
10 µL × 6 + 90 µL × 6
5 µL × 6 + 95 µL × 6
2 µL × 7 + 98 µL × 7
QD volume + Cell media volume
75 µL × 6 + 25 µL × 6
10 µL × 6 + 90 µL × 6
Total volume in each eppendorf vial:
100 µL × 6

Figure 10.2.5. Schematic procedure to prepare the QD dispersions in Test 3.b, for further analysis with AlamarBlue® assay.

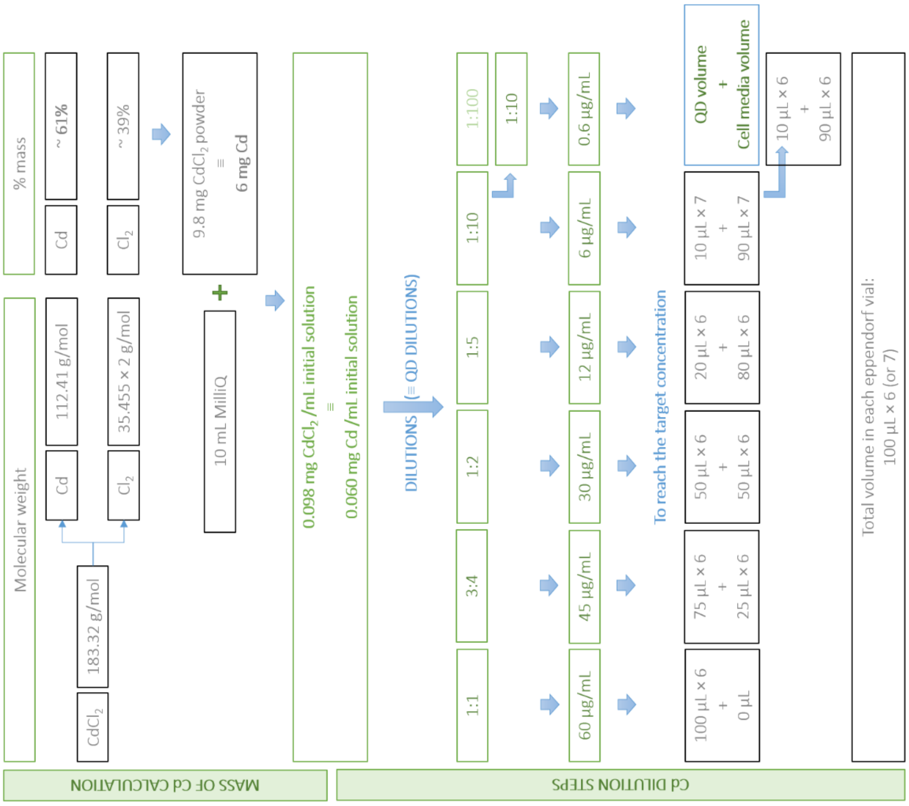
MASS OF Cd CALCULATION
Molecular weight
CdCl$_2$
183.32 g/mol
Cd
112.41 g/mol
Cl$_2$
35.455 × 2 g/mol
% mass
Cd
~ 61%
Cl$_2$
~ 39%
9.8 mg CdCl$_2$ powder
=
6 mg Cd
10 mL MilliQ
0.098 mg CdCl$_2$ /mL initial solution
=
0.060 mg Cd /mL initial solution
Cd DILUTION STEPS
DILUTIONS (= QD DILUTIONS)
1:1
3:4
1:2
1:5
1:10
1:100
1:10
60 µg/mL
45 µg/mL
30 µg/mL
12 µg/mL
6 µg/mL
0.6 µg/mL
To reach the target concentration
100 µL × 6 + 0 µL
75 µL × 6 + 25 µL × 6
50 µL × 6 + 50 µL × 6
20 µL × 6 + 80 µL × 6
10 µL × 7 + 90 µL × 7
QD volume + Cell media volume
10 µL × 6 + 90 µL × 6
Total volume in each eppendorf vial:
100 µL × 6 (or 7)

Figure 10.2.6. Schematic representation of the calculation of the Cd counterpart from CdCl$_2$, and procedure to obtain diluted solutions for further AlamarBlue® assay analysis.

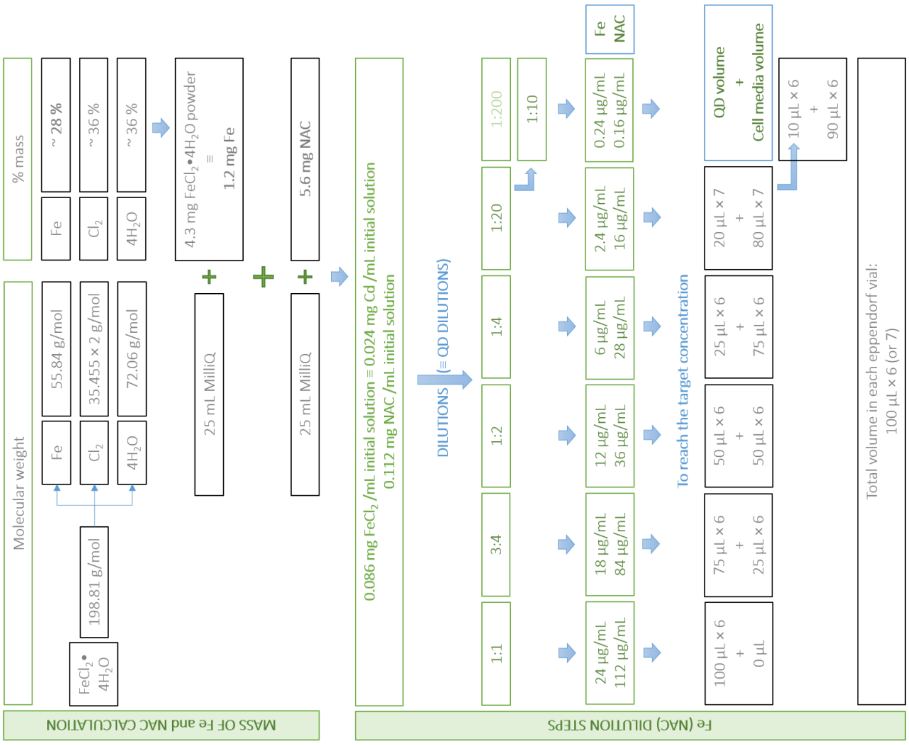
MASS OF Fe and NAC CALCULATION
Molecular weight
FeCl$_2$•4H$_2$O
198.81 g/mol
Fe
55.84 g/mol
Cl$_2$
35.455 × 2 g/mol
4H$_2$O
72.06 g/mol
% mass
Fe
~ 28 %
Cl$_2$
~ 36 %
4H$_2$O
~ 36 %
4.3 mg FeCl$_2$•4H$_2$O powder
=
1.2 mg Fe
25 mL MilliQ
5.6 mg NAC
25 mL MilliQ
0.086 mg FeCl$_2$ /mL initial solution = 0.024 mg Cd /mL initial solution
0.112 mg NAC /mL initial solution
Fe (NAC) DILUTION STEPS
DILUTIONS (= QD DILUTIONS)
1:1
3:4
1:2
1:4
1:20
1:200
1:10
Fe
NAC
24 µg/mL
112 µg/mL
18 µg/mL
84 µg/mL
12 µg/mL
36 µg/mL
6 µg/mL
28 µg/mL
2.4 µg/mL
16 µg/mL
0.24 µg/mL
0.16 µg/mL
To reach the target concentration
100 µL × 6 + 0 µL
75 µL × 6 + 25 µL × 6
50 µL × 6 + 50 µL × 6
25 µL × 6 + 75 µL × 6
20 µL × 7 + 80 µL × 7
QD volume + Cell media volume
10 µL × 6 + 90 µL × 6
Total volume in each eppendorf vial:
100 µL × 6 (or 7)

Figure 10.2.7. Schematic representation of the calculation of the Fe counterpart from FeCl$_2$ and of the NAC organic ligand, and procedure to obtain diluted solutions for further AlamarBlue® assay analysis.

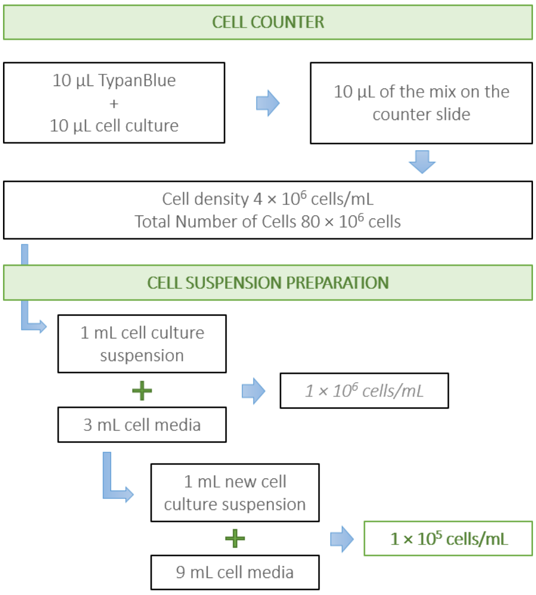
CELL COUNTER
10 µL TypanBlue + 10 µL cell culture
10 µL of the mix on the counter slide
Cell density 4 × 10^6 cells/mL
Total Number of Cells 80 × 10^6 cells
CELL SUSPENSION PREPARATION
1 mL cell culture suspension
3 mL cell media
1 × 10^6 cells/mL
1 mL new cell culture suspension
9 mL cell media
1 × 10^5 cells/mL

Figure 10.2.8. Example of cell counting and cell suspension preparation.

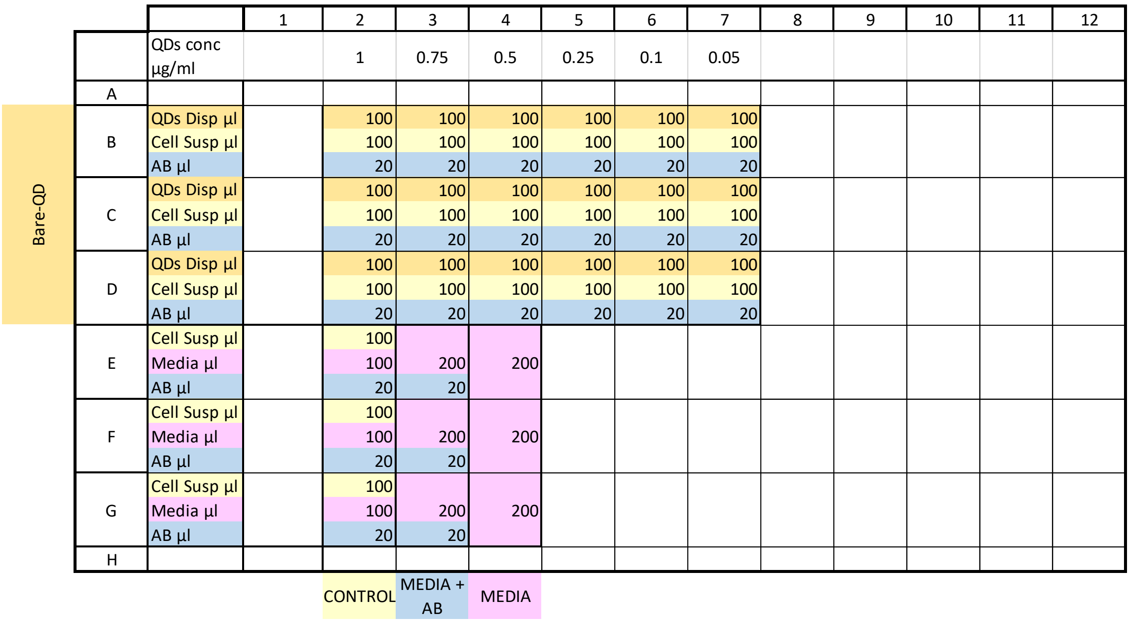

			1	2	3	4	5	6	7	8	9	10	11	12
		QDs conc µg/ml		1	0.75	0.5	0.25	0.1	0.05					
	A													
Bare-QD	B	QDs Disp µl		100	100	100	100	100	100					
		Cell Susp µl		100	100	100	100	100	100					
		AB µl		20	20	20	20	20	20					
	C	QDs Disp µl		100	100	100	100	100	100					
		Cell Susp µl		100	100	100	100	100	100					
		AB µl		20	20	20	20	20	20					
	D	QDs Disp µl		100	100	100	100	100	100					
		Cell Susp µl		100	100	100	100	100	100					
		AB µl		20	20	20	20	20	20					
	E	Cell Susp µl		100										
		Media µl		100	200	200								
		AB µl		20	20									
	F	Cell Susp µl		100										
		Media µl		100	200	200								
		AB µl		20	20									
	G	Cell Susp µl		100										
		Media µl		100	200	200								
		AB µl		20	20									
	H													
				CONTROL	MEDIA + AB	MEDIA								

Figure 10.2.9. Well plate layout of example of samples of Test 1 or Test 2.

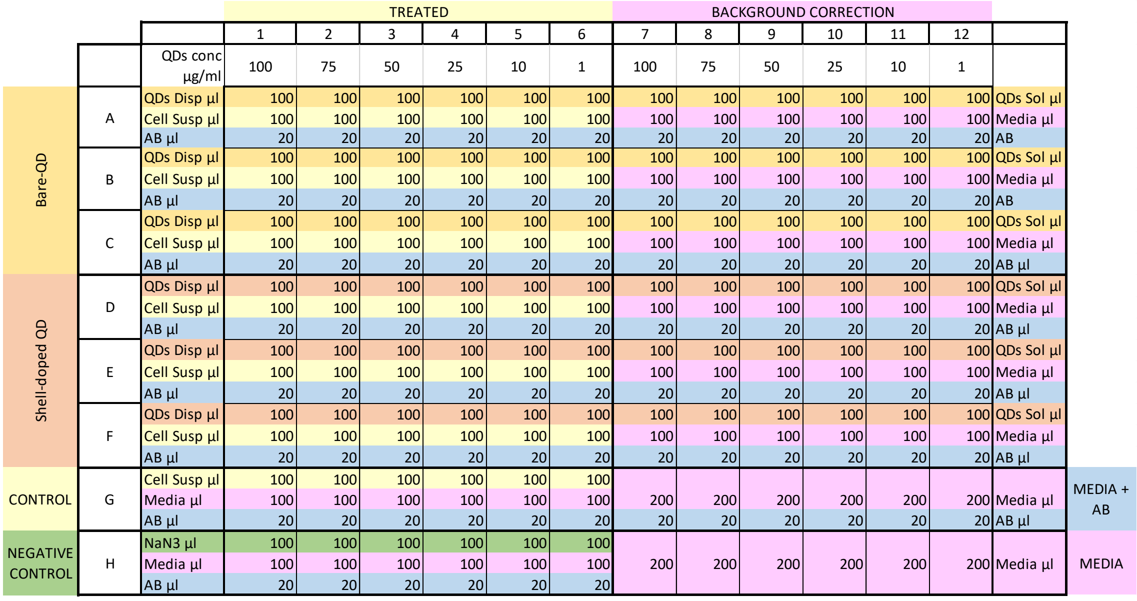

			TREATED						BACKGROUND CORRECTION							
			1	2	3	4	5	6	7	8	9	10	11	12		
		QDs conc µg/ml	100	75	50	25	10	1	100	75	50	25	10	1		
Bare-QD	A	QDs Disp µl	100	100	100	100	100	100	100	100	100	100	100	100	QDs Sol µl	
		Cell Susp µl	100	100	100	100	100	100	100	100	100	100	100	100	Media µl	
		AB µl	20	20	20	20	20	20	20	20	20	20	20	20	AB	
	B	QDs Disp µl	100	100	100	100	100	100	100	100	100	100	100	100	QDs Sol µl	
		Cell Susp µl	100	100	100	100	100	100	100	100	100	100	100	100	Media µl	
		AB µl	20	20	20	20	20	20	20	20	20	20	20	20	AB	
	C	QDs Disp µl	100	100	100	100	100	100	100	100	100	100	100	100	QDs Sol µl	
		Cell Susp µl	100	100	100	100	100	100	100	100	100	100	100	100	Media µl	
		AB µl	20	20	20	20	20	20	20	20	20	20	20	20	AB µl	
Shell-doped QD	D	QDs Disp µl	100	100	100	100	100	100	100	100	100	100	100	100	QDs Sol µl	
		Cell Susp µl	100	100	100	100	100	100	100	100	100	100	100	100	Media µl	
		AB µl	20	20	20	20	20	20	20	20	20	20	20	20	AB µl	
	E	QDs Disp µl	100	100	100	100	100	100	100	100	100	100	100	100	QDs Sol µl	
		Cell Susp µl	100	100	100	100	100	100	100	100	100	100	100	100	Media µl	
		AB µl	20	20	20	20	20	20	20	20	20	20	20	20	AB µl	
	F	QDs Disp µl	100	100	100	100	100	100	100	100	100	100	100	100	QDs Sol µl	
		Cell Susp µl	100	100	100	100	100	100	100	100	100	100	100	100	Media µl	
		AB µl	20	20	20	20	20	20	20	20	20	20	20	20	AB µl	
CONTROL	G	Cell Susp µl	100	100	100	100	100	100								MEDIA + AB
		Media µl	100	100	100	100	100	100	200	200	200	200	200	200	Media µl	
		AB µl	20	20	20	20	20	20	20	20	20	20	20	20	AB µl	
NEGATIVE CONTROL	H	NaN3 µl	100	100	100	100	100	100								
		Media µl	100	100	100	100	100	100	200	200	200	200	200	200	Media µl	MEDIA
		AB µl	20	20	20	20	20	20								

Figure 10.2.10. Well plate layout of bare-QD and shell-doped QD-spiked samples Test 3.a or b.

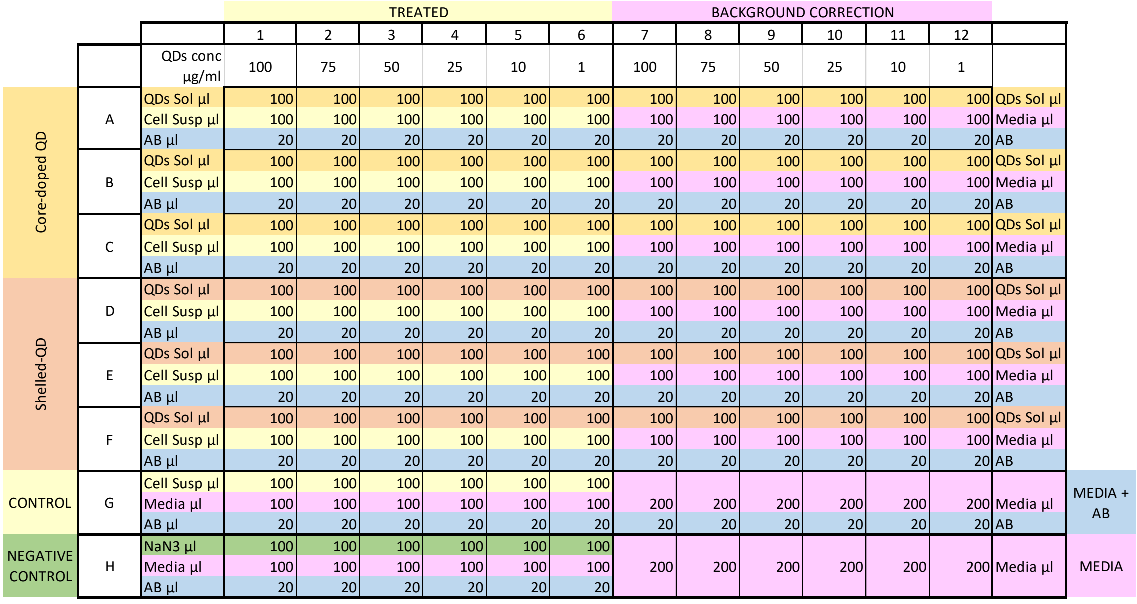

			TREATED						BACKGROUND CORRECTION							
			1	2	3	4	5	6	7	8	9	10	11	12		
		QDs conc µg/ml	100	75	50	25	10	1	100	75	50	25	10	1		
Core-doped QD	A	QDs Sol µl	100	100	100	100	100	100	100	100	100	100	100	100	QDs Sol µl	
		Cell Susp µl	100	100	100	100	100	100	100	100	100	100	100	100	Media µl	
		AB µl	20	20	20	20	20	20	20	20	20	20	20	20	AB	
	B	QDs Sol µl	100	100	100	100	100	100	100	100	100	100	100	100	QDs Sol µl	
		Cell Susp µl	100	100	100	100	100	100	100	100	100	100	100	100	Media µl	
		AB µl	20	20	20	20	20	20	20	20	20	20	20	20	AB	
	C	QDs Sol µl	100	100	100	100	100	100	100	100	100	100	100	100	QDs Sol µl	
		Cell Susp µl	100	100	100	100	100	100	100	100	100	100	100	100	Media µl	
		AB µl	20	20	20	20	20	20	20	20	20	20	20	20	AB	
Shelled-QD	D	QDs Sol µl	100	100	100	100	100	100	100	100	100	100	100	100	QDs Sol µl	
		Cell Susp µl	100	100	100	100	100	100	100	100	100	100	100	100	Media µl	
		AB µl	20	20	20	20	20	20	20	20	20	20	20	20	AB	
	E	QDs Sol µl	100	100	100	100	100	100	100	100	100	100	100	100	QDs Sol µl	
		Cell Susp µl	100	100	100	100	100	100	100	100	100	100	100	100	Media µl	
		AB µl	20	20	20	20	20	20	20	20	20	20	20	20	AB	
	F	QDs Sol µl	100	100	100	100	100	100	100	100	100	100	100	100	QDs Sol µl	
		Cell Susp µl	100	100	100	100	100	100	100	100	100	100	100	100	Media µl	
		AB µl	20	20	20	20	20	20	20	20	20	20	20	20	AB	
CONTROL	G	Cell Susp µl	100	100	100	100	100	100								MEDIA + AB
		Media µl	100	100	100	100	100	100	200	200	200	200	200	200	Media µl	
		AB µl	20	20	20	20	20	20	20	20	20	20	20	20	AB	
NEGATIVE CONTROL	H	NaN3 µl	100	100	100	100	100	100								
		Media µl	100	100	100	100	100	100	200	200	200	200	200	200	Media µl	MEDIA
		AB µl	20	20	20	20	20	20								

Figure 10.2.11. Well plate layout of core-doped QD and shelled-QD-spiked samples, Test 3.a or b.

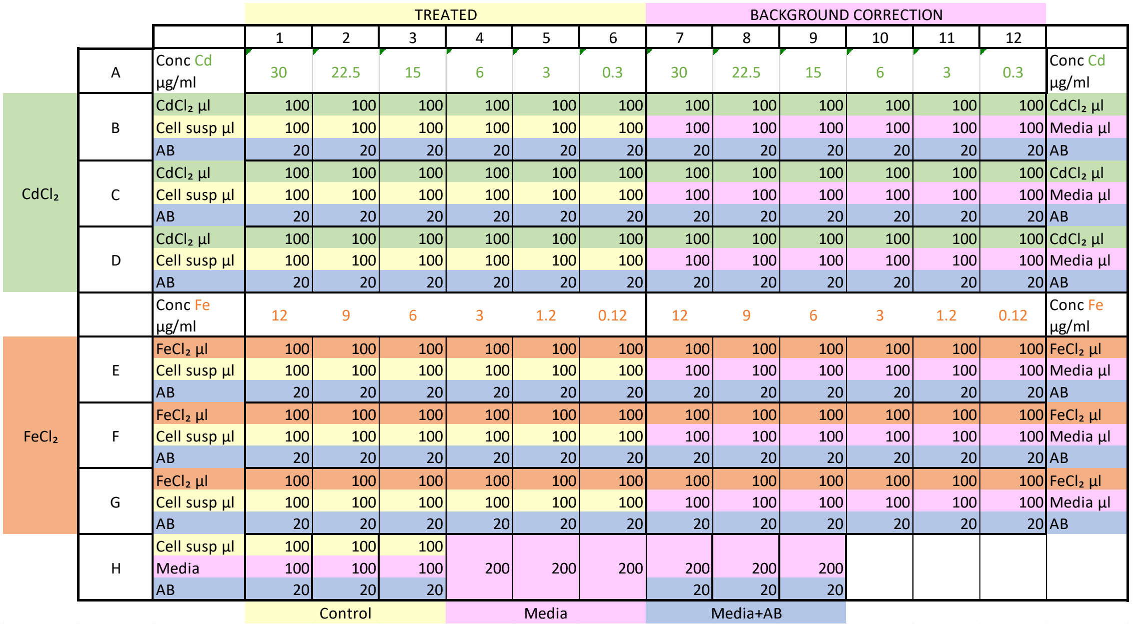

			TREATED						BACKGROUND CORRECTION						
			1	2	3	4	5	6	7	8	9	10	11	12	
	A	Conc Cd µg/ml	30	22.5	15	6	3	0.3	30	22.5	15	6	3	0.3	Conc Cd µg/ml
$CdCl_2$	B	$CdCl_2$ µl	100	100	100	100	100	100	100	100	100	100	100	100	$CdCl_2$ µl
		Cell susp µl	100	100	100	100	100	100	100	100	100	100	100	100	Media µl
		AB	20	20	20	20	20	20	20	20	20	20	20	20	AB
	C	$CdCl_2$ µl	100	100	100	100	100	100	100	100	100	100	100	100	$CdCl_2$ µl
		Cell susp µl	100	100	100	100	100	100	100	100	100	100	100	100	Media µl
		AB	20	20	20	20	20	20	20	20	20	20	20	20	AB
	D	$CdCl_2$ µl	100	100	100	100	100	100	100	100	100	100	100	100	$CdCl_2$ µl
		Cell susp µl	100	100	100	100	100	100	100	100	100	100	100	100	Media µl
		AB	20	20	20	20	20	20	20	20	20	20	20	20	AB
		Conc Fe µg/ml	12	9	6	3	1.2	0.12	12	9	6	3	1.2	0.12	Conc Fe µg/ml
$FeCl_2$	E	$FeCl_2$ µl	100	100	100	100	100	100	100	100	100	100	100	100	$FeCl_2$ µl
		Cell susp µl	100	100	100	100	100	100	100	100	100	100	100	100	Media µl
		AB	20	20	20	20	20	20	20	20	20	20	20	20	AB
	F	$FeCl_2$ µl	100	100	100	100	100	100	100	100	100	100	100	100	$FeCl_2$ µl
		Cell susp µl	100	100	100	100	100	100	100	100	100	100	100	100	Media µl
		AB	20	20	20	20	20	20	20	20	20	20	20	20	AB
	G	$FeCl_2$ µl	100	100	100	100	100	100	100	100	100	100	100	100	$FeCl_2$ µl
		Cell susp µl	100	100	100	100	100	100	100	100	100	100	100	100	Media µl
		AB	20	20	20	20	20	20	20	20	20	20	20	20	AB
	H	Cell susp µl	100	100	100										
		Media	100	100	100	200	200	200	200	200	200				
		AB	20	20	20				20	20	20				
			Control			Media			Media+AB						

Figure 10.2.12. Well plate layout of ionic counterparts sample. $CdCl_2$ is displayed in green and $FeCl_2$ in orange, Test 3.b.

10.3 SAMPLE PREPARATION FOR FLUORESCENCE MICROSCOPY

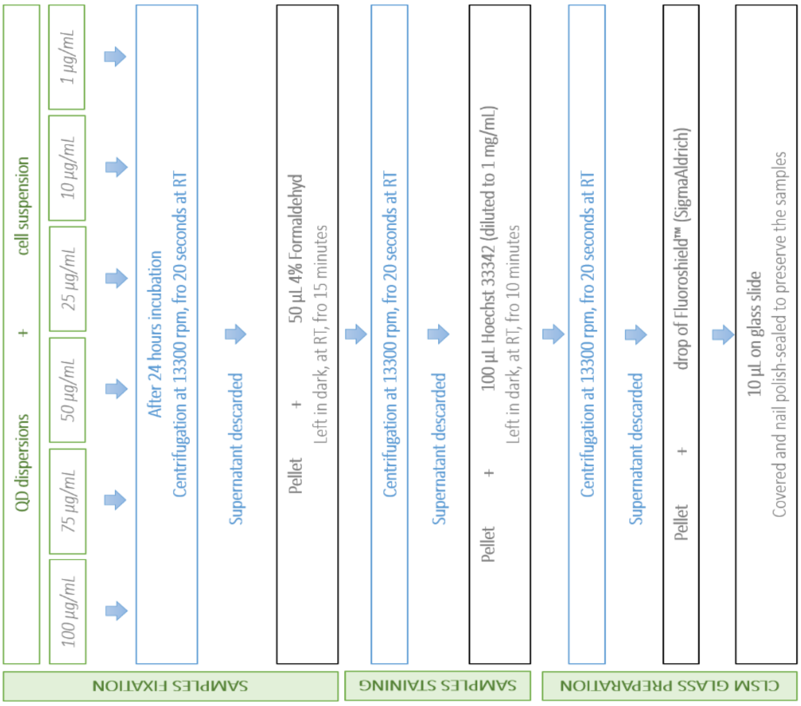
QD dispersions + cell suspension
1 µg/mL
10 µg/mL
25 µg/mL
50 µg/mL
75 µg/mL
100 µg/mL
After 24 hours incubation
Centrifugation at 13300 rpm, fro 20 seconds at RT
Supernatant descarded
Pellet + 50 µL 4% Formaldehyd
Left in dark, at RT, fro 15 minutes
Centrifugation at 13300 rpm, fro 20 seconds at RT
Supernatant descarded
Pellet + 100 µL Hoechst 33342 (diluted to 1 mg/ml)
Left in dark, at RT, fro 10 minutes
Centrifugation at 13300 rpm, fro 20 seconds at RT
Supernatant descarded
Pellet + drop of Fluoroshield™ (SigmaAldrich)
10 µL on glass slide
Covered and nail polish-sealed to preserve the samples
SAMPLES FIXATION
SAMPLES STAINING
CLSM GLASS PREPARATION

Figure 10.3.1. Procedure for fixation, staining and glass preparation of the six samples, for fluorescence microscopy analysis.

10.4 ALAMARBLUE® ASSAY INCUBATION TIMES RESULTS

Attempts for method improvement increase of QD concentrations - Test 2

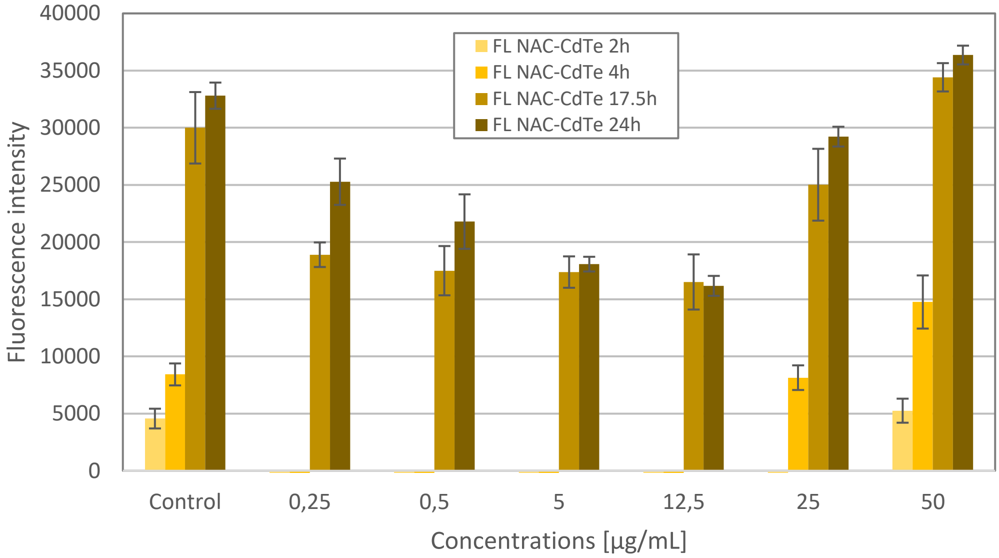

Figure 10.4.1. Comparison of fluorescence intensity of U937 incubated with NAC-CdTe, Test 2

.

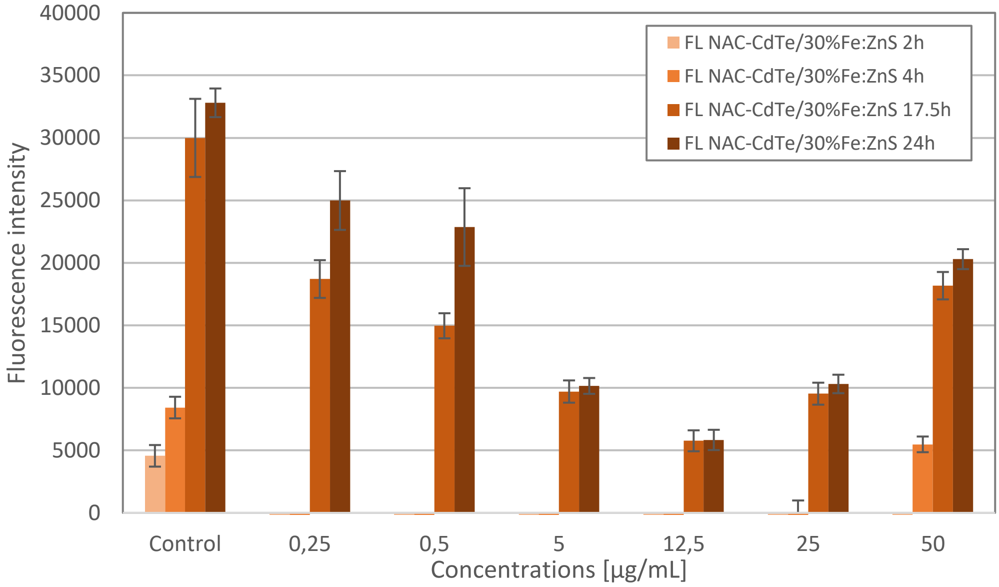

Figure 10.4.2. Comparison of fluorescence intensity of U937 incubated with NAC-CdTe/30%Fe:ZnS, Test 2.

Determination of dose-response curve and IC$_{50}$ values and CdCl$_2$ and FeCl$_2$•H$_2$0 samples – Test 3.a-b

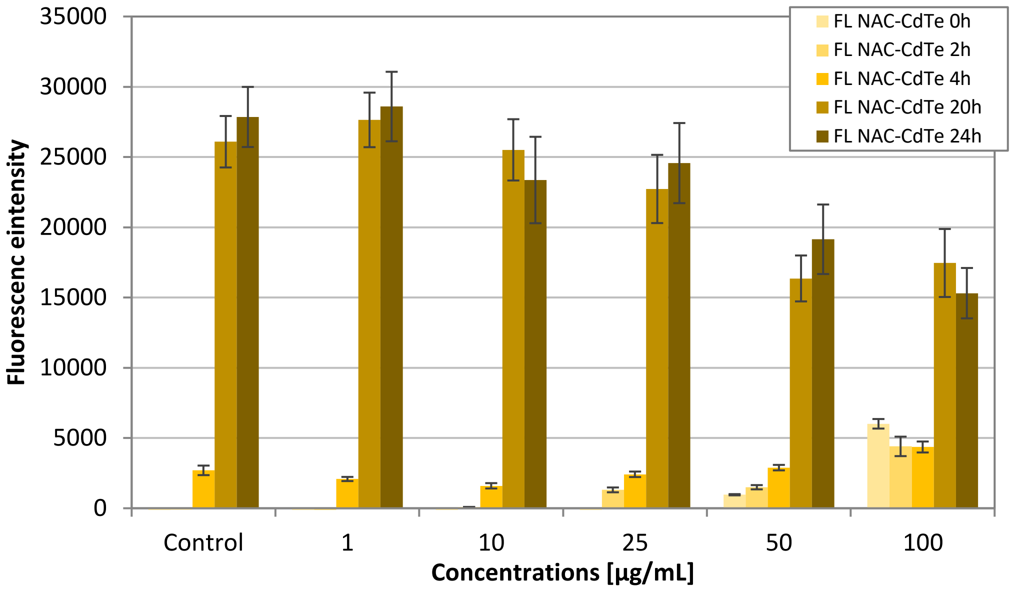

Figure 10.4.3. Comparison of fluorescence intensity of U937 incubated with NAC-CdTe, Test 3.a.

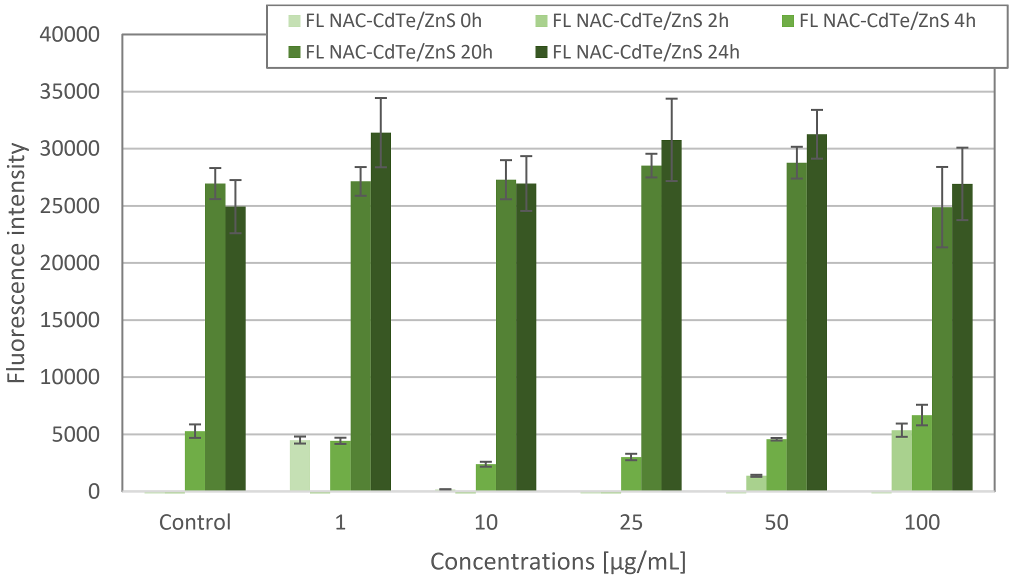

Figure 10.4.4. Comparison of fluorescence intensity of U937 incubated with NAC-CdTe/ZnS, Test 3.a.

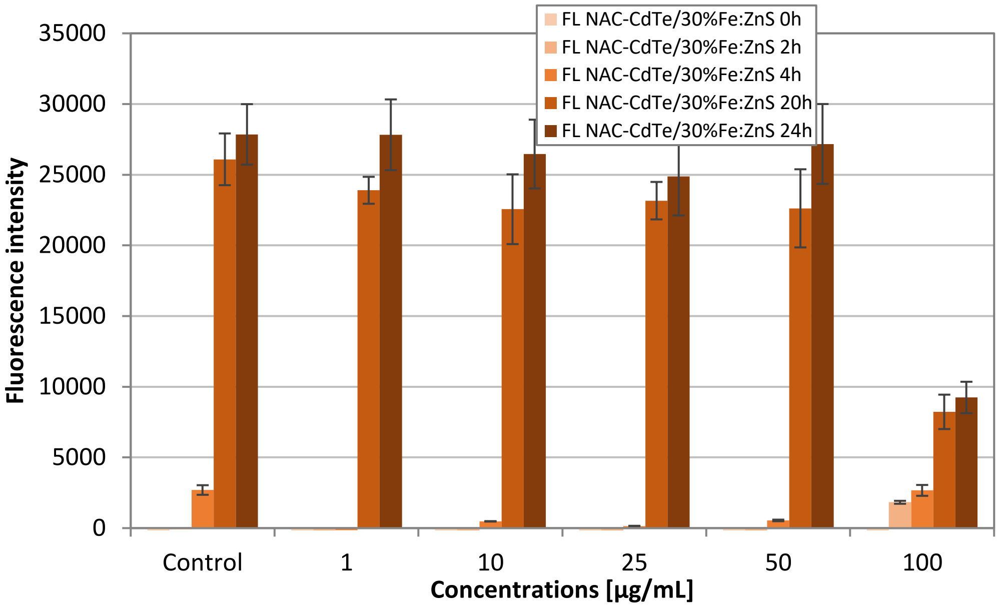

Figure 10.4.5. Comparison of fluorescence intensity of U937 incubated with NAC-CdTe/30%Fe:ZnS, Test 3.a.

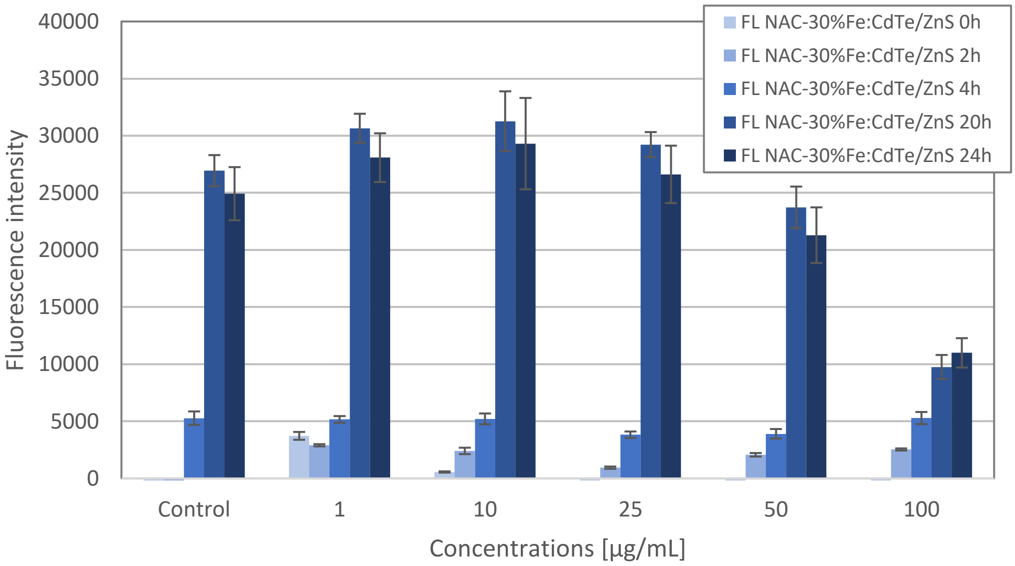

Figure 10.4.6. Comparison of fluorescence intensity of U937 incubated with NAC-30%Fe:CdTe/ZnS, Test 3.a.

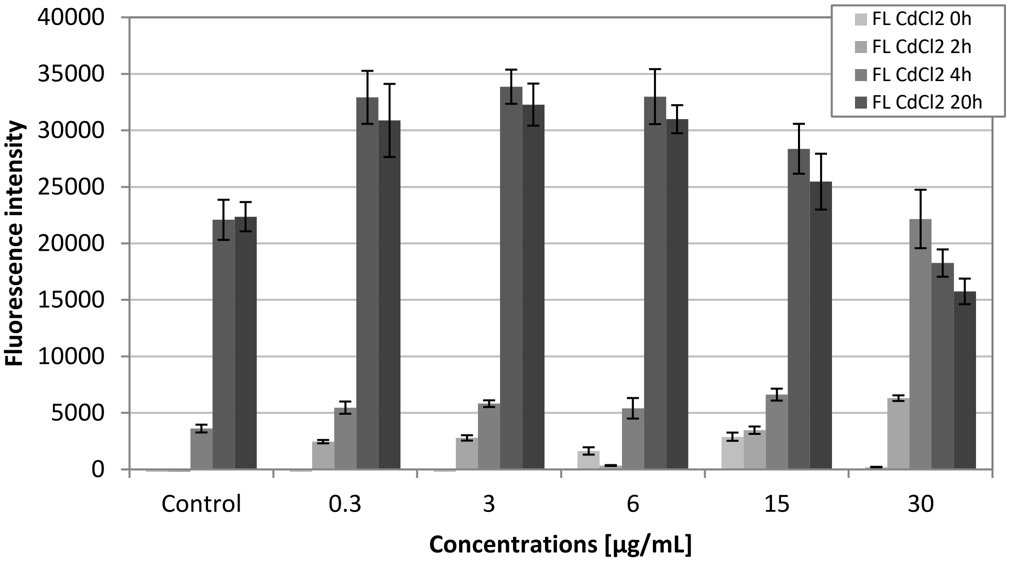

Figure 10.4.7. Comparison of fluorescence intensity of U937 incubated with $CdCl_2$, Test 3.a.

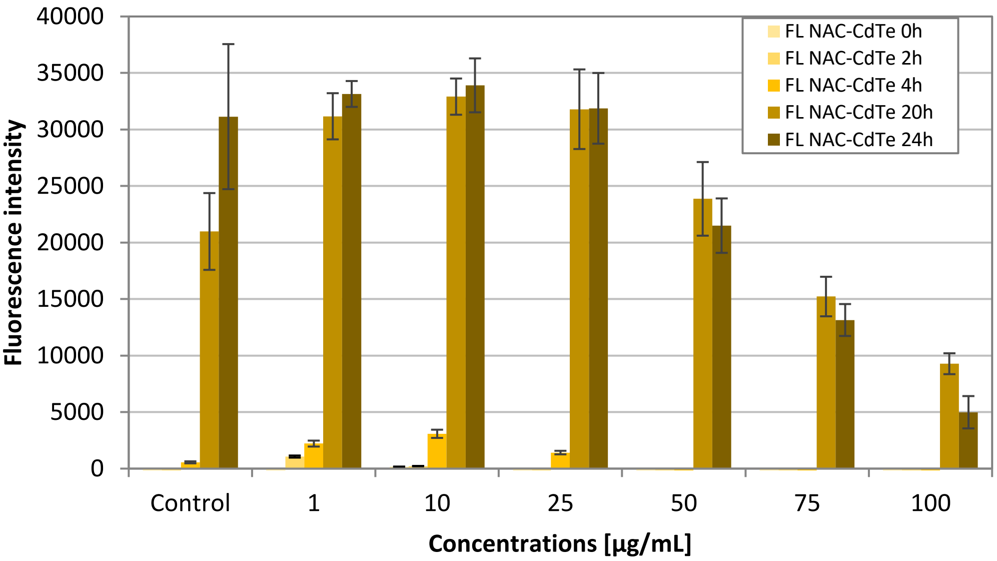

Figure 10.4.8. Comparison of fluorescence intensity of U937 incubated with NAC-CdTe, Test 3.b.

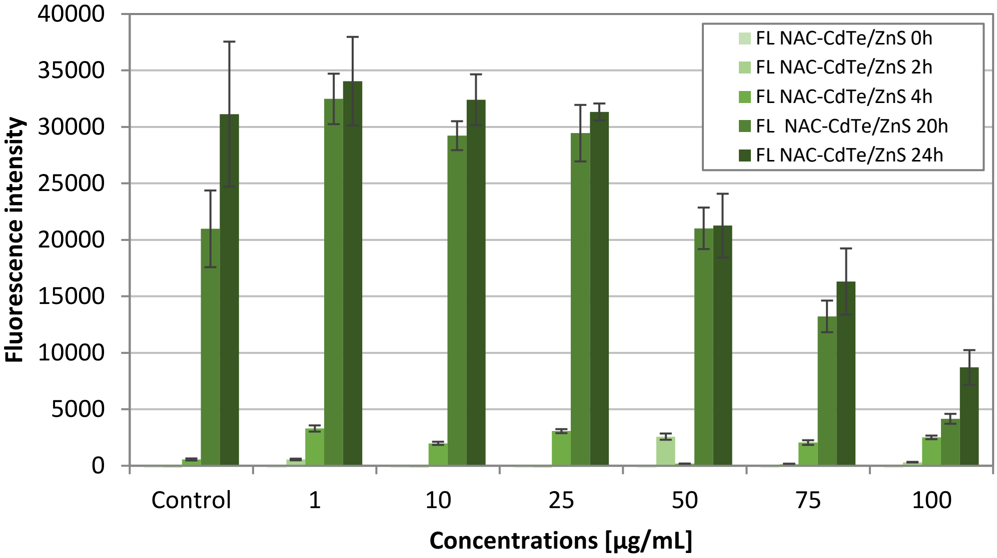

Figure 10.4.9. Comparison of fluorescence intensity of U937 incubated with NAC-CdTe/ZnS, Test 3.b.

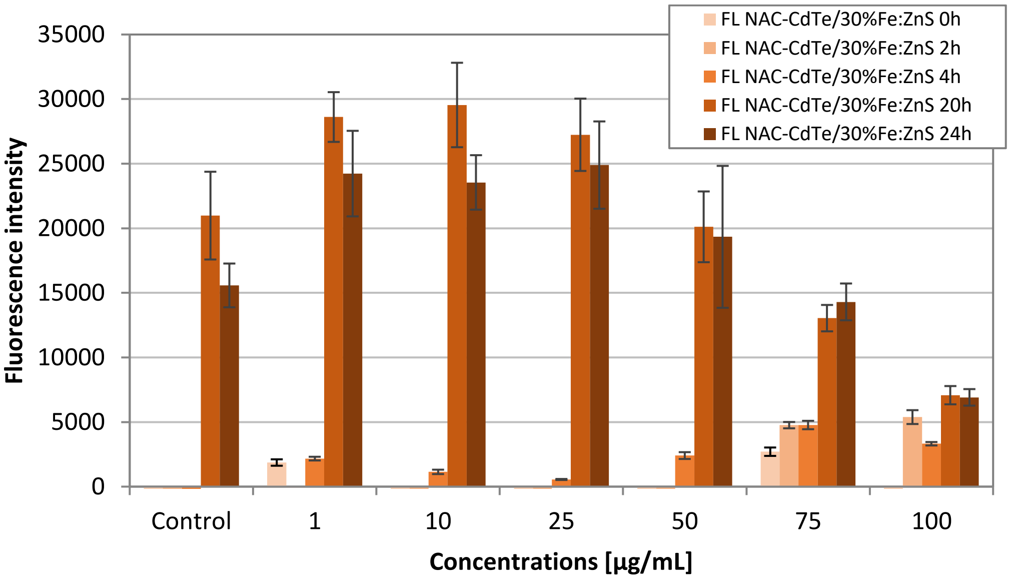

Figure 10.4.10. Comparison of fluorescence intensity of U937 incubated with NAC-CdTe/30%Fe:ZnS, Test 3.b.

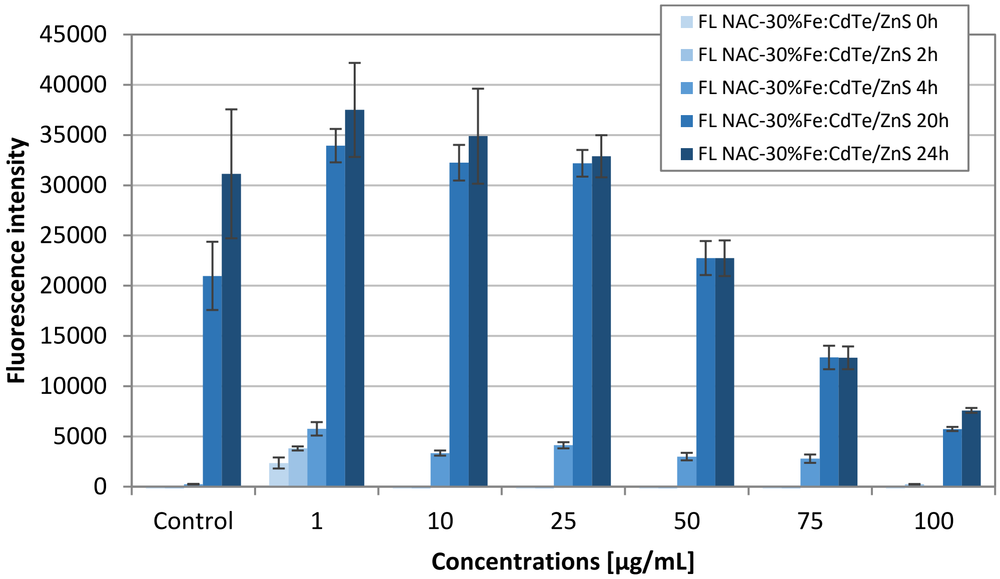

Figure 10.4.11. Comparison of fluorescence intensity of U937 incubated with NAC-30%Fe:CdTe/ZnS, Test 3.b.

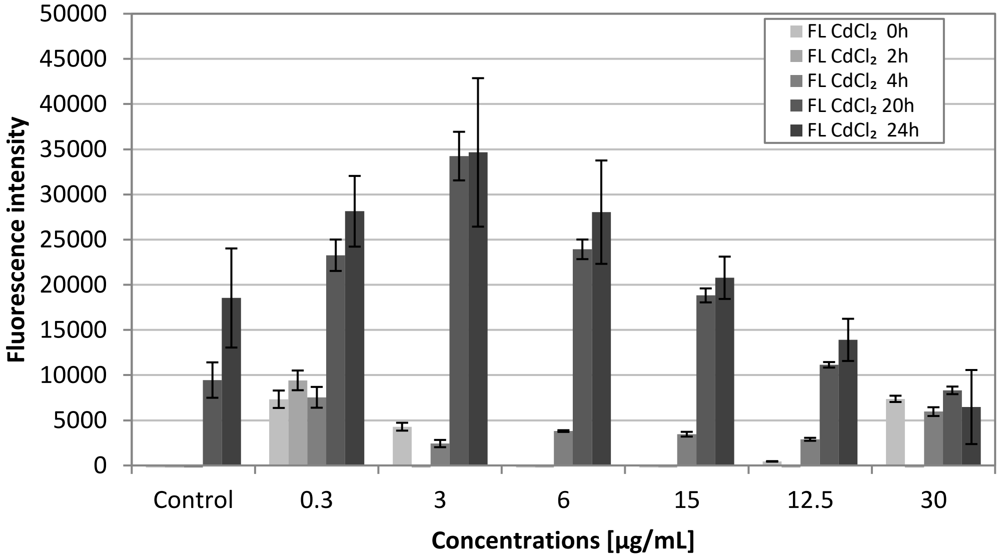

Figure 10.4.12. Comparison of fluorescence intensity of U937 incubated with $CdCl_2$, Test 3.b.

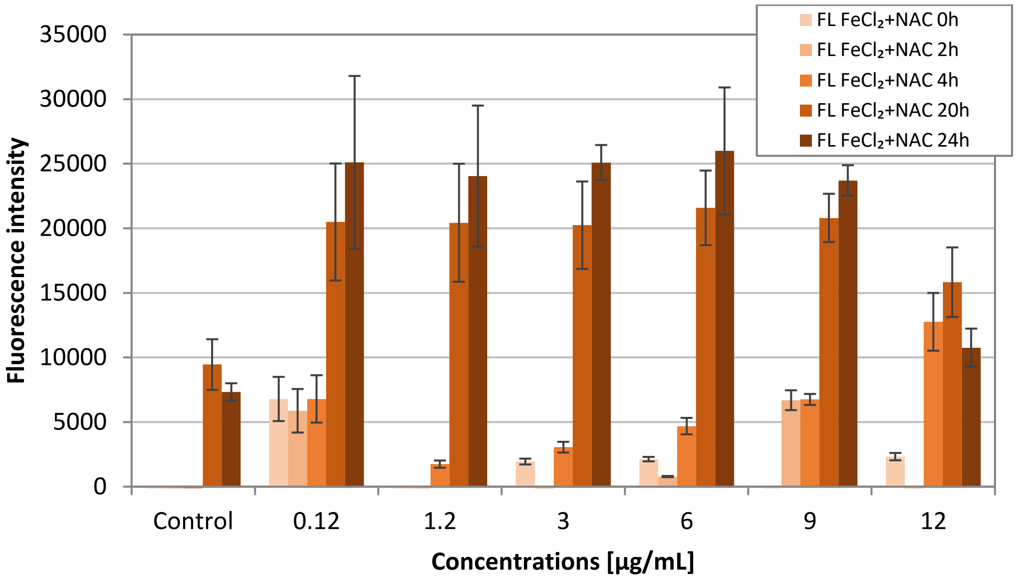

Figure 10.4.13. Comparison of fluorescence intensity of U937 incubated with $FeCl_2$, Test 3.b.